On parton showers and multi parton interaction

Martin von den Driesch

December 9, 2016

Über Partonschauer und Multipartonwechselwirkungen

Martin von den Driesch

December 9, 2016

On parton showers and multi parton interaction

Dissertation

zur Erlangung des Doktorgrades
der Physik Fakultät
der Universität Hamburg

vorgelegt von

Martin von den Driesch

aus Hamburg

Hamburg
2016

Gutachter/in der Dissertation:	PD Dr. Hannes Jung Prof. Dr. Peter Schleper
Gutachter/in der Disputation:	PD Dr. Hannes Jung Prof. Dr. Johannes Haller
Datum der Disputation:	16.11. 2016
Vorsitzende des Prüfungsausschusses:	Prof. Dr. Daniela Pfannkuche
Vorsitzender des Promotionsausschusses:	Prof. Dr. Wolfgang Hansen
Dekan der MIN-Fakultät:	Prof. Dr. Heinrich Graener

Abstract

In high energy hadron-hadron collisons (like for example at LHC) Drell Yan processes are important. For a precise determination of the inclusive cross section higher order calculations must be taken into account. In the region of phase space near threshold (where soft gluon emission dominates) large double logarithmic corrections become important. Thus it is necessary to perform a resummation to all orders in perturbation theory. In this thesis we analyze the energy fraction in Drell Yan processes. For that we apply a new parton shower formalism that was originally developed in [1]. It will be shown that the result is equivalent (under certain conditions) to a result given in [2] where the distribution of the energy fraction has been derived by standard resummation techniques. The goal is to confirm the reliability of this new formalism. Further also a comparison with the Monte Carlo event generator PYTHIA will be done.
We further investigate a jet algorithm that should detect multi parton interactions. It will be shown that this algorithm works for an idealised case but that it cannot detect multi parton interaction in a realistic scenario.

Zusammenfassung

In hochenergetischen Hadron-Hadron Kollisionen (wie z.B. am LHC) sind Drell Yan Prozesse wichtig. Für eine präzise Bestimmung des inklusiven Wirkungsquerschnittes müssen Rechnungen höherer Ordnung berücksichtigt werden. In der Region nahe an der Grenze des Phasenraumes (wo weiche Gluonenemission dominiert) werden große doppelte Logarithmen wichtig. Es ist daher notwendig, eine Resummation in allen Ordnungen der Störungstheorie durchzuführen. In dieser Arbeit analysieren wir den Energieanteil in Drell Yan Prozessen. Dafür wenden wir einen neuen Partonschauerformalismus an, der urprünglich in [1] entwickelt wurde. Es wird gezeigt, dass das Resultat unter bestimmten Bedingungen äquivalent zu einem anderen Resultat von [2] ist, wo die Verteilung des Energieanteils mit Standardresummationtechniken hergeleitet wurde. Das Ziel ist, die Zuverlässigkeit des neuen Formalismus zu bestätigen. Desweiteren wird auch ein Vergleich mit dem Monte Carlo Generator PYTHIA gemacht werden.
Wir untersuchen desweiteren einen Jetalgorithmus, der Multipartonwechselwirkungen ausfindig machen soll. Es wird gezeigt werden, dass dieser Algorithmus für ein idealisiertes Szenario funktioniert, aber dass er Multipartonwechselwirkungen nicht in einem realistischen Szenario bestimmen kann.

Danksagung

Zunächst möchte ich mich an dieser Stelle bei all denjenigen bedanken, die mich während der Anfertigung dieser Doktorarbeit unterstützt und motiviert haben.
Vor allem möchte ich meinen beiden Betreuern Hannes Jung und Zoltan Nagy danken. Desweitern geht mein Dank an Carsten Niebuhr.
Ganz besonderer Dank gilt dabei Zoltan Nagy, der viel zur Unterstützung dieser Arbeit beigetragen hat. Er nahm sich sehr viel Zeit, mir meine Fragen zu beantworten und mir mit Kritik, Anregungen und Tipps zu helfen.
Der Partonshauerformalismus, der in dieser Arbeit eine wichtige Rolle spielt, ist maßgeblich von ihm ausgearbeitet worden. Desweiteren geht die grundlegende Idee des Jetalgorithmus, der in dieser Arbeit untersucht wird, auch auf ihn zurück.

Desweiteren gilt mein Dank Manuel Hohmann, Martin Brinkmann, Albert Knutsson, Yuri Solovjev, Leif Joennson, Krzysztof Kutak und Michal Deak.
Besonderer Dank geht dabei an meine Mutter, die mich auch finanziell unterstützt hat.

Acknowledgement

First of all I would like to thank all those who have supported and motivated me during making my PhD thesis.
Especially I would like to thank my two supervisors Hannes Jung and Zoltan Nagy. Furthermore my thanks go to Carsten Niebuhr.
Special thanks go to Zoltan Nagy who has contributed much to the support of this thesis. He took a lot of time to answer me my questions and to help me with criticism, suggestions and tips.
The parton shower formalism that plays a major role in this thesis has been worked out by him to a major extent. Furthermore the jet algorithm that is investigated in this thesis goes back to him, too.

Furthermore my thanks go to Manuel Hohmann, Martin Brinkmann, Albert Knutsson, Yuri Solovjev, Leif Joennson, Krzysztof Kutak und Michal Deak.
Special thanks go to my mother who has supported me financially.

Contents

Chapter 1

Introduction

The general picture

For the investigation of the strong interaction, collider experiments are indespensable. There are several types of possible collisions: electron-positron, electron-proton, positron-proton, protron-antiproton and proton-proton. For the analysis of the strong interaction the most simple choice are electron-positron collisions[1]: the incoming electron and the incoming positron radiate before they form a γ or a Z^0 boson several photons. These radiation processes are well understood inside the frame of QED and can be treated pertubatively. We can call the formation of the γ or the Z^0 boson the "hard" subprocess as it happens on higher energy scales than the processes before and afterwards. After the formation of the virtual γ or Z^0 boson it must decay into a fermion-antifermion pair. It can be a lepton-antilepton pair (for example e^-e^+, $\mu^-\mu^+$, $\nu_e\bar{\nu}_e$ etc.) or a quark-antiquark pair. Only the latter case is interesting for the study of the strong interaction. The outcoming quarks undergo subsequent radiation of gluons as the incoming lepton-pair has undergone subsequent radiation of photons[2]. The outgoing gluons themselves can undergo further branchings: splitting into a gluon pair (in contrast to photons which cannot radiate photons by themselves) or splitting into a quark-antiquark pair. Those branchings can be treated inside the frame of perturbation theory and the branching can undergo further iterations until the nonperturbative domain has been reached. In the

[1] As we must deal here with the strong interaction in the final state only. In the other cases also the inital state must be taken into account for the analysis of the strong interaction.

[2] Though the outgoing quarks can also radiate photons those processes play no siginificant role in comparison to the radiation of gluons.

nonperturbative domain the outgoing partons must form hadrons due to *confinement*. This process is called *hadronization*. An important point that must be kept in mind in this context are the *factorization theorems*. They state that the cross section for the process $e^-e^+ \rightarrow Z^0/\gamma \rightarrow hadrons$ can be factored into a part $\hat{\sigma}$ that can be calculated with perturbative methods and a nonperturbative part that stands for hadronization. The perturbative cross section $\hat{\sigma}$ is always defined on parton level and is suited for the description of parton branching we have talked above. Physically the factorization theorems stand for the fact that perturbative and non-perturbative processes happen on different time scales: the time scale for perturbative processes is magnitudes lower than the one of non-pertubative processes. Therefore they can be treated seperately.
There are also factorization theorems in the case of deep inelastic scattering (DIS) (electron-proton or positron-proton collision) both for the incoming proton and for the outgoing hadrons. In that case the cross section factors into a non-perturbative part that stands for the incoming proton, a perturbative part $\hat{\sigma}$ that describes the quark that is struck by the virtual photon and its parton branching before and after the hard interaction and a non-perturbative part that stands for hadronization in the final state. The incoming proton is described by parton density functions (PDFs) which describe the momentum distributions of the incoming partons.
Similar is the situation in the case of hadron-hadron collisions. We have those processes at Tevatron (proton-antiproton) and at LHC (proton-proton). In the perturbative regime the incoming partons of the two hadrons can undergo parton branching (splitting of a gluon into a quark-antiquark pair or a gluon pair, radiation of a gluon from a quark or antiquark). This is in correspondence to the case of photon radiation in the case of a e^+e^- collision we have already mentioned above with the difference that gluons themselves can radiate further gluons. Afterwards they can undergo a hard interaction. The partons that come out of the hard interaction are themselves subject to further branching. An important point that must be kept in mind is that it is only meaningful to speak of parton branchings with respect to a *resolution scale*. As it is well known we encounter divergences in the case of soft and collinear branchings. This has to do with the fact that for example a quark that has emitted a soft or a collinear gluon[3] is completely undistinguishable from a quark that has emitted no gluon at all. The same applies to the case of a gluon which undergoes a soft or a collinear branching. By introduc-

[3]We have the problem of collinear gluons emitted by a quark only for the case that the quark's mass can be neglected.

ing a resolution scale we can distinguish between *resolvable* branchings and *nonresolvable* branchings. Thus it is possible for a quark that comes into a hard interaction to loose energy without emitting any resolved gluons[4]. The lower the resolution scale (for example for the case of an incoming quark) is set the more we see emitted gluons which are almost soft or collinear with respect to the resolution scale. This number goes to infinity when the resolution scale goes to zero. This is the physical meaning of the collinear and soft divergency.

In the case of proton-proton or antiproton-proton collisions further processes exist besides the one hard interaction. These additional processes are called the *underlying event*. First it is possible that besides the one hard interaction there are softer interactions that can be dealt within perturbative QCD. This is called *multi parton interaction*. The incoming and outcoming partons from these further interactions must also undergo parton branching.

Then it should be noted that besides the partons that came out of parton branching or directly from the hard interactions we have also remnants from the incoming hadrons. This is called the *beam remnant*. The beam remnant must also be taken into account for the formation of hadrons in the final state.

Monte Carlo event generators

After the description of the general physical picture of hadron-hadron collisions in a qualitative manner, the next question that arises is: how do we model this quantitatively? In practice a computer simulation is used which reproduces the probability distributions we expect from theory. Such a program is called a *Monte Carlo event generator* (MC).
The first step for such a program is to simulate the incoming particles. In the case of LHC and Tevatron they are hadrons. As already mentioned due to factorization theorems the incoming hadrons can be described by PDFs if there is a hard interaction for the incoming partons. For the case of two incoming hadrons (where two incoming partons undergo a hard interaction)

[4]This will become important in chapter (4).

we can write the cross section as[5]

$$\sigma(P_1, P_2) = \sum_{i;j} \int dx_1 dx_2 \; f_i(x_1, \mu^2) f_j(x_2, \mu^2) \hat{\sigma}_{ij}(p_1, p_2, \alpha_S(\mu^2), Q^2/\mu^2) \; . \tag{1.1}$$

Here is μ the factorization scale which separates the long- and the short-distance physics while Q characterizes the scale of the hard process. We note here that the scale μ should be of the order of the hard scale Q. The object $\hat{\sigma}_{ij}$ is the cross section of two incoming partons i and j which participate in the hard interaction. This entity can be calculated inside the frame of perturbative QCD. This is possible because the coupling at high energies (which is equivalent to short distances) is small. This implies that it does not depend on the details of the hadronic wave function or the flavors of the incoming hadrons. It only depends on the momenta and flavors of the incoming partons which come out of the hadrons. The functions $f_i(x, \mu^2)$ are the well known parton density functions evaluated at factorization scale μ. It should be noted that eq.(1.1) does not apply to the majority of events in hadron-hadron collisions. Most collsions only yield soft particles in the final state. Nevertheless it is essential for the analysis of those type of events where we do have a hard interaction as this is important for the understanding of perturbative QCD. The momenta of the two incoming partons are given by $p_1 = x_1 P_1$ and $x_2 P_2$ where P_1 and P_2 are the momenta of the two incoming hadrons while x_1 and x_2 are the momentum fractions of the partons. The parton density functions stand for the non-perturbative part of the process or to be more precise their dependence on the momentum fractions x cannot be derived inside the frame of perturbative QCD. What however can be treated inside perturbation theory is their dependence on the scale μ. This leads to a set of evolution equations which are known as the DGLAP equations. The DGLAP equations effectively sum up leading powers of $[\alpha_S \log Q]^n$ which come from multigluon emission in a region of phase space where the gluons have strongly-ordered transverse momenta[6]. The DGLAP equations are based on the assumption that $\log Q$ is much bigger than $\log\left(\frac{1}{x}\right)$.

Though DGLAP is the usual approach for dealing with the scale dependency of the parton density functions it is important to mention that for example at HERA Q^2 is not so large at very small x. Here the application of DGLAP is not appropriate. The alternative is to sum up all terms proportional to $\alpha_S \log\left(\frac{1}{x}\right)$ while retaining the full Q^2 dependence and not just the leading

[5] See for that eq.(7.1) in [3].

[6] See for that chapter (4) of [3].

$\log Q^2$ terms. This leads to the BFKL[7] evolution equations where integration is performed for the full k_T space of the gluons and not just for the strongly ordered part. It ought to be mentioned that for BFKL another factorization is used than the one given in eq.(1.1).
A third set of evolution equations are the CCFM equations (see for that [7], [8], [9] and [10].). They have the advantage that in contrast to BFKL they are better suited for implementation into a Monte Carlo event generator (see for that [11] and [12]). They are an approach to cover both the infrared regions and the collinear regions by treating color coherence effects; in the limit of asymptotic energies they are almost equivalent to the BFKL and DGLAP equations.

For hadron-hadron collisions where we have at least one hard interaction, the next step inside a Monte Carlo event generator is to simulate the parton branching mentioned above. The first choice for those kind of processes are matrix elements as they are inside the frame of perturbative QCD. Here the exact kinematics, full interference and helicity structure are taken into account. Unfortunately the application of matrix elements becomes more and more complicated[8] in higher orders especially for loop graphs. Thus the parton shower approach is introduced where certain approximations for the parton splitting in the soft and collinear limit are made in order to deal with the parton branching we have discussed above. There the process of parton splitting is modeled like a process in classical statistical mechanics[9]. An explicit expression of a matrix element is only used in MC event generators for the hard scattering while the parton shower appproach is applied for branchings that occur before (initial state splitting) and after the hard scattering (final state splitting).

In the generator we have a bunch of partons which come out from the hard interaction and the parton branching. Inside a physical detector we see however not partons but hadrons. The transition is beyond the scope of perturbative QCD and cannot be treated up to now from first principles. Thus we need inside the event generator a phenemenological algorithm which conducts the transition from partons. Such a kind of algorithm is called a *hadronization model*.

[7] See for that section (4.6.4) and section (4.6.5) in [3]; the original set up of the BFKL equations was done in [4–6].

[8] See for that chapter (2) in [13].

[9] For a more detailed description of this see the next chapter and section (2.2) in chapter (2).

There are nowadays two ways to simulate hadronization in a Monte Carlo event generator: string fragmentation and cluster fragmentation. Further many variants and hybrids exist, too[10]. String fragmentation is used in the JETSET hadronization scheme which is applied in PYTHIA and ARIADNE (see for that [13], [14, 15] and [16]) . An example for the use of cluster fragmentation is HERWIG (see for that [17, 18]).

We note here that the decay of unstable hadrons after their formation plays also a role.

In a hadron-hadron collision the incoming partons (which first can radiate and then undergo the hard process) take only a part of the momenta of the incoming hadrons. Thus the beam remnant must be taken into account in the simulation in order to treat the whole physical process properly.

What will be discussed in more detail in this thesis is the possibility of multi parton interaction. It is possible that a parton from one hadron scatters with several partons from the other or that several parton pairs from the two hadrons take part in several distinct hard interactions. It is presumed due to combinatorial reasons that the latter is favored; this is taken into account in an event generator like PYTHIA[11].

Jets

A point that will be important in this thesis is the subject of *jets*. We have an algorithm that combines several outgoing hadrons which we call jets. There are several types of jet algorithms like k_T (see [19]), SiScone (see [20]) or anti-k_T (see [21]).

The underlying reasoning behind those algorithms is this: the outgoing partons after the hard scattering (they are considered inside the frame of perturbative QCD) are colored objects; the outgoing hadrons which are directly observed in the detector are color free[12]. We have already mentioned that this problem is handled by hadronization models which are phenomenological and not based on first principles. It is on the other hand helpful to treat this problem from the other side in a jet algorithm where the final state hadrons are attributed to distinct jets. The idea behind this is that the outgoing partons are the origin of those jets and that fragmentation does not change the momentum distribution much. An important application for jet algorithms are events of the type $e^+e^- \to hadrons$. On parton level we have

[10] See section (2.4) in [13].

[11] See section (2.3) in [13].

[12] See also chapter (5).

$e^+e^- \to q\bar{q}$ and $e^+e^- \to q\bar{q}g$ where g is supposed to be a hard gluon. The seperation into 2 jet and 3 jet events gives us insight how often a hard gluon is emitted. By this method it is possible to determine the strong coupling constant α_S. We note that also 4 jet events and events with an even higher jet multiplicity are observed. However they are rather suppressed.
Another example where the application of jet algorithms becomes important is given by the analysis of hadron-hadron collision where we have in the final state three jets. Under the prerequisite that these jets are well seperated in phase space it is possible by using a jet algorithm to compare the three jet cross section with perturbative QCD. The result is a big success for the theory[13].
This success of perturbative QCD and jet algorithms triggered the hope by introducing a new kind of jet algorithm we could distinguish multi-parton interactions from the major hard interaction. In chapter (5) we will discuss this in more detail.

This thesis is orgainized as follows

1. In chapter (2) we summarise the application both for PS and MPI inside Monte Carlo event generators.

2. In chapter (3) we introduce an analytical parton shower formalism. This is a summary of [1] where this formalism was devoloped for the first time. Its advantage lies in the fact that it takes also interference effects into account. We present this formalism as its results will play a role in chapter (4).

3. In chapter (4) we apply the formalism presented in chapter (3) to the case of Drell Yan processes. This will be compared afterwards with the resummation in perturbative QCD. By that the energy fraction in Drell Yan processes was derived inside the frame of conventional methods. This was done in [2] and [24]. In section (4.4) the results will be compared with the energy fraction inside a conventional parton shower generated by PYTHIA.

4. In chapter (5) we discuss an algorithm that is supposed to distinguish between the hard interaction and multi parton interaction.

5. In chapter (6) we summarize the results of this thesis.

[13] See section (7.7) in [3]; further [22] and [23]

Chapter 2

Monte Carlo event generators

2.1 Why do we need Monte Carlo generators?

We want to compare predictions from a theory like QCD with experimental measurements. In contrast to QED, however, it is not possible just to calculate the matrix element of a particular process and then derive the cross section which can be compared to data. The first complication arises with the break down of perturbation theory at low momentum transfer. With our present tools we are not able to deal with nonperturbative physics from first principles. We must therefore use phenomenological models like for example hadronization models for dealing with the final state[1]. But even inside the frame of perturbative QCD it is not meaningful to just calculate the matrix element: although it is true that the matrix element approach is preferable - since exact kinematics, the full interference and the helicity structure are treated - the calculation of matrix elements for higher orders becomes increasingly difficult especially for loop graphs. Until recently only for special cases diagrams have been computed for more than one loop and in many cases no loops at all have been treated. Now it is possible to apply automated NLO calls like aMC@NLO or Blackhat (see [25]).
In order to deal with this problem the parton shower approach is used. This can be done in numerical computer programs like Monte Carlo event generators (see this chapter) or in an analytical formalism (see for that chapter (3)). The basic idea of a parton shower is to have an iterative algorithm of branchings $a \to bc$. In a QCD shower the type of branchings we have are

[1] See for a discussion of it for example section (5.6) of [3].

$q \to qg$, $\bar{q} \to \bar{q}g$, $g \to gg$ and $g \to q\bar{q}$. (It is in principle also possible to include QED type processes $q \to q\gamma$, $\gamma \to l\bar{l}$ etc.) In contrast to the matrix element approach the number of the outgoing partons is not fixed anymore[2]. The probability of a branching is derived from the soft and collinear limit where we have a pole. The kinematics, the interference and helicity structure is simplified in contrast to the matrix element approach. In contrast to a matrix element loop graphs are not considered. Non-resolvable branchings and virtual corrections are taken into account by the fact that the probability of non-emission can be simply derived from the probability of emission[3]. Thus the matrix element approach and the parton shower approach should be viewed as complementary in many aspects (see section (2.2) of [13]). In the following section we introduce the parton shower approach for Monte Carlo event generators. For a full description of hadron-hadron collisions Monte Carlo event generators are indispensible. The aim is to have a computer program that simulates events as detailed as possible as they would be seen in reality by a perfect detector. It is however not feasible to perform this in one single step. Instead the process is 'factored' into several parts where each can be treated by a computer program in a proper way. In practice this means that the algorithm starts with the hard interaction, then parton shower or bremsstrahlung is generated and as a final step we have hadronization.
Those 'events' which are generated with the computer program are supposed to have the same average behaviour and the same fluctuations as real data. The fluctuations in data have their origin in quantum effects. These fluctuations are simulated in an algorithm by Monte Carlo techniques where all relevant variables are selected according to the probability distributions which lead to the desired (quasi-)randomness. Unfortunatley we must anticipate some loss of information as Monte Carlo algorithms work with probabilities and not with amplitudes which are the basis for quantum physics. This problem is not too severe, since only rarely we must deal with interference phenomena that cannot be treated inside the frame of probabilistic language.
We summarize the main applications for Monte Carlo event generators in particle physics:

- Monte Carlo event generators show us for every model (for example the Standard model) how events are supposed to look like and at what

[2]While in the matrix element approach for any configuration of the final state partons a transitional amplitiude is calculated.

[3]One or the other of the two processes must happen.

rates. These results can later be compared to data.

- Monte Carlo event generators are useful for the planning of new detectors so that detector performance can be optimized. The simulation of the detector is done with programs like GEANT (see [26] and [27]).
- Monte Carlo event generators are also useful for work on analysis strategies on real data in order to enhance the signal-to-background conditions.
- A Monte Carlo generator can be also used as a tool in order to estimate detector acceptance corrections which can be applied to data in order to obtain the 'real' physical signal.

For a full description of hadron-hadron collisions a Monte Carlo algorithm needs necessarily the following ingredients:

- matrix elements, lorentzinvariant phase space
- parton density functions
- parton showers
- beam remnants
- multi parton interactions

2.2 Parton showers

We start the discussion with a concrete example namely e^+e^- annihilation to hadrons[4]. The leading order process is $e^+e^- \to q\bar{q}$. We denote its cross section by $\sigma_{q\bar{q}}$.
The next step is to consider the next-to-leading order process, the radiation of a gluon $e^+e^- \to q\bar{q}g$. We parametrize the three-parton phase space by θ (which is the opening angle between the quark and the gluon) and the energy fraction of the gluon with respect to the beam energy which we denote by z. With the matrix element we obtain

$$\frac{\mathrm{d}\sigma_{q\bar{q}g}}{\mathrm{d}\cos\theta dz} \approx \sigma_{q\bar{q}} C_F \frac{\alpha_S}{2\pi} \frac{2}{\sin^2\theta} \frac{1+(1-z)^2}{z} \ , \tag{2.1}$$

[4]We follow here the description of [28] page 22-28.

where we have $C_F = \frac{N_c^2-1}{2N_c}$ which can be considered as the color charge squared of a quark. According to eq.(2.1) the cross section for $q\bar{q}g$ is proportional to the cross section for $q\bar{q}$. Thus we may consider the rest of the equation as the probability of gluon emission, differential in the kinematics of the gluon.
We must note there are divergencies:

1. $\theta \to 0$ corresponds to the case where the gluon becomes collinear with the quark.

2. $\theta \to \pi$ corresponds to the case where the gluon becomes back-to-back with the quark which implies that it becomes collinear with the antiquark.

3. $z \to 0$ means that the gluon energy becomes zero. This is the soft case.

We focus now on the two collinear cases. We can seperate the two collinear regions

$$\frac{2}{\sin^2\theta} = \frac{1}{1-\cos\theta} + \frac{1}{1+\cos\theta} \approx \frac{1}{1-\cos\theta} + \frac{1}{1-\cos\bar{\theta}} \ . \tag{2.2}$$

So we can write the cross section as a sum of these two processes. $\bar{\theta}$ is here the angle between the gluon and the antiquark. Thus we may write

$$\mathrm{d}\sigma_{q\bar{q}g} \approx \sigma_{q\bar{q}} \sum_{\text{partons}} C_F \frac{\alpha_S}{2\pi} \frac{\mathrm{d}\theta^2}{\theta^2} \mathrm{d}z \frac{1+(1-z)^2}{z} \ . \tag{2.3}$$

Here is θ now the opening angle between the parton and the gluon that has been emitted by the former. A series expansion of the trigonometric functions was used for this expression so we come to the $\frac{d\theta^2}{\theta^2}$ expression for the $\theta \to 0$ limit in eq.(2.3). We note that the form of this equation does not change when we substitute θ by any other variable that is proportional to θ like the virtuality $q^2 = z(1-z)\theta^2E^2$ or the gluon's transverse momentum with respect to the parent's quark direction. Because of $k_\perp^2 = z^2(1-z)^2\theta^2E^2$ we can write for $\theta \to 0$

$$\frac{\mathrm{d}\theta^2}{\theta^2} = \frac{\mathrm{d}q^2}{q^2} = \frac{\mathrm{d}k_\perp^2}{k_\perp^2} \ . \tag{2.4}$$

We note that any of these forms gives the same result in the collinear limit but differs in the region away from it which means different finite terms are included in addition to the divergent piece.

It is possible to generalize eq.(2.3). We can write for a hard process where a parton of flavor i together with a parton j (which has momentum fraction z) is produced

$$\mathrm{d}\sigma \approx \sigma_0 \sum_{\text{partons},i} \frac{\alpha_S}{2\pi} \frac{\mathrm{d}\theta^2}{\theta^2} \mathrm{d}z P_{ji}(z,\phi)\mathrm{d}\phi \ . \tag{2.5}$$

$P_{ji}(z,\phi)$ are the splitting functions. They are a set of flavor dependent functions. The angle ϕ (the azimuth of j around the axis of i) indicates that they are also spin dependent. The spin-averaged functions are given by

$$\begin{aligned} P_{qq}(z) &= C_F \frac{1+z^2}{1-z}, & P_{gq}(z) &= C_F \frac{1+(1-z)^2}{z}, \\ P_{gg}(z) &= C_A \frac{z^4+1+(1-z)^4}{z(1-z)}, & P_{qg}(z) &= T_R(z^2+(1-z)^2) \ . \end{aligned} \tag{2.6}$$

$C_A = N_c$ can be considered as the color charge squared of a gluon. T_R is a further factor that is by convention set to $\frac{1}{2}$. Another choice would make a different definition of α_S necessary. The splitting functions P_{qq}, P_{gq}, P_{gg} and P_{qg} are related to the splitting-processes $q \to qg$, $q \to gq$, $g \to gg$ and $g \to q\bar{q}$.

These results are valid for the collinear limit where they do not depend on the precise definition of z. This variable can be the energy fraction or the light-cone momentum fraction (or something similar) of parton j with respect to parton i.

The next step is to treat the divergencies in the splitting functions. For the moment we focus on the collinear divergencies. The soft case will be considered later. The collinear divergency means that we cannot distinguish between non-emission and a collinear pair of partons. This corresponds to a process that has no physical effect and is unmeasurable.

In order to get meaningful results we require that we take only resolvable branchings into account. For the resolution scale there are several possible choices. One choice is the relative transverse momentum between two partons above a cutoff scale Q_0.

Let us consider some ordering variable q (for example the virtuality). The total probability of a branching of a parton of type i between q^2 and q^2+dq^2 is given by

$$d\mathcal{P}_i = \frac{\alpha_S}{2\pi} \frac{dq^2}{q^2} \int_{Q_0^2/q^2}^{1-Q_0^2/q^2} dz P_{ji} \ . \tag{2.7}$$

We want to find out the probability that no branchings above a virtuality q^2 happen given that its maximum possible value is Q^2. We call this function

$\Delta_i(Q^2, q^2)$. If we change the quantity q^2 by a small value the non branching probability Δ_i will change by the branching probability $d\mathcal{P}_i$. The change $\mathrm{d}\Delta_i$ itself is proportional to the non emission probability Δ_i. Thus we have

$$\frac{\mathrm{d}\Delta_i(Q^2, q^2)}{dq^2} = \Delta_i(Q^2, q^2)\frac{\mathrm{d}\mathcal{P}_i}{\mathrm{d}q^2} \ . \tag{2.8}$$

The solution of this equation is given by

$$\Delta_i(Q^2, q^2) = \exp\left\{ -\int_{q^2}^{Q^2} \frac{\mathrm{d}k^2}{k^2}\frac{\alpha_S}{2\pi}\int_{Q_0^2/k^2}^{1-Q_0^2/k^2} \mathrm{d}z P_{ji}(z)\right\} . \tag{2.9}$$

Of special interest is the total probability to produce no *resolvable* branching at all:

$$\begin{aligned}\Delta_i(Q^2, q^2) &= \exp\left\{ -\int_{Q_0^2}^{Q^2} \frac{\mathrm{d}k^2}{k^2}\frac{\alpha_S}{2\pi}\int_{Q_0^2/k^2}^{1-Q_0^2/k^2} \mathrm{d}z P_{ji}(z)\right\} \\ &\sim \exp\left\{ -C_F\frac{\alpha_S}{2\pi}\log^2\frac{Q^2}{Q_0^2}\right\} .\end{aligned} \tag{2.10}$$

This is the Sudakov factor. It is the basic building block to be implemented into a Monte Carlo simulation program.
Previously we considered the collinear case. We also know that there is a soft divergency. Due to destructive interference it is possible to include soft gluon effects into a collinear parton shower algorithm if out of all possible evolution scales, the opening angle is used. This leads to angular-ordered (or coherence-improved) parton showers like for example in HERWIG[5] (for the description of HERWIG see [29]). Angular ordering is also used in the generators CASCADE (see [30]), PYTHIA (see [13] and [31]) and ARIADNE (see [16]).

2.2.1 Implementation into a Monte Carlo event generator

We introduce here the most simple way to simulate parton branching in a Monte Carlo event generator[6]. We do not take into account more complicated effects like different possible branchings and QCD coherence effects. For the purpose of convenience we write $t := q^2$. First we consider the case of spacelike branching. In this case t evolves towards the hard scale Q^2. Let us start with t_1 as a starting value for the virtuality. Then we want to

[5] See for that section (4.3) of [28].
[6] The description follows mainly section (5.3) and (5.4) of [3].

generate with the correct probability distribution t_2. We already know that the probabilty to evolve from t_1 to t_2 without resolvable branching is given by $\Delta(t_2)/\Delta(t_1)$. We generate t_2 by solving the equation

$$\frac{\Delta(t_2)}{\Delta(t_1)} = \mathcal{R} \ . \tag{2.11}$$

$\mathcal{R}$ is here a random number with a uniform distribution in the interval $[0, 1]$. For the case that t_2 exceeds Q^2 we have no further branching. Else further branching is possible. Then we must consider[7] the proper distribution of z. The distribution is supposed to be proportional to $(\alpha_S/2\pi)P(z)$ where $P(z)$ is the corresponding splitting function. The value of z can be generated by solving the following equation

$$\int_{\epsilon}^{x_2/x_1} dz \frac{\alpha_S}{2\pi} P(z) = \mathcal{R}^{'} \int_{\epsilon}^{1-\epsilon} dz \frac{\alpha_S}{2\pi} P(z) \ . \tag{2.12}$$

$\mathcal{R}^{'}$ is here a further random number in the interval $[0, 1]$ while ϵ is the infrared cut-off for resolvable branching. The azimuthal angles of the emission are in the simplest case generated uniformly in the range $[0, 2\pi]$.
Now we focus on the timelike case. Here t evolves downwards to the cut-off scale t_0. Now the probability for evolution from t_1 to t_2 is given by $\Delta(t_1)/\Delta(t_2)$. Thus we substitute for the timelike case eq.(2.11) by

$$\frac{\Delta(t_1)}{\Delta(t_2)} = \mathcal{R} \ . \tag{2.13}$$

We remark that because of $\Delta(t_0) = 1$ there is no solution for $t_2 > t_0$ if we have $\mathcal{R} < \Delta(t_1)$. If timelike branching does happen the procedure for generating z is the same as in the spacelike case.
The whole procedure continues until no branchings occur. Then the cascade stops. This depends on the cut-off scale t_0. After parton branching ceases the outgoing partons are transformed into hadrons. This is called *hadronization*. There are several hadronization models available for a Monte Carlo event generator.

We have now dealt with *forward* parton evolution. Here a parton with timelike momentum produces new partons so that they evolve towards lower virtual mass-squared. In spacelike cascades it is however more convenient to consider *backward* evolution. If we applied forward evolution for initial

[7] If the incoming particles are hadrons we have $z = x_2/x_1$.

state radiation we would have no guarantee that a hard subprocess can be generated. Instead in many cases we would have no hard process at all. This would make the whole algorithm inefficient. Instead we start with the hard subprocess and evolve the parton shower back. This is called *backward* evolution. However we cannot just use the forward algorithm and run it in the reverse. If for example the incoming particles are hadrons eq.(2.12) could produce an incoming parton with $x_1 > 1$. Again in many cases we would obtain useless results that must be rejected so that we would have low efficiency either.
The solution to this problem is given by a modified form factor which also incorporates the parton density functions $f(x,t)$. It is given by

$$\Pi(t_1, t_2; x) = \frac{f(x,t_1)\Delta(t_2)}{f(x,t_2)\Delta(t_1)} \ . \tag{2.14}$$

It is the probability for backward evolution from (t_2, x) to (t_1, x) without branching. Thus the Sudakov factor $\Delta(t_i)$ is substituted by $\Delta(t_i)/f(x,t_i)$. The algorithm yields t_1 by solving the equation

$$\Pi(t_1, t_2; x) = \mathcal{R} \tag{2.15}$$

where $\mathcal{R}$ is again a random number uniformly distributed in the interval $[0,1]$. The next step is to generate x_1. With $z = x_2/x_1$ the probability distribution for x_1 is supposed to be proportional to

$$\frac{\alpha_S}{2\pi}\frac{P(z)}{z} f(x_2/z, t_1) \tag{2.16}$$

with $P(z)$ as the corresponding splitting function. The extra factor $f(x_1,t_1)$ will be divided out in the next backward step in t. With the above expression z is generated with a similar procedure as in forward evolution (see for that eq.(2.12)). As an alternative it is possible to write for Π

$$\Pi(t_1, t_2; x) = \exp\left\{ -\int_{t_1}^{t_2} \frac{dt}{t} \int \frac{dz}{z} \frac{\alpha_S}{2\pi} \hat{P}(z) \frac{f(x/z,t)}{f(x,t)} \right\} \ . \tag{2.17}$$

It should be noted here that the ratio of parton distributions in eq.(2.14) leads to a suppresion of branching at large x as $f(x,t)$ is a decreasing function of t there. On the other side it enhances branching at low x because $f(x,t)$ is increasing with decreasing x. The physical meaning of this is that partons at high x are less likely to have undergone branching (which always reduces x) what means that it is very likely for the parton to have come

directly from one of the two hadrons.
Corresponding to that we have in the distribution of z a suppression of branchings in regions where the parton density $f(x_2/z, t_1)$ is low. This factor guarantees that the value of $x_1 = x_2/z$ is always less than unity.

2.3 Multi parton interaction

Besides the hard interaction and the parton showering (which are dealt with perturbative methods) there are further processes in hadron-hadron collisions. Due to the composite nature of hadrons (they can be considered as 'bunches' of partons) even within perturbative QCD we expect that most inelastic hadron-hadron collisions contain several calculable interactions. Such interactions, even if they are soft compared to the hardest interaction, can cause non-trivial changes in the color topology of the system which could lead to drastic changes of the particle multiplicity of the final state.
These further interactions (which are part of the so called 'underlying event') were not considered to be interesting in the past because perturbative QCD emissions play a more important role in the production of multijets than seperate multiple interactions. The underlying event was dismissed as a mess of soft QCD emissions that cannot be treated inside the frame of perturbative physics but must be parametrized. Those parametrizations were successful in describing the average underlying activity. They fail however for the treatment of correlations and fluctuations. This affects the description of jet pedestals, jet profiles and random shifts in jet energies. Thus those models are not trustworthy beyond the fit region despite the fact that they can describe a few distributions well.
In order to deal with this it is postulated that *all* particle production in inelastic hadronic collisions has its origin in the multiple-interactions mechanism. This does not exclude the possibility that nonperturbative effects and other phenomena will play a role in the transition from perturbative physics to visible hadrons. But we start in the frame of perturbative physics. This implies that a typical Tevatron hadron-hadron collision has about 2-6 interactions while at the LHC one expects[8] about 4-10.

[8]The material for this section has been taken out from [32] (page 1 to 8) and [13] (page 329-334 and 342-344).

2.3.1 Basics of multi parton interaction

The following follows closely the description of [28,32]. Information from [13] on multi parton interaction has been included, too.
The cross section for QCD hard $2 \to 2$ processes can be written as a function of the $p_\perp^2$ as

$$\frac{\mathrm{d}\sigma_{\mathrm{int}}}{\mathrm{d}p_\perp^2} = \sum_{i,j,k} \int \mathrm{d}x_1 \int \mathrm{d}x_2 \int \mathrm{d}\hat{t} f_i(x_1, Q^2) f_j(x_2, Q^2) \frac{\mathrm{d}\hat{\sigma}_{ij\to kl}}{\mathrm{d}\hat{t}} \delta\left(p_\perp^2 - \frac{\hat{t}\hat{u}}{\hat{s}}\right) \tag{2.18}$$

with $\hat{s} = x_1 x_2 s$. As each interaction gives rise to two jets, the jet cross section σ_{jet} is twice as large. We will now always refer to the interaction cross section and not the jet cross section. As the hard scale we take the transverse momentum $p_\perp$ thus $Q^2 = p_\perp^2$. We must note however that some objections could be made against the use of the above equation for small values of $p_\perp$. For small $p_\perp$ values the low x region yields major contribution to the integrals. The theoretical understanding of parton distributions in this region however is difficult (BFKL, CCFM, Regge-limit behaviour, dense-packing problems etc.). In the low x region there are measurements of parton density functions from HERA ([33,34] and [35]). We must therefore face the problem that different sets of parton density functions could give different results for the phenomenolgy of interest. A further problem could be higher order corrections to the jet rates, K factors, beyond what is given by parton shower corrections. The following processes contribute to the QCD $2 \to 2$ cross section: $\mathrm{qq}' \to \mathrm{qq}'$, $\mathrm{q\bar{q}} \to \mathrm{q}'\bar{\mathrm{q}}'$, $\mathrm{q\bar{q}} \to \mathrm{gg}$, $\mathrm{qg} \to \mathrm{qg}$, $\mathrm{gg} \to \mathrm{gg}$ and $\mathrm{gg} \to \mathrm{q\bar{q}}$. The cross section itself is dominated by t-channel exchange processes.
For the $|t| \ll \hat{s}$ case where we have $p_\perp^2 = \hat{t}\hat{u}/\hat{s} \approx |\hat{t}|$ the following relation holds

$$\frac{\mathrm{d}\sigma_{\mathrm{int}}}{\mathrm{d}p_\perp^2} \approx \int\int \frac{\mathrm{d}x_1}{x_1} \frac{\mathrm{d}x_2}{x_2} F(x_1, p_\perp^2) F(x_2, p_\perp^2) \frac{\mathrm{d}\hat{\sigma}}{\mathrm{d}p_\perp^2} \tag{2.19}$$

with

$$\frac{\mathrm{d}\hat{\sigma}}{\mathrm{d}p_\perp^2} = \frac{8\pi\alpha_S(p_\perp^2)}{9p_\perp^4} \tag{2.20}$$

and

$$F(x, Q^2) = \sum_q \left(xq(x, Q^2) + x\bar{q}(x, Q^2)\right) + \frac{9}{4} xg(x, Q^2) \ . \tag{2.21}$$

We remark here that in this region the only difference between quark and gluon interactions are the color factors.

Note that for constant α_S the integrated cross section above some $p_{\perp\min}$ becomes divergent in the limit $p_\perp \to 0$:

$$\sigma_{\rm int}(p_{\perp\min}) = \int_{p_{\perp\min}}^{\sqrt{s}/2} \frac{{\rm d}\sigma}{{\rm d}p_\perp} {\rm d}p_\perp \propto \frac{1}{p^2_{\perp\min}} \ . \tag{2.22}$$

We have here neglected the x integrals. That the integral for $p_\perp \to 0$ becomes divergent should not surprise us because this is already the well known collinear divergency. But the integrated cross section can exceed the total cross section pp/p$\bar{\rm p}$ (in the parametrization of [36]) when $p_\perp$ reaches the order of a few GeV. As this is well above $\Lambda_{\rm QCD}$ this problem cannot be dismissed as the result of nonperturbative effects. In order to solve the problem we must consider the following:

1. We must take into account that the interaction cross section is an inclusive number. Events with two interactions contribute twice to $\sigma_{\rm int}$ but only once to $\sigma_{\rm tot}$. The same applies for higher multiplicities. Thus $\langle n \rangle(p_{\perp\min}) = \sigma_{\rm int}(p_{\perp\min})/\sigma_{\rm tot}$ can be identified with the average number of interactions above $p_{\perp\min}$ per event. This quantity can be well above unity.

2. The effects of energy-momentum conservation have not been included in our derivation. The problem is that the number of interactions increases faster than the average of $\hat{s}$ decreases if $p_{\perp\min}$ becomes smaller and smaller. Thus the total amount of partonic energy would become infinite. One way to solve this problem is by introducing multi-parton correlated parton distributions inside a hadron. This is not part of the standard perturbative QCD formalism and it is not implemented into eq. (2.22). Those functions reduce the $\langle n \rangle(p_{\perp\min})$ number but not strong enough to describe measurements. It leads to a picture where too little of the incoming energy remains in the small-angle beam-jet region.

3. In order to tame the rise of $\langle n \rangle(p_{\perp\min})$ it is important to take into account that hadrons are color singlet objects. A gluon with a $p_\perp$ has a correspondingly large wavelength and cannot anymore resolve individual color charges. Thus the effective coupling decreases. We note here that perturbative QCD deals with partons that are assumed to be free and not with partons inside of hadrons. Thus it cannot deal with this kind of nonperturbative screening effect. In the simplest model a sharp cut-off at some scale $p_{\perp\min}$ is introduced, while a more

smooth dampening is assumed for a complex scenario.
A naive estimate for an effective lower cut-off would be

$$p_{\perp\min} = \frac{\hbar}{r_{\mathrm{p}}} \approx \frac{0.2\,\mathrm{GeV}\cdot\mathrm{fm}}{0.7\,\mathrm{fm}} \approx 0.3\,\mathrm{GeV} \simeq \Lambda_{\mathrm{QCD}}\ . \tag{2.23}$$

The proton radius r_{p} itself must be replaced by the typical color screening distance which is not known from first principles but is assumed. In PYTHIA the default value for such a cut-off is given by[9]

$$p_{\perp\min}(s) = (1.9\,\mathrm{GeV})\left(\frac{s}{1\,\mathrm{TeV}^2}\right)^{0.08}\ . \tag{2.24}$$

In addition to the coupling also the pQCD ME diverges for small $p_\perp$, such that we obtain $\sim \frac{\alpha_S^2}{p_\perp^4}$. Instead of just introducing a step function a smooth transition is obtained by multiplying $\alpha_S^2/p_\perp^4$ with

$$\frac{\alpha_{\mathrm{S}}^2(p_{\perp 0}^2 + p_\perp^2)}{\alpha_{\mathrm{S}}^2(p_\perp^2)} \frac{p_\perp^4}{(p_{\perp 0}^2 + p_\perp^2)^2} \tag{2.25}$$

with $p_{\perp\,0}$ as a free parameter that must be tuned to data. Empirically we have $p_{\perp\min} \approx p_{\perp\min}$. Both entities are of order 2 GeV.

Simple model for multi parton interactions ("Old" model)

We follow here the description of the "old" model given in section (11.2.2) of [13]. The "old" and the "new" model (the "new" model will be discussed in the next section) are brought up here as they will be used for our jet studies in chapter (5).
Since elastic or diffractive physics are not considered, the partonic cross section $\sigma_{\mathrm{int}}(p_{\perp\min}, s)$ or $\sigma_{\mathrm{int}}(p_{\perp 0}, s)$ builds the σ_{nd} nondiffractive one. The average number of interactions per event is then given by $\langle n\rangle = \sigma_{\mathrm{int}}/\sigma_{\mathrm{nd}}$. First let us assume that all hadron collisions are equivalent, that means without impact parameter dependence, and that the parton-parton interactions take place completely independent from each other. This implies that the number of interactions per event is then distributed according to a Poisson distribution with mean $\langle n\rangle$, $\mathcal{P}_n = \langle n\rangle^n \exp(-\langle n\rangle)/n!$.
A naive approach would be to choose the actual number of interactions per event n according to the Poissonian and then to pick the $np_\perp$ values independently according to eq.(2.18). The problem with this kind of approach however is that it does not take into account correlations like energy-momentum

[9] See section (11.2.1) of [13].

conservation.
It is convenient to impose an ordering. As an ordering variable we can choose $p_\perp$ or $x_\perp = 2p_\perp/E_{\rm cm}$. The scatterings are then arranged in a falling sequence of the $p_\perp$ values. In this picture the 'first' scattering is the hardest one while the subsequent ones (the 'second' one, the 'third' one, etc.) are successively softer. This kind of ordering however must not be confused with a time-ordering. In a simplified picture where the incoming hadrons are due to Lorentz contraction like flat pancakes, the different interactions have the tendency to be causally separated. Averaging over all configurations of soft partons yields the standard QCD phenomenology of a hard scattering together with parton density functions.
For the use in a Monte Carlo event generator let us consider the following function

$$f(x_\perp) = \frac{1}{\sigma_{\rm nd}(s)} \frac{{\rm d}\sigma}{{\rm d}x_\perp} \ . \tag{2.26}$$

${\rm d}\sigma/{\rm d}x_\perp$ is here corresponding to eq.(2.18). The function $f(x_\perp)$ can be considered as the probability for a parton-parton interaction at $x_\perp$ for the case that the collision of the two hadrons is nondiffractive and inelastic.
The probability distribution for the hardest interaction is

$$f(x_\perp) \exp\left\{ -\int_{x_{\perp 1}}^1 f(x'_\perp){\rm d}x'_\perp \right\} \tag{2.27}$$

with $x_{\perp 1}$ being the $x_\perp$ of the hardest interaction. This is the probability to have a scattering at $x_{\perp 1}$ multiplied by the probability that no scattering above $x_{\perp 1}$ has occurred. This corresponds to the Sudakov form factor which we have used for parton showers in Monte Carlo generators. The probability to have an ith scattering at a $x_{\perp i} < x_{\perp i-1} \cdots < x_{\perp 1} < 1$ sequence is given by

$$f(x_{\perp i}) \frac{1}{(i-1)!} \left(\int_{x_{\perp i}}^1 f(x'_\perp){\rm d}x'_\perp \right)^{i-1} \exp\left\{ -\int_{x_{\perp i}}^1 f(x'_\perp){\rm d}x'_\perp \right\} . \tag{2.28}$$

We see that according to this expression the total probability that a scattering happens at $x_{\perp i}$ (independently whether it is the first, the second and so on) is given by $f(x_{\perp i})$.

The ordinary parton distributions are used for the hard scattering. This scattering takes energy from the system away. Thus for the subsequent scatterings we must also take into account the energies and flavors of the

preceeding interactions. In practice the parton distributions are not evaluated at x_i (the x value for the i-th scattering) but at a rescaled value

$$x_i' = \frac{x_i}{1 - \sum_{j=1}^{i-1} x_j} \ . \tag{2.29}$$

This modification prevents that more energy is taken by the individual scatterings than available from the incoming hadrons.
Some events do not include scatterings above $x_{\perp\min}$ at all. Here we reach the domain of nonperturbative physics which is not treated here.
For a hard interaction the situation can become quite complex especially when we have to deal with several hard scatterings and as the number of possible color configurations increases. What makes the situation even worse is that we must extend the standard string fragmentation description in order to deal with events where we have two or more valence quarks being kicked out of an incoming hadron by seperate interactions.
Some simplifications are necessary. For the first interaction (the hardest one) full freedom for the choice of flavor and color topology is assumed while for the subsequent interactions we have only three possibilities in the model:

- Processes of the type $gg \to gg$ where the two gluons are in a color-singlet state. A double string is stretched between the two gluons that are decoupled from the rest of the system.

- Processes of the type $gg \to gg$ where each of the two gluons are connected to one of the strings already present. There are several possibilities for connecting the colors of the gluons. The one which minimizes the total increase in string length is chosen. This is in contrast to the previous situation where we have a maximization (within reason) of the string length.

- Processes of the type $gg \to q\bar{q}$ where the final pair is required to be in a color-singlet state. Thus a single string is stretched between the outgoing q and $\bar{q}$.

Originally it was presumed that the probabilities of the three possibilities are equal. Comparison with measurements however suggests that the minimal string length topology dominates.
Initial- or final state showers can change the nature of a $gg \to gg$ or $q\bar{q}$ scattering as it could turn into a qg-process. Thus radiation is only included for the hardest interaction. The treatment of beam remnants is a bit modified if we have multiple interactions. After the generation of the hard scattering (together with its associated initial- nad final state radiation) additional

multiple interactions are generated. Only then are beam remnants attached to the initiator partons of the hardest interaction. For the treatment of beam remnants see section (11.1) of [13].

Complex model for multiparton interactions ("new" model)

In the "old" model we considered initial and final state radiation only for the hardest interaction. The reason for this was the inability to treat junction string topologies. Thus a simplification was needed. It can be argued that the subsequent interactions have the tendency to be soft with rather low transverse momentum near $p_{\perp\min}$ or $p_{\perp 0}$ and are therefore not associated with additional hard interaction. However it still remains a simplification.
The "new" model (see for that section (11.4) of [13]) uses transverse momentum ordered showers. The transverse momentum $p_\perp$ is therefore the evolution variable both for multiple interactions and for parton showers although the definition of it is slightly different in the two cases.
Regarding the parton showers it should be possible to apply final state radiation only after the simulation of initial state radiation (ISR) and multiple interactions. This is supposed to be a good approximation because FSR does not change the total energy of the system. Instead it only redistributes the energy among more partons. In contrast to that a further ISR or a further interaction takes energy from the beam particles.
It is required that multi parton interactions are ordered according to a sequence of falling $p_\perp$ values. The ISR emissions are incorporated into the $p_\perp$ sequence. This means that a hard interaction is generated before an ISR emission of the hardest interaction. This can be done as $p_\perp$ is now the common evolution variable.
We note here that the choice of $p_\perp$ as an evolution variable is a generalization of backward evolution: we consider a configuration at a given $p_\perp$ and then deal with the kind of configuration with lower $p_\perp$ it could have come.
A further point is that the new model does not have the limitations regarding string configuration as the old model.

Chapter 3

Parton shower formalism

3.1 Introduction

In this chapter we present a new analytical formalism developed in [1] that describes parton showers. This formalism will be the basis for the calculation in chapter (4) where the distribution of the energy fraction[1] τ in Drell Yan processes is derived. The exact definition of this observable can be found in the beginning of chapter (4).
Parton showers are usually dealt within a Monte Carlo event generator. The basic principles how a parton shower is generated inside a Monte Carlo event generator can be found in section (2.2.1): thus in a conventional Monte Carlo generator the physical events are modeled as processes in classical statistical mechanics. Here we have a set of partons that have been produced in the hard scattering. Then it is possible for each parton to split into two partons with a probability determined from theory. This process continues until a complete "parton shower" has been formed.
The splitting probability becomes biggest if the two daughter partons are collinear or soft ($p = 0$) or both. In this case they must be also almost massless.
In the soft and in the collinear case the amplitude for $m+1$ partons factorizes into a splitting function and the matrix element for m partons.
Usually also the following approximations are used:

1. It is possible that a soft gluon can be emitted from one hard parton or from another. These two diagrams interfere. This interference is approximated with the "angular ordering" approximation.

[1] For its definition see eq.(4.32).

2. Colors are simplified. This approximation is valid if $1/N_c^2 \to 0$. Here, however, $N_c = 3$ is the number of colors.

3. The angular distribution of the daughter partons after splitting is dependent on the mother parton spin and also on the interference between different mother parton spins. This is usually neglected.

The purpose of the parton shower formalism formulated in [1] was to construct a parton shower formalism where these approximations are not made. This leads to a formulation where quantum statistical states instead of classical statistical states are used. With the application of the soft/collinear approximation the treatment becomes rather simple. The formulation works with a density operator in color $\otimes$ spin space.
In the next sections we give an overview of the formalism and its construction. The details are given in [1]. For the momentum mapping[2] we apply the formalism of [37]. The rest of this chapter is organised as follows:

1. In section (3.2) we introduce the concept of parton density states. These span a vector space in parallel to ordinary quantum states. Formally they have the same structure as density operators known from statistical physics.

2. In section (3.3) we introduce the concept of shower evolution. This is in direct analogy to shower evolution in a Monte Carlo event generator (see chapter (2) and section (2.2)). Thus we compile an evolution equation for the density state ρ. This is dependent on the shower time t (that must not be confused with real physical time but is a running parameter which will be later connected to kinematical parameters).

3. In section (3.4) we introduce the concept of parton mapping.

4. In section (3.5) we deal with parton splitting on the level of quantum amplitudes. There we show for one example how the splitting amplitudes are derived[3]. In section (3.5.3) these results are used to derive the splitting operator. With that we are in a position to construct the evolution equation that will be used in chapter (4).

[2] What momentum mapping is and what is its purpose see section (3.4).
[3] For further derivations see [1].

3.2 The parton shower formalism

We describe a parton shower formalism following the description of [1]. We start with a proper notation. This notation will be used for the description of a quantum state with two initial state partons and m final state partons. All partons shall have an index. The indices "a" and "b" denote initial state partons, $1, \ldots, m$ denote final state partons. For each parton we have a momentum p, a spin index s and a color index c. Further each parton has a flavor $f \in \{\mathrm{g},\mathrm{u},\bar{\mathrm{u}},\mathrm{d},\bar{\mathrm{d}},\ldots\}$. The quantum numbers of such a state are described by

$$\{p,f,s,c\}_m \equiv \{\eta_a,a,s_a,c_a;\eta_b,b,s_b,c_b;p_1,f_1,s_1,c_1;\ldots;p_m,f_m,s_m,c_m\} \ . \tag{3.1}$$

The momentum fractions of the incoming partons are η_a and η_b. We assume the incoming hadrons are massless. Thus we may write

$$\begin{aligned} p_A^2 &= 0 \ , \\ p_B^2 &= 0 \ , \\ 2p_A \cdot p_B &= s \ . \end{aligned} \tag{3.2}$$

We assume the initial state partons to be on-shell. They have no transverse momentum. In [1] their momenta are written as

$$\begin{aligned} p_a &= \eta_a p_A + \frac{m^2(f_a)}{\eta_a s} p_B \ , \\ p_b &= \eta_b p_B + \frac{m^2(f_b)}{\eta_b s} p_A \ , \end{aligned} \tag{3.3}$$

where the masses of the partons were taken into account. In our notation the flavor of parton "a" is simply a, and the flavor of parton "b" is simply b. This notation will also be used for the parton distribution functions: $f_{a/A}(\eta_a,\mu_F^2)$ and $f_{b/B}(\eta_b,\mu_F^2)$. For the flavors of antiquarks we write $-\mathrm{u} = \bar{\mathrm{u}}, -\bar{\mathrm{u}} = \mathrm{u}, -\mathrm{g} = \mathrm{g}$. In [37] it was assumed that all partons are massless:

$$\begin{aligned} p_a &= \eta_a p_A \ , \\ p_b &= \eta_b p_B \ . \end{aligned} \tag{3.4}$$

As we shall use the results of [37] in chapter (4) (where we will derive the energy fraction[4] in Drell Yan processes with the formalism discussed here)

[4]The definition of the energy fraction is found there.

we will from now on assume that all partons are massless.
For a matrix element we can write

$$M(\{p,f\})^{c_a,c_b,c_1,\ldots,c_m}_{s_a,s_b,s_1,\ldots,s_m} \ . \tag{3.5}$$

M is here supposed to be a function of the parton momenta $\{p,f\}_m$, the colors $c_a, c_b, c_1 \ldots, c_m$ and the parton spins $s_a, s_b, s_1, \ldots, s_m$.
M can be seen as a vector in color-spin space

$$|M(\{p,f\}_m)\rangle \ . \tag{3.6}$$

In the color-spin space we can define a scalar product

$$\langle M'|M\rangle \ . \tag{3.7}$$

This is given by multiplying an element M of $|M(\{p,f\}_m)\rangle$ with M'^* and then summing over the spins and colors.
We can view an observable F as a set of functions $F(\{p,f\}_m)$ which act as linear operators on the color-spin space. For the cross section of an observable F we can write

$$\begin{aligned}\sigma[F] = \sum_m \frac{1}{m!}\int [d\{p,f\}_m] \frac{f_a/A(\eta_a,\mu_F^2) f_{b/B}(\eta_b,\mu_F^2)}{4n_c(a)n_c(b)2\eta_a\eta_b p_A\cdot p_B} \\ \times\langle M(\{p,f\}_m)|F(\{p,f\}_m)|M(\{p,f\}_m)\rangle \ .\end{aligned} \tag{3.8}$$

The integration over momenta is defined as

$$\begin{aligned}\int [d\{p,f\}_m] g(\{p,f\}_m) = \prod_{i=1}^m \left\{ \sum_{f_i} \int \frac{d^4p_i}{(2\pi)^4} 2\pi\delta_+(p_i^2 - m^2(f_i))\right\} \\ \times \sum_a \int_0^1 d\eta_a \sum_b \int_0^1 d\eta_b (2\pi)^4 \delta\left(p_a + p_b - \sum_{i=1}^m p_i\right)\theta(m_H^2 < \eta_a\eta_b s) g(\{p,f\}) \ .\end{aligned} \tag{3.9}$$

Here $g(\{p,f\}_m)$ is an arbitrary test function.
$f_{a/A}$ and $f_{b/B}$ are the parton distribution functions, $n_c(a)$ stands for the number of colors a parton of flavor a can have, $N_c = 3$ for quarks and $N_c = 8$ for gluons. By the factor $4n_c(a)n_c(b)$ the sum over spins and colors for initial state partons is changed into an average over spins and colors. m_H stands here for the mass[5] of the heaviest quark involved in the interaction.

[5] In [1] it was assumed that quarks have masses.

As we make here the simplification only to deal with massless partons we can remove the θ function inside the phase space element. We note that the distribution δ_+ is defined by

$$\delta_+(p^2) = \theta(E > 0)\delta(p^2) \ , \tag{3.10}$$

so that the energy is only positively defined.
We give for every final state parton a label $i \in \{1, \ldots, m\}$. We denote the label of momentum, flavor, spin and color of particle i by $\{p_i, f_i, s_i, c_i\}$. Now we introduce the density operator in color $\otimes$ spin space as

$$\rho(\{p,f\}_m) = |M(\{p,f\}_m)\rangle \frac{f_a/A(\eta_a, \mu_F^2) f_{b/B}(\eta_b, \mu_F^2)}{4n_c(a)n_c(b)2\eta_a\eta_b p_A \cdot p_B} \langle M(\{p,f\}_m)| \ . \tag{3.11}$$

With that we can write for the cross section

$$\sigma[F] = \sum_m \frac{1}{m!} \int [d\{p,m\}] \mathrm{Tr}\{\rho(\{p,f\}_m) F(\{p,f\}_m)\} \ . \tag{3.12}$$

The density operator ρ can be written in color $\otimes$ spin space as

$$\rho(\{p,f\}_m) = \sum_{s,c} \sum_{s',c'} |\{s,c\}_m\rangle \rho(\{p,f,s',c',s,c\}_m) \langle \{s',c'\}_m| \ . \tag{3.13}$$

The function $\rho(\{p,f,s',c',s,c\}_m)$ depends on the momenta and flavors of the m partons $\{p,f\}_m$ and on the labels $\{s,c\}_m$ for the "ket" quantum state and the labels $\{s',c'\}_m$ for the conjugate "bra" state. The state labels are written as $\{p,f,s',c',s,c\}_m$. We can therefore view the entities $\rho(\{p,f,s',c',s,c\}_m)$ as matrix elements of the density operator. We choose an orthonormal basis for the spin space

$$\langle \{s'\}_m | \{s\}_m \rangle = \delta_{\{s\}_m}^{\{s'\}_m} \ . \tag{3.14}$$

However we do not assume that the basic color states are orthogonal for reasons that shall become later clear[6]. $\langle \{c\}_m | \{c\}_m \rangle$ is only approximately one. $\langle \{c'\}_m | \{c\}_m \rangle$ in general is not zero for $\{c\}_m \neq \{c'\}_m$.
We can expand a vector $|\psi\rangle$ by

$$|\psi\rangle = \sum_{\{c\}_m} |\{c\}_m\rangle a(\{c\}_m) \ . \tag{3.15}$$

And now we define a dual basis by

$${}_D\langle \{c'\} | \{c\}_m \rangle = \delta_{\{c\}_m}^{\{c'\}_m} \ . \tag{3.16}$$

[6]See for that section (3.5.2).

Thus we can obtain the expansion coefficients $a(\{c\}_m)$ by

$$ {}_D\langle\{c\}_m|\psi\rangle = a(\{c\}_m) \ . \tag{3.17}$$

With a dual basis we can also formulate a completeness relation

$$ 1 = \sum_{\{c\}_m} |\{c\}_m\rangle \ {}_D\langle\{c\}_m| \ , \tag{3.18}$$

and

$$ 1 = \sum_{\{c\}_m} |\{c\}_m\rangle_D \ \langle\{c\}_m| \ . \tag{3.19}$$

Please note the difference between eq.(3.18) and eq.(3.19): in eq.(3.18) the bravector has the label D while in eq.(3.19) the ketvector has the label D. These two completeness relations are a convenient tool for dealing with linear operators.
Let us call such a linear operator O. Consider the expansion coefficients $a'(\{c'\}_m)$ of the state $|\psi'\rangle = O|\psi\rangle$. They are given by

$$ a'(\{c'\}_m) = \sum_{\{c\}_m} o(\{c'\}_m, \{c\}_m) a(\{c\}_m) \ , \tag{3.20}$$

where $o(\{c'\}_m, \{c\}_m)$ are the matrix elements of O with respect to the basis $|\{c\}_m\rangle$. With the help of the dual basis ${}_D\langle\{c'\}_m|$ we may write

$$ o(\{c'\}_m, \{c\}_m) = {}_D\langle\{c'\}_m|O|\{c\}_m\rangle \ . \tag{3.21}$$

Statistical states

The density operators ρ form a vector space just as the quantum states $|\psi\rangle$. We call a statistical state $|\rho)$. We can also define a dual space where we have basis vectors $(\{p, f, s', c', s, c\}_m|$. With that we may write

$$ \rho(\{p, f, s', c', s, c\}_m) = (\{p, f, s', c', s, c\}_m|\rho) \ . \tag{3.22}$$

There is further a completeness relation

$$ 1 = \sum_m \frac{1}{m!} \int [d\{p, f, s', c', s, c\}_m] |\{p, f, s', c', s, c\}_m)(\{p, f, s', c', s, c\}_m| \ . \tag{3.23}$$

The integration measure $[d\{p,f,s',c',s,c\}_m]$ is a generalization of the integration measure given in eq.(3.9)

$$\int [d\{p,f,s',c',s,c\}_m] = \int [d\{p,f\}_m] \sum_{s_a,s'_a,c_a,c'_a} \sum_{s_b,s'_b,c_b,c'_b} \prod_{i=1}^{m} \Big\{ \sum_{s_i,s'_i,c_i,c'_i} \Big\} \, . \tag{3.24}$$

The inner product of basic states is given by

$$\begin{aligned} &(\{p,f,s',c',s,c\}_m | \{\tilde{p},\tilde{f},\tilde{s}',\tilde{c}',\tilde{s},\tilde{c}\}_{\tilde{m}}) = \\ &\delta_{m,\tilde{m}} \delta(\{p,f,s',c',s,c\}_m; \{\tilde{p},\tilde{f},\tilde{s}',\tilde{c}',\tilde{s},\tilde{c}\}_m) \, . \end{aligned} \tag{3.25}$$

The function δ is an extension of the ordinary δ-function and defined in the following way:

$$\begin{aligned} &\frac{1}{m!} \int [d\{p,f,s',c',s,c\}_m] \delta(\{p,f,s',c',s,c\}_m; \tilde{p},\tilde{f},\tilde{s}',\tilde{c}',\tilde{s},\tilde{c}\}_m) \\ &\times h(\{p,f,s',c',s,c\}_m) = h(\tilde{p},\tilde{f},\tilde{s}',\tilde{c}',\tilde{s},\tilde{c}\}_m) \, , \end{aligned} \tag{3.26}$$

with h as an ordinary test function.
Let us consider a covector $(F|$ which corresponds to an observable F so that the following relation holds

$$(F|\{p,f,s',c',s,c\}_m) = \langle \{s',c'\}_m | F(\{p,f\}_m) | \{s,c\}_m \rangle \, . \tag{3.27}$$

With that we obtain

$$\sigma[F] = (F|\rho) \, . \tag{3.28}$$

Here we used the completeness relation (3.23), the formula for the cross section given in eq.(3.12), eq.(3.22) and eq.(3.13).
If F is an operator proportional to the unit operator we may write

$$\begin{aligned} (F|\rho) = \sum_m \frac{1}{m!} \int [d\{p,f,s',c',s,c\}_m] F(\{p,f\}_m) \langle \{s'\}_m | \{s\}_m \rangle \langle \{c'\}_m | \{c\}_m \rangle \\ \times \rho(\{p,f,s',c',s,c\}_m) \, . \end{aligned} \tag{3.29}$$

3.3 Parton evolution

In the previous sections we have introduced the concept of a density state operator ρ. It is supposed to describe a parton shower[7]. From now on we

[7]For what a parton shower is see also chapter (1), section (3.1) and section (2.2).

call ρ a parton shower state. This parton shower state evolves with the parton shower time t. Please note that t is not a physical time, it is a running parameter on which ρ is dependent. In section (3.5.4) it will be discussed how t is connected to the kinematical parameters of the system, for example virtuality[8]. Then increasing t can mean decreasing virtuality. We start with the value $t = 0$. Here we have no parton shower at all what means that we start with the hard interaction. Then t increases towards a final value t_{f} at which the application of shower evolution is no longer meaningful. Please note that also initial state evolution can only occur for $t > 0$. Thus we have here again the backward evolution principle we discussed in section (2.2.1).

In this context it is important to consider the issue of a *resolution scale*. As already mentioned in chapter (1) a parton shower is only well defined with respect to a resolution scale: else it is not meaningful to distinguish between resolvable and nonresolvable branching. This is however essential for the definition of the two splitting operators $\mathcal{H}$ and $\mathcal{V}$ which are later given in eq.(3.35) and eq.(3.36) and will be defined there.
Let us call the scale of the hard interaction Q_0^2. Then the resolution scale μ^2 must be always smaller or equal to Q_0^2. Interactions whose scales are bigger than μ^2 are resolvable. They are included in the $|M\rangle\langle M|$ part of the density operator ρ. Interactions whose scales are smaller than μ^2 (nonresolvable branchings) are either included into the parton density functions[9] (if they are initial state) or are simply integrated out if they belong to the final state. In order to guarantee that the parton density functions in eq.(3.11) include all branchings below the resolution scale μ^2 we demand $\mu_F^2 = \mu^2$ where μ_F^2 is the factorization scale of the parton density functions.
The resolution scale μ^2 starts from the scale of the hard interaction Q_0^2 and becomes lower down to a cut-off value[10]. The lower μ^2 is set the more parton branching we see. This is in the reverse order of the shower t which starts from the hard interaction at value 0 and increases to some cut-off value t_{f}. It is therefore meaningful to assume the following relation

$$\mu^2 = Q_0^2 e^{-t} \ . \tag{3.30}$$

Further also the issue of *infrared safety* of an observable F ought to be mentioned. A physical observable can be represented by a set of functions

[8] Another possibility would be transverse momentum.
[9] That is the functions given in eq.(3.11).
[10] It is not meaningful to go down directly to zero as we would see then an infinite number of partons.

$F(\{p,f\}_m)$ which are invariant under label interchange. Strictly speaking it is called infrared safe if $F(\{p,f\}_{m+1}) \to F(\{p,f\}_m)$ for the case that parton $m+1$ becomes soft or collinear with parton l. This definition refers to any scale.
A broader notion of infrared safety can be given by considering infrared safety with reference to a scale μ^2. This means that

$$F(\{\hat{p},\hat{f}\}_{m+1}) \approx F(\{p,f\}_m) \tag{3.31}$$

holds[11] for $|2\hat{p}_{m+1}\cdot\hat{p}_l| < \mu^2$. So $(F|\rho)$ does not change for $\mu^2 \to \mu^2 + \delta\mu^2$ which is equal or larger than μ^2. $(F|\rho)$ can however in this case change for scales which are smaller than μ^2.

Now we formulate the axioms for shower evolution. In the next sections we will relate the operators which appear in the evolution equation to the Feynman rules at tree level QCD. For the evolution equation we assume a linear operator $\mathcal{U}$ so[12] that we have

$$|\rho(t)) = \mathcal{U}(t,t')|\rho(t')\ . \tag{3.32}$$

In order to have consistency we demand

$$\mathcal{U}(t,t) = 1\ . \tag{3.33}$$

Further we must require that the $\mathcal{U}$ operators fullfill the group compository rule

$$\mathcal{U}(t_3,t_2)\mathcal{U}(t_2,t_1) = \mathcal{U}(t_3,t_1)\ . \tag{3.34}$$

We demand

$$\frac{d}{dt}\mathcal{U}(t,t') = [\mathcal{H}(t) - \mathcal{V}(t)]\mathcal{U}(t,t')\ . \tag{3.35}$$

The operator $\mathcal{H}(t)$ describes real splitting (the number of partons and their momenta are changed) while $\mathcal{V}(t)$ describes virtual splitting (virtual graphs and unresolved graphs). It does not change the spin, number and momenta of the partons but it can change their colors. Thus the evolution equation can be also written as

$$\frac{d}{dt}|\rho(t)) = [\mathcal{H}(t) - \mathcal{V}(t)]|\rho(t))\ . \tag{3.36}$$

[11] Up to now there is no exact condition formulated how precise the approximation has to be.

[12] Note that this formalism is not intended for dealing with saturation effects.

In lowest order, $\mathcal{H}(t)$ describes the change from a state with m partons to a state with $m+1$ partons. $\mathcal{H}(t)$ is specified by its matrix elements

$$(\{\hat{p},\hat{f},\hat{s}',\hat{c}',\hat{s},\hat{c}\}_{m'}|\mathcal{H}(t)|\{p,f,s',c',s,c\}_m) \ . \tag{3.37}$$

In the following sections we will derive these matrix elements from the Feynman rules at tree level QCD.
We can construct the virtual splitting operator $\mathcal{V}(t)$ from the real splitting operator $\mathcal{H}$. Here we must take into account that the showering itself is independent from the hard process. This means that the total cross section is not changed during shower evolution. We note here however that this statement is only true for processes like $e^+ + e^- \rightarrow hadrons$. For the case of hadron-hadron collisions the total cross section does not have a well defined perturbative expansion. If $|\rho(0)\big)$ is however "hard" in the sense that $(\{p,f,s^{'},c^{'},s,c\}_m|\rho(0)\big) \neq 0$ holds only for configurations with a large transverse momentum we can postulate that the contribution from $|\rho(t)\big)$ to the total cross section does not change.
The observable that measures everything (that is the total cross section) is

$$F_1(\{p,f\}_m) = 1 \ . \tag{3.38}$$

The density state that corrsponds to $F_1(\{p,f\}_m)$ should be $(1|$. This means that we have

$$\sigma_{total} = (1|\rho) \ . \tag{3.39}$$

At this point it is important to note that the unit vector $(1|$ satisfies the following condition

$$(1|\{p,f,s',c',s,c\}_m) = \langle\{s'\}_m|\{s\}_m\rangle\langle\{c'\}_m|\{c\}_m\rangle \ , \tag{3.40}$$

which we obtain from equation (3.27). As shower evolution does not change the total cross section, the following relation holds

$$(1|\mathcal{U}(t^{'},t)|\rho) = (1|\rho) \ . \tag{3.41}$$

Thus we obtain:

$$\begin{aligned} \frac{d}{dt}\sigma_{total} &= 0 \\ &= (1|\mathcal{H}(t) - \mathcal{V}(t)|\rho(t)) \ . \end{aligned} \tag{3.42}$$

So the following relation holds

$$0 = (1|[\mathcal{H}(t) - \mathcal{V}(t)] \ , \tag{3.43}$$

which results in:

$$(1|\mathcal{V}(t)|\{p,f,s',c',s,c\}_m) = (1|\mathcal{H}(t)|\{p,f,s',c',s,c\}_m) \ . \tag{3.44}$$

3.4 Momentum and flavor mapping

For the description of collision processes the first choice are matrix elements. In contrast to the incoming and outcoming partons the partons in the intermediate state are described by propagators and are therefore not on mass shell. In a matrix element the in- and outcoming partons are well defined. In contrast to that, the parton shower approach is an iterative process. It is a priori not clear when to stop. For simplicity we want to keep therefore the partons on mass shell. In order to preserve momentum conservation we need therefore a momentum mapping $\{p\}_m \leftrightarrow \{\hat{p}\}_{m+1}$ where the momenta of all or at least some of the partons before and after the splitting are related to each other. There are different possible ways to define a momentum mapping. One of them is the method of Catani and Seymour [38]. It is an example of local mapping where only three partons are involved: $(p_l, p_k) \leftrightarrow (\hat{p}_l, \hat{p}_{m+1}, \hat{p}_k)$. Parton k is thereby a spectator parton which is color connected to parton l. The momenta of the other partons remain unchanged[13].
On the other hand in the case of a global mapping the momenta of all partons are changed. This was the case in [1] and [37]. As we will use in chapter (4) the results of [37] we introduce the momentum mapping that was presented there. First of all we consider initial state splitting. Consider parton a with momentum p_a that splits in backward evolution into parton $m+1$ with momentum $\hat{p}_{m+1}$ and a parton with momentum $\hat{p}_a$. The momentum of parton b remains unchanged. Then we define the following momentum mapping with splitting variables (y, z, ϕ)[14]

$$\begin{aligned} \hat{p}_{m+1} &= \frac{1-z}{z}(1+y)p_a + z\frac{y}{1+y}p_b + k_\perp \ , \\ \hat{p}_a &= \frac{1+y}{z}p_a \ , \\ \hat{p}_b &= p_b \ . \end{aligned} \tag{3.45}$$

Here is $k_\perp$ a space-like vector which is the part of $\hat{p}_{m+1}$ that is orthogonal to both p_a and p_b.
According to eq.(3.45) we have

$$y = \frac{2\hat{p}_{m+1} \cdot \hat{p}_a}{2p_a \cdot p_b} \tag{3.46}$$

[13] Please note that there is an exception to this rule in the case of inital state splitting.
[14] Regarding initial state splitting: in [37] in section (4.4) the momentum mapping was only defined by the momenta themselves and not by splitting variables.

and

$$\frac{\hat{p}_{m+1} \cdot p_b}{\hat{p}_a \cdot p_b} = 1 - z \ . \tag{3.47}$$

The fraction variable z is in the range $0 < z < 1$. For the momentum fractions of the two partons we have

$$\begin{aligned} \hat{\eta}_a &= \frac{1+y}{z}\eta_a \ , \\ \hat{\eta}_b &= \eta_b \ . \end{aligned} \tag{3.48}$$

As we discussed in the previous section the density state ρ of the system is dependent on the shower time t. We choose as in [37] the following relation

$$t = \log\left(\frac{Q^2}{2\hat{p}_{m+1} \cdot \hat{p}_a}\right) \ . \tag{3.49}$$

Here can be, for example, $\sqrt{Q^2}$ the mass of the Z-boson in a Drell Yan process. Both t and y can be seen as virtuality variables. We have the following relation

$$y = \frac{Q^2}{2p_a \cdot p_b} e^{-t} \ . \tag{3.50}$$

As the emitted parton $m+1$ is supposed to be lightlike we can derive the following relation for

$$\begin{aligned} 0 &= \hat{p}_{m+1}^2 \\ &= (1-z)y2p_a \cdot p_b - \mathbf{k}_\perp^2 \\ &= (1-z)Q^2 e^{-t} - \mathbf{k}_\perp^2 \ . \end{aligned} \tag{3.51}$$

So we get

$$\mathbf{k}_\perp^2 = (1-z)Q^2 e^{-t} \ . \tag{3.52}$$

We note here that in the case that we have $y \neq 0$ the momentum difference $\hat{p}_a - \hat{p}_{m+1}$ is not exactly p_a. We therefore must face the problem of momentum conservation. The problem is solved by taking some momentum from the final state partons at the time of the splitting. This means that each parton j with momentum $p_j, j \in \{1, 2, \ldots, m\}$ has after the splitting a new momentum $\hat{p}_j$. This also applies to the Z-boson as an example. The momenta $\hat{p}_j$ after splitting are related to the ones before the splitting by a Lorentz transformation $\hat{p}_j = \Lambda p_j$. Hence the following relation holds

$$\hat{p}_\mathrm{a} + \hat{p}_\mathrm{b} - \hat{p}_{m+1} = \Lambda(p_\mathrm{a} + p_\mathrm{b}) \ . \tag{3.53}$$

There are different choices for a Lorentz transformation possible.
It must be mentioned that in contrast to the $\hat{p}_j$ we have

$$\begin{aligned} \hat{p}_a &\neq \Lambda p_a \ , \\ \hat{p}_b &\neq \Lambda p_b \ . \end{aligned} \tag{3.54}$$

Further we remark that in the case of final state splitting the daughter partons are also put on mass shell. In [1] it was chosen to let the momenta of the inital state partons unchanged while the momenta of the spectator final state partons are changed by a Lorentz transfortmation, too.

The next point we must face is flavor mapping. First of all we consider final state splitting. The parton that splits is denoted as parton l. Thus we write

$$\hat{f}_j = f_j \ , \qquad j \notin \{l, m+1\} \ . \tag{3.55}$$

The flavor of the two partons l and $m+1$ is given by the value of the variable $\zeta_{\mathrm{f}} = (\hat{f}_l, \hat{f}_{m+1})$. The different possible values that ζ_{f} can take, span a set $\Phi(f_l)$ which is dependent on the mother parton's flavor. For parton l being a quark or an antiquark the only possible way of splitting is the radiation of a gluon. As we have freedom to assign labels we choose to label the remaining quark or antiquark after the splitting as parton l and the emitted gluon as parton $m+1$. Then the set $\Phi_l(f_l)$ can have only one element

$$\Phi(f_l) = \{(f_l, \mathrm{g})\} \ , \qquad f_l \neq \mathrm{g} \ . \tag{3.56}$$

A bit different is the case when parton l is a gluon. Then ζ_{f} is a pair of gluons or a quark-antiquark pair $(q, \bar{q})$ of any flavor

$$\Phi_l(\mathrm{g}) = \{(\mathrm{g}, \mathrm{g}), (\mathrm{u}, \bar{\mathrm{u}}), (\mathrm{d}, \bar{\mathrm{d}}), \dots\} \ . \tag{3.57}$$

For $\mathrm{g} \to q + \bar{q}$ we have again the freedom to assign labels. We call the daughter quark parton l and the daughter antiquark parton $m+1$.
We have now discussed the flavor mapping in final state splitting. Let us turn to initial state splitting. The flavors of the two incoming partons which are involved in the hard interactions are before and after the splitting called $f_{\mathrm{a}}, \hat{f}_{\mathrm{a}}, f_{\mathrm{b}}$ and $\hat{f}_{\mathrm{b}}$. With the exception of those partons that have the label "a" or $m+1$ the flavors are not changed

$$\hat{f}_j = f_j \ , \qquad j \notin \{\mathrm{a}, m+1\} \ . \tag{3.58}$$

We call the splitting variable $\zeta_{\mathrm{f}} = (\hat{f}_{\mathrm{a}}, \hat{f}_{m+1})$. The set of the splitting variables is named $\Phi_{\mathrm{a}}(f_{\mathrm{a}})$. It is dependent on the flavor of the mother parton.

The set has only two elements for parton "a" being a quark or an antiquark

$$\Phi_{\mathrm{a}}(f_{\mathrm{a}}) = \{(f_{\mathrm{a}}, \mathrm{g}), (\mathrm{g}, f_{\mathrm{a}})\} \ , \qquad f_{\mathrm{a}} \neq \mathrm{g} \ . \tag{3.59}$$

We have these two possibilities because both the gluon or the quark/antiquark can go into the hard interaction. The parton that does not participate in the hard interaction and therefore goes directly to the final state partons is called $m+1$. For the case that parton "a" is a gluon, ζ_{f} can be a pair of gluons or a quark-antiquark of any flavor $(q, \bar{q})$ or $(\bar{q}, q)$ (as far as momentum conservation allows it)

$$\Phi_{\mathrm{a}}(\mathrm{g}) = \{(\mathrm{g}, \mathrm{g}), (\mathrm{u}, \bar{\mathrm{u}}), (\bar{\mathrm{u}}, \mathrm{u}), (\mathrm{d}, \bar{\mathrm{d}}), (\bar{\mathrm{d}}, \mathrm{d}), \dots\} \ . \tag{3.60}$$

We have here several possibilities as a gluon, a u-quark or a $\bar{\mathrm{d}}$-quark etc. can participate in the hard interaction. Again the parton that goes directly to the final state is labeled $m+1$. The mapping of momenta and flavors is symbolically written as

$$\{\hat{p}, \hat{f}\}_{m+1} = R_l(\{p, f\}_m, \{\zeta_{\mathrm{p}}, \zeta_{\mathrm{f}}\}). \tag{3.61}$$

We mention here that the transformation has an inverse. For a more detailed discussion see [1] and [37].

3.5 Splitting for the statistical states

Here it is our goal to derive an expression for the operator $\mathcal{H}$. According to equation (3.43) we can then derive an expression for the virtual splitting operator $\mathcal{V}$. In order to derive an expression for $\mathcal{H}$ we use the Feynman rules for the corresponding matrix element. Before we consider the density state operator ρ we must investigate the quantum scattering amplitude $|M(\{p, f\})\rangle$. It belongs to color $\otimes$ spin space. Thus we can write it as

$$|M(\{p, f\}_m)\rangle = \sum_{\{c\}_m} |\{c\}_m\rangle \sum_{\{s\}_m} |\{s\}_m\rangle M(\{p, f, s, c\}_m) \ . \tag{3.62}$$

Please note that the color vectors are not orthogonal to each other in contrast to the spin vectors. Here the following relation holds

$$\langle\{s'\}_m|\{s\}_m\rangle = \delta_{m',m}\delta_{\{s'\}_m,\{s\}_m} \ . \tag{3.63}$$

Let us consider now the QCD scattering amplitude $|M(\{\hat{p}, \hat{f}\}_{m+1})\rangle$. Further the splitting operators $t_l^\dagger$ (which acts on the color part) and $V_l^\dagger$ (which acts on the spin part) are introduced. Thus the following relation holds

$$|M_l(\{\hat{p}, \hat{f}\}_{m+1})\rangle = t_l^\dagger(f_l \to \hat{f}_l + \hat{f}_{m+1}) V_l^\dagger(\{\hat{p}, \hat{f}\}_{m+1}) |M(\{p, f\}_m)\rangle \ . \tag{3.64}$$

For the case that two partons (we call them l and $m+1$) are almost collinear we may write

$$|M(\{\hat{p},\hat{f}\}_{m+1})\rangle \sim |M_l(\{\hat{p},\hat{f}\}_{m+1})\rangle \ . \tag{3.65}$$

If p_{m+1} becomes soft we have

$$|M(\{\hat{p},\hat{f}\}_{m+1})\rangle \sim \sum_l |M_l(\{\hat{p},\hat{f}\}_{m+1})\rangle \ . \tag{3.66}$$

The definition of $|M_l(\{\hat{p},\hat{f}\}_{m+1})\rangle$ in eq.(3.64) has the feature that eq.(3.66) and eq.(3.65) become exact in the soft and collinear limit respectively.

3.5.1 Splitting on the spin level

The spin dependent splitting operator $V_l^\dagger(\{\hat{p},\hat{f}\}_{m+1})$ can be characterized by its matrix elements

$$\langle\{\hat{s}\}_{m+1}|V_l^\dagger(\{\hat{p},\hat{f}\}_{m+1})|\{s\}_m\rangle \ . \tag{3.67}$$

As we have chosen an orthonormal basis for the spin states we can write the operator $V_l^\dagger$ in the following way

$$\langle\{\hat{s}\}_{m+1}|V_l^\dagger(\{\hat{p},\hat{f}\}_{m+1})|\{s\}_m\rangle = \Bigg(\prod_{j\notin\{l,m+1\}} \delta_{\hat{s}_j,s_j}\Bigg) v_l(\{\hat{p},\hat{f}\}_{m+1},\hat{s}_{m+1},\hat{s}_l,s_l) \ . \tag{3.68}$$

The factor $\prod_{j\notin\{l,m+1\}} \delta_{\hat{s}_j,s_j}$ is on the right side of the equation as the whole expression must be diagonal in the spectator spins. By this equation we define the splitting functions $v_l(\{\hat{p},\hat{f}\}_{m+1},\hat{s}_{m+1},\hat{s}_l,s_l)$. The various splitting functions are derived in [1].
As an example we show here in detail the derivation for one splitting (initial state $q \to q+g$ splitting, quark scatters). For the other amplitudes see section (6) of [1].
For the kinematics of the whole process we write

$$\begin{aligned} &p = p_a \ , \eta = \eta_a \ , \\ &\hat{p} = \hat{p}_a \ , \hat{\eta} = \hat{\eta}_a \ , \\ &q = \hat{p}_{m+1} \ , m = m(f_a) = m(\hat{f}_a) \ , \\ &\hat{s} = \hat{s}_a \ , \varepsilon_\mu = \varepsilon_\mu(\hat{p}_{m+1},\hat{s}_{m+1};\hat{Q}) \ , \end{aligned} \tag{3.69}$$

where p_{m+1} stands for the momentum of the emitted gluon. It must be noted that ε is defined to be orthogonal to $\hat{Q} = \hat{p}_a + \hat{p}_b = p_a + p_b$.

According to the Feynman rules for QCD we have for a quark-gluon vertex (see for that page 10 of [3]):

$$-ig(\mathrm{t}^A)_{cb}(\gamma^\alpha)_{ji} \ . \tag{3.70}$$

The factor g stands here for the strong coupling constant (in analogy to the fine structure constant α in QED) while $(\mathrm{t}^A)_{cb}$ is the color matrix. Thus we have for the amplitude $|M(\{\hat{p},\hat{f}\}_{m+1})\rangle$ the following expression

$$M = H\frac{\not{P}-m}{P^2-m^2}gt^c\not{\epsilon}^*U(\hat{p},\hat{s}) \ . \tag{3.71}$$

The factor $-i$ has been absorbed into H that stands here for the hard interaction we are not interested in at the moment. The entity $U(\hat{p},\hat{s})$ stands for the incoming initial state quark while $\not{\epsilon}^*$ stands for the outcoming real gluon that is emitted in the process. Further, $\not{P}$ is given by

$$\not{P} = P_\mu\gamma^\mu \ . \tag{3.72}$$

We see here also the propagator for the off-shell quark (the quark after the emission of the gluon). Its momentum is given by

$$P = \hat{p} - q \ . \tag{3.73}$$

We want to make an approximation of M for the soft and the collinear case; our goal is to derive the scalar expression v given in eq.(3.68).
For that we insert into M a "one" factor

$$M = H\frac{\not{n}(\not{p}-m)+(\not{p}+m)\not{n}}{2p\cdot n}\frac{\not{P}+m}{P^2-m^2}(gt^c\not{\epsilon}^*)U(\hat{p},\hat{s}) \ . \tag{3.74}$$

We assume n to be the lightlike vector p_B. In order to see that the inserted factor $\frac{\not{n}(\not{p}-m)+(\not{p}+m)\not{n}}{2p\cdot n}$ is truly equal to one we remind that the following relation is valid for general 4 vectors A and B (see eq. (A.19a) of [39])

$$\not{A}\not{B} = 2A\cdot B - \not{B}\not{A} \ . \tag{3.75}$$

Let us focus on the first term in M

$$M_{\mathrm{ns}} = H\frac{\not{n}(\not{p}-m)}{2p\cdot n}\frac{\not{P}+m}{P^2-m^2}(gt^c\not{\epsilon}^*)U(\hat{p},\hat{s}) \ . \tag{3.76}$$

With[15]

$$p = P + (p+q-\hat{p}) \tag{3.77}$$

[15] See eq.(3.73).

and

$$(\not{P} - m)(\not{P} + m) = P^2 - m^2 \tag{3.78}$$

we can write for $M_{\rm ns}$

$$\begin{aligned} M_{\rm ns} = & H \frac{\not{n}}{2n \cdot p} (g t^c \not{\varepsilon}^*) U(\hat{p}, \hat{s}) \\ & + H \frac{\not{n} \ (\not{p} \ + \not{q} - \not{\hat{p}})}{2p \cdot n} \frac{\not{P} \ + m}{P^2 - m^2} (g t^c \not{\varepsilon}^*) U(\hat{p}, \hat{s}) \ . \end{aligned} \tag{3.79}$$

We remind here that the 4-momentum of the emitted gluon is given by q. As the first term is independent from q we have no divergency both for the soft and collinear limit of q.
In the soft limit we see that the expression $(p+q-\hat{p})$ is proportional to one power of q. Also the denominator $P^2 - m^2 = -2\hat{p} \cdot q$ is proportional to one power of q. So the expression $M_{\rm ns}$ as a whole remains finite in the soft limit.
For the treatment of the collinear limit we resolve the entity q into two parts

$$q = q_\perp + q_{||} \ . \tag{3.80}$$

Here is $q_\perp$ a spacelike vector; it is non-zero and fulfills

$$q_\perp \cdot p = 0 \ . \tag{3.81}$$

In the collinear limit the denominator of the second term of $M_{\rm ns}$ has two powers of $q_\perp$. The numerator $(\not{p} + \not{q} - \not{\hat{p}})$ contributes with one power of $q_\perp$ while the other numerator $\not{P} \ + m$ also with one. Thus both cancel each other and $M_{\rm ns}$ remains finite both in the soft and in the collinear limit.
Thus the divergent part of M remains

$$M_{\rm sing} = H \frac{(\not{p} \ + m) \not{n}}{2p \cdot n} \frac{\not{P} \ + m}{P^2 - m^2} (g t^c \not{\varepsilon}^*) U(\hat{p}, \hat{s}) \ . \tag{3.82}$$

According to eq.(A.22) of [40] we have

$$\not{p} \ + m = \sum_s U(p,s) \bar{U}(p,s) \ . \tag{3.83}$$

The factor $U(p,s)$ can be viewed as a real incoming quark that comes into the hard process. Thus we consider it to be meaningful to absorb this factor into the hard scattering amplitude H. We define therefore as a splitting function

$$v_{\rm a} = - \frac{\sqrt{4\pi\alpha_s}}{(\hat{p} - q)^2 - m^2} \varepsilon^*_\mu \frac{\bar{U}(p,s) \not{n} \ (\not{\hat{p}} - \not{q} + m) \gamma^\mu U(\hat{p}, \hat{s})}{2p \cdot n} \ . \tag{3.84}$$

We note here that by definition the color matrix t^c acts only on the color part of $|M\rangle$. For the splitting function $v_{\rm a}$ only the spin part of $|M\rangle$ is relevant (see for that eq.(3.68)). For the treatment of the other splittings see section 6 of [1].

3.5.2 Splitting on the color level

In the previous section we discussed the splitting operators on spin level. Now we want to say something about splitting on color level. In eq. (3.64) the splitting operators both on color and on spin level have been introduced. As an example we could write for the emission of a gluon by a parton:

$$|\hat{\psi}\rangle = t_l^\dagger(f_l \to f_l + g)|\psi\rangle \ . \tag{3.85}$$

The question is: how can this be properly described?
For that we write the quantum amplitude in a vector expansion

$$|M(\{p,f\}_m)\rangle_{\rm C,S} = \sum_{\{c\}_m} |\{c\}_m\rangle_{\rm C} \otimes \sum_{\{s\}_m} |\{s\}_m\rangle_{\rm S} M(\{p,f,s,c\}_m) \ . \tag{3.86}$$

$|\{c\}_m\rangle$ is here a vector in color space while $|\{s\}_m\rangle$ is a vector in spin space. With that $|M(\{p,f\}_m)\rangle_{\rm C,S}$ is a vector in the combined color-spin space. Eq.(3.86) can be written in a component notation. The spin is denoted by the index λ_l which takes the values $\pm\frac{1}{2}$ for quarks and the values ± 1 for gluons. For color the indices are denoted by a_l which takes the values $1,\ldots,3$ for quarks and the values $1,\ldots,8$ for gluons. Regarding color, an initial state quark corresponds to a final state antiquark and an initial state antiquark corresponds to a final state quark. Hence in this section "q" and "quark" can mean both a final state quark or an initial state antiquark and "$\bar{q}$" respectively "antiquark" a final state antiquark or an initial state quark. Now M can be expanded in the following way

$$\begin{aligned} M(\{p,f\}_m)^{a_{\rm a},a_{\rm b},a_1,\ldots,a_m}_{\lambda_{\rm a},\lambda_{\rm b},\lambda_1,\ldots,\lambda_m} &= \sum_{\{c\}_m} \Psi(\{c\}_m)^{a_{\rm a},a_{\rm b},a_1,\ldots,a_m} \\ &\times \sum_{\{s\}_m} \Xi(\{s\}_m)_{\lambda_{\rm a},\lambda_{\rm b},\lambda_1,\ldots,\lambda_m} M(\{p,f,s,c\}_m) \ . \end{aligned} \tag{3.87}$$

The $\Psi(\{c\}_m)$ form here a basis in the space of color singlets with color labels $\{c\}_m$. In addition the $\Xi(\{s\}_m)$ form a basis in the space of spins with spin labels $\{s\}_m$.

We assume that the spin labels λ stand for parton helicities. They are already properly normalized. Therefore we have

$$\Xi(\{s\}_m)_{\lambda_a\lambda_b,\lambda_1,\ldots,\lambda_m} = \delta_{s_a}^{\lambda_a}\delta_{s_b}^{\lambda_b}\delta_{s_1}^{\lambda_1}\ldots\delta_{s_m}^{\lambda_m} \ . \tag{3.88}$$

We already mentioned in section (3.2) the situation for color is a bit more complicated. As the amplitude $|M(\{p,f\}_m)\rangle$ is supposed to be a physical state it must be invariant under gauge transformations. Thus a basis in the color space must be introduced where each basis vector is a color singlet. For that the concept of *color strings* is introduced (see for that [41–44]). Here a color basis vector $|\{c\}_m\rangle$ is considered to be a *color string configuration* $\{c\}$. Such a configuration is considered to be a set of one or more *strings* S. There are two types of strings: *open strings* and *closed strings*.
An open string $S = [l_1, l_2, \ldots, l_{n-1}, l_n]$ is respresented by a set of parton indices where l_1 is the label of a quark, $l_2, \ldots, l_{n-1}$ are the labels of gluons and l_n is a label for an antiquark.
A closed string $S = (l_1, l_2, \ldots, l_{n-1}, l_n)$ is represented by at least two parton indices where all the partons are gluons. Sets which are related by cyclic permutation are treated as the same.
Now we focus on the basis states. We write $\Psi(\{c\}_m)$ as

$$\Psi(\{c\}_m)^{a_1,\ldots,a_m} = \Psi(S_1)^{\{a\}_{[1]}}\Psi(S_2)^{\{a\}_{[2]}}\ldots\Psi(S_K)^{\{a\}_{[K]}} \ . \tag{3.89}$$

The set of color indices in string k is given by

$$\{a\}_{[k]} = \{a_{l_1}, \ldots, a_{l_n}\} \ . \tag{3.90}$$

We define for an open string

$$\Psi(S)^{\{a\}} = n(S)^{-1/2}[t^{a_2}t^{a_3}\ldots t^{a_{n-1}}]_{a_1 a_n} \ . \tag{3.91}$$

Here t^a are the SU(3) generator matrices. The normalization factor is

$$n(S) = N_c C_F^{n-2} \ . \tag{3.92}$$

So that we have

$$\langle S|S\rangle \equiv \sum_{\{a\}} |\Psi(S)^{\{a\}}|^2 = 1 \ . \tag{3.93}$$

For a closed string we define

$$\Psi(S)^{\{a\}} = n(S)^{-1/2}\mathrm{Tr}[t^{a_1}t^{a_2}\ldots t^{a_n}] \ . \tag{3.94}$$

Where we have

$$n(S) = C_F^n \ . \tag{3.95}$$

So we obtain

$$\langle S|S\rangle \equiv \sum_{\{a\}} |\Psi(S)^{\{a\}}|^2 = 1 - \left(\frac{-1}{2N_c C_F}\right)^{n-1} \ , \tag{3.96}$$

which becomes one for a large number of colors.
With the definition of color strings we can now construct basis states for color singlet states. They are defined as a product of string states. They have a normalization factor $n(\{c\}_m)^{-1/2}$ with

$$n(\{c\}_m) = n(S_1)n(S_2)\dots n(S_K) \ . \tag{3.97}$$

For the normalization of the states we have

$$\langle \{c\}_m | \{c\}_m \rangle = \prod_k \langle S_k | S_k \rangle \ . \tag{3.98}$$

These factors are given by eq.(3.93) and eq.(3.96). We have therefore $\langle \{c\}_m | \{c\}_m \rangle \approx 1$ for the large N_c limit.
The set of basis vectors $|\{c\}_m\rangle$ is not orthonormal but for the large limit we have

$$\langle \{c'\}_m | \{c\}_m \rangle = \mathcal{O}(1/N_c^2) \qquad \{c'\}_m \neq \{c\}_m \ . \tag{3.99}$$

Now splitting on color level can be described. For that we go back to eq.(3.85). In component notation it can be written as

$$\hat{\psi}^{a_{\rm a},a_{\rm b},a_1,\dots,a_l,\dots,a_m,a_{m+1}} = \sum_{\tilde{a}_l} T(f_l)^{a_{m+1}}_{a_l,\tilde{a}_l} \psi^{a_{\rm a},a_b,a_1,\dots,\tilde{a}_l,\dots,a_m} \tag{3.100}$$

where the $T(f_l)^{a_{m+1}}_{a_l,\tilde{a}_l}$ stand for a representation of the SU(3) group. For the case that we have $f_l = \mathrm{g}$ it is given by

$$T(\mathrm{g})^a_{bc} = i f_{bac} \ . \tag{3.101}$$

The f_{bac} are the structure constants of the SU(3) group. They are defined by the commutator relation[16]

$$[t^a, t^b] = i f_{abc} t^c \ . \tag{3.102}$$

[16]We remind that we have the summation convention there; see further section (15.2) and section (15.4) of [40].

The application of the splitting operator T to one basis state $|\{c\}_m\rangle$ leads to

$$\sum_{a_l} T(g)^{\tilde{a}_{m+1}}_{\tilde{a}_l,a_l}\ t^{a_l} = \sum_{a_l} i f_{\tilde{a}_l,\tilde{a}_{m+1},a_l} t^{a_l} = t^{\tilde{a}_l} t^{\tilde{a}_{m+1}} - t^{\tilde{a}_{m+1}} t^{\tilde{a}_l}\ , \tag{3.103}$$

which can be written as

$$t_l^\dagger(g \to g+g)|\{c\}_m\rangle = \left[\frac{n(\{\hat{c}_+\}_{m+1})}{n(\{c\}_m)}\right]^{1/2} |\{\hat{c}_+\}_{m+1}\rangle - \left[\frac{n(\{\hat{c}_-\}_{m+1}}{n(\{c\}_m)}\right]^{1/2} |\{\hat{c}_-\}_{m+1}\rangle \tag{3.104}$$

with

$$\frac{n(\{\hat{c}_\pm\}_{m+1})}{n(\{c\}_m)} = C_F\ . \tag{3.105}$$

Eq. (3.104) can be also written as an operator equation

$$t_l^\dagger(g \to g+g) = \sqrt{C_F} a_+^\dagger(l) - \sqrt{C_F} a_-^\dagger(l)\ . \tag{3.106}$$

For a precise definition of the splitting operators a see section (7.2) of [1].
If f_l is a quark we have

$$T(q)^a_{ij} = t^a_{ij} \tag{3.107}$$

and if f_l is an antiquark the following relation holds

$$T(\bar{q})^a_{ij} = -t^a_{ji}\ . \tag{3.108}$$

By that also the splitting operators $T_l^\dagger$ for other processes (like for example $q \to q+g$) can be derived. For a more detailed discussion see section (7.3) of [1].

3.5.3 Splitting for the density operator

In the previous sections we have dealt with parton splitting on the level of the quantum states $|M\rangle$. Now we want to consider how a splitting is described on the level of the density states. In eq.(3.64) the splitting operators $t_l^\dagger$ and $V_l^\dagger$ have been introduced which act on the quantum aplitude $|M\rangle$.
Now we need an operator $\mathcal{S}$ that acts on the density state ρ so that the following relation holds

$$|\hat{\rho}) = \mathcal{S}|\rho)\ . \tag{3.109}$$

Here $|\rho)$ stands for the density state before the splitting while $|\hat{\rho})$ stands for the density state after the splitting. Before a splitting we can describe a

state with m partons in the final state and two partons in the initial state by

$$(\{p, f, s', c', s, c\}_m|\rho) \ . \tag{3.110}$$

After a splitting we have $m+1$ partons in the final state that is described by

$$(\{\hat{p}, \hat{f}, \hat{s}', \hat{c}', \hat{s}, \hat{c}\}_{m+1}|\rho) \ . \tag{3.111}$$

Parton i can split in $|M(\{p, f\}\rangle$ while parton j can split in $\langle M(\{p, f\}_m)|$. The simplest possibility is $i = j$. It is the only one that is incorporated into Monte Carlo event generators as they simulate only probability distributions (in collinear approximation) and not amplitudes. Thus they do not simulate interference effects.
We cannot ignore, however, the case where we have $i \neq j$ for the following reason: it is possible that we obtain after splitting the same flavors and momenta $\{\hat{p}, \hat{f}\}_{m+1}$. An integration over $\{\hat{p}\}_{m+1}$ would yield a logarithmic divergency. Please note that this is not only true for the collinear case but in general. An example for that would be parton i in $|M(\{p, f\}_m)\rangle$ emitting a gluon $m+1$ while parton j emits a gluon in $\langle M(\{p, f\}_m)|$. An interference graph for this does not contain a collinear divergence from p_{m+1} being collinear with respect to $\hat{p}_i$ or $\hat{p}_j$. We obtain a soft divergence when $\hat{p}_{m+1}$ goes to zero. Thus we must take the case $i \neq j$ into account. Now the question arises which momentum mapping ought to be used for $i \neq j$:

$$\{\hat{p}, \hat{f}\}_{m+1} = R_l(\{p, f\}_m, \{\zeta_{\mathrm{p}}, \zeta_{\mathrm{f}}\}) \ . \tag{3.112}$$

There are different options: mapping with $l = i$ or with $l = j$. In [1] it was chosen to average the two possibilities in an equal manner:

$$\begin{aligned}
\hat{\rho}(\{\hat{p}, \hat{f}_{m+1}\}) &= \sum_l \hat{\rho}_{ll}^{(l)}(\{\hat{p}, \hat{f}\}_{m+1}) \\
&+ \sum_{\substack{i,j \\ i\neq j}} \Big\{ A_{ij}(\{\hat{p}\}_{m+1}) \hat{\rho}_{ij}^{(i)}(\{\hat{p}, \hat{f}\}_{m+1}) + A_{ji}(\{\hat{p}\}_{m+1}) \hat{\rho}_{ij}^{(j)}(\{\hat{p}, \hat{f}\}_{m+1}) \Big\} \\
&= \sum_l \Bigg\{ \hat{\rho}_{ll}^{(l)}(\{\hat{p}, \hat{f}\}_{m+1}) \\
&+ \sum_{k\neq l} A_{lk}(\{\hat{p}\}_{m+1}) \Big[\hat{\rho}_{lk}^{(l)}(\{\hat{p}, \hat{f}\}_{m+1}) + \hat{\rho}_{kl}^{(l)}(\{\hat{p}, \hat{f}\}_{m+1} \Big] \Bigg\} \ .
\end{aligned} \tag{3.113}$$

The sum runs over the set $\{\mathrm{a}, \mathrm{b}, 1, \ldots, m\}$. The A_{ij} are here weight factors. In [1] $A_{ij} = \frac{1}{2}$ was taken but also other choices are possible. A_{ij} stands

here for momentum mapping R_l while A_{ji} stands for momentum mapping R_l with $l = j$. If we have $i = j$ we take the mapping with $l = i = j$. Then the different contributions to $\hat{\rho}(\{\hat{p}, \hat{f}_{m+1}\})$ need to be considered. We have for the case $i = j$ according to eq.(3.64)

$$\begin{aligned}\rho_{ll}^{(l)}(\{\hat{p}, \hat{f}_{m+1}\}) = t_l^\dagger(f_l \to \hat{f}_l + \hat{f}_{m+1}) V_l^\dagger(\{\hat{p}, \hat{f}\}_{m+1}) \rho(\{p, f\}) \\ \times V_l(\{\hat{p}, \hat{f}\}_{m+1}) t_l(f_l \to \hat{f}_l + \hat{f}_{m+1}) \\ \times S_l(\{\hat{f}_{m+1}) \ .\end{aligned} \tag{3.114}$$

Here is $S_l(\{\hat{f}_{m+1})$ a normalisation factor

$$S_l(\{\hat{f}\}_{m+1}) = \begin{cases} 1/2 \ , & l \in \{1, \ldots, m\}, \ \hat{f}_l = \hat{f}_{m+1} = \mathrm{g} \\ 1 \ , & l \in \{1, \ldots, m\}, \ \hat{f}_l \neq \mathrm{g}, \hat{f}_{m+1} = \mathrm{g} \\ 0 \ , & l \in \{1, \ldots, m\}, \ \hat{f}_l = \mathrm{g}, \hat{f}_{m+1} \neq \mathrm{g} \\ 1 \ , & l \in \{1, \ldots, m\}, \ \hat{f}_l = q, \hat{f}_{m+1} = \bar{q} \\ 0 \ , & l \in \{1, \ldots, m\}, \ \hat{f}_l = \bar{q}, \hat{f}_{m+1} = q \\ 1 \ , & l \in \{\mathrm{a}, \mathrm{b}\} \end{cases} \ . \tag{3.115}$$

In the first case the normalisation factor is 1/2. The reason for this is because this stands for the process $\mathrm{g} \to \mathrm{g} + \mathrm{g}$. The splitting probability is symmetric under interchange of the labels l and $m + 1$ so that integration over $\hat{p}_l$ and $\hat{p}_{m+1}$ would count the same physical configuration twice. The factor 1/2 compensates this. For the case that we have $\hat{f}_l = \mathrm{g}$ and $\hat{f}_{m+1} = q$ or $\hat{f}_{m+1} = \bar{q}$ the counting factor must be zero, so that then the emitted gluon should be counted as parton $m + 1$. Similar to that the factor is zero for $\hat{f}_l = \bar{q}$ and $\hat{f}_{m+1} = q$ so that for $\mathrm{g} \to q + \bar{q}$ the final daughter antiquark ought to be parton $m + 1$. By that the flavor mapping is enforced as discussed in section (3.4).

For the case $i \neq j$ we have

$$\begin{aligned}\hat{\rho}_{ij}^{(l)}(\{\hat{p}, \hat{f}_{m+1}) = & t_i^\dagger(f_l \to \hat{f}_i + \hat{f}_{m+1}) V_i^{\dagger,\mathrm{soft}}(\{\hat{p}, \hat{f}\}_{m+1}) \rho(\{p, f\}) \\ & \times V_j^{\mathrm{soft}}(\{\hat{p}, \hat{f}\}_{m+1}) t_j(f_j \to \hat{f}_j + \hat{f}_{m+1}) \ .\end{aligned} \tag{3.116}$$

Here we have used the simpler splitting operator V^{soft}. We mention here that both $V_i^{\dagger,\mathrm{soft}}$ and V_j^{soft} are equal to zero when parton $m + 1$ is not a gluon.[17] So $\hat{\rho}_{ij}^{(l)}(\{\hat{p}, \hat{f}_{m+1})$ vanishes for $i \neq j$ except for the case that parton $m + 1$ is a gluon.
So we can write now

$$|\hat{\rho}_{ij}^{(l)}) = \mathcal{S}_{ij}^{(l)} |\rho) \ . \tag{3.117}$$

[17]For a treatment of the soft splitting function see section (6.6) of [1].

$|\hat{\rho}_{ij}^{(l)})$ stands for the statistical state after splitting while $|\rho)$ stands for the statistical state before splitting. $\mathcal{S}_{ij}^{(l)}$ is the splitting operator.
We can write this as

$$\begin{aligned}(\{\hat{p},\hat{f},\hat{s}',\hat{c}',\hat{s},\hat{c}\}_{m+1}|\mathcal{S}_{ij}^{(l)}|\rho) = \frac{1}{m!}\int [d\{p,f,s',c',s,c\}_m] \\ \times(\{\hat{p},\hat{f},\hat{s}',\hat{c}',\hat{s},\hat{c}\}_{m+1}|\mathcal{S}_{ij}^{(l)}|\{p,f,s',c',s,c\}_m) \\ \times(\{p,f,s',c',s,c\}_m|\rho)\ .\end{aligned} \tag{3.118}$$

We can write the splitting operator in the following form

$$\begin{aligned}(\{p,f,s',c',s,c\}_{m+1}|\mathcal{S}_{ij}^{(l)}|\{p,f,s',c',s,c\}_m) = \\ (\{\hat{c}',\hat{c}\}_{m+1}|\mathcal{G}(i,j;\{\hat{f}\}_{m+1})|\{c',c\}_m) \\ \times(\{\hat{s}',\hat{s}\}_{m+1}|\mathcal{W}(i,j;\{\hat{f},\hat{p}\}_{m+1})|\{s',s\}_m) \\ \times(\{\hat{p},\hat{f}\}_{m+1}|\mathcal{P}_l|\{p,f\}_m) \\ \times(m+1)\frac{n_c(a)n_c(b)\eta_a\eta_b}{n_c(\hat{a})n_c(\hat{b})\hat{\eta}_a\hat{\eta}_b}\frac{f_{\hat{a}/A}(\hat{\eta}_a,\mu_F^2)f_{\hat{b}/B}(\hat{\eta}_b,\mu_F^2)}{f_{a/A}(\eta_a,\mu_F^2)f_{b/B}(\eta_b,\mu_F^2)}\ .\end{aligned} \tag{3.119}$$

The single factors are given by a color part

$$\begin{aligned}&(\{\hat{c}',\hat{c}\}_{m+1}|\mathcal{G}(i,j;\{\hat{f}\}_{m+1})|\{c',c\}_m) = \\ &{}_D\langle\{\hat{c}\}_{m+1}|t_i^\dagger(f_i\to\hat{f}_i+\hat{f}_{m+1})|\{c\}_m\rangle\langle\{c'\}_m|t_j(f_j\to\hat{f}_j+\hat{f}_{m+1})|\{\hat{c}'\}_{m+1}\rangle_D\end{aligned} \tag{3.120}$$

and a spin part $(\{\hat{s}',\hat{s}\}_{m+1}|\mathcal{W}(l,l;\{\hat{f},\hat{p}\}_{m+1})|\{s',s\}_m)$. For $i=j$ and under the exclusion of the process $\mathrm{g}\to\mathrm{g}+\mathrm{g}$ this can be written as

$$\begin{aligned}&(\{\hat{s}',\hat{s}\}_{m+1}|\mathcal{W}(l,l;\{\hat{f},\hat{p}\}_{m+1})|\{s',s\}_m) \\ &= S_l(\{\hat{f}\}_{m+1})\langle\{\hat{s}\}_{m+1}|V_l^\dagger(\{\hat{p},\hat{f}\}_{m+1})|\{s\}_m\rangle\langle\{s'\}_m|V_l(\{\hat{p},\hat{f}\}_{m+1})|\{\hat{s}'\}_{m+1}\rangle\ .\end{aligned} \tag{3.121}$$

For $i=j$ the splitting operator $\mathcal{W}$ can be written as[18]

$$\begin{aligned}&(\{\hat{s}',\hat{s}\}_{m+1}|\mathcal{W}(l,l;\{\hat{f},\hat{p}\}_{m+1})\{s',s\}_m) = \\ &= S_l(\{\hat{f}\}_{m+1})\Big\{\langle\{\hat{s}\}_{m+1}|V_l^\dagger(\{\hat{p},\hat{f}\}_{m+1})|\{s\}_m\rangle\langle\{s'\}_m|V_l(\{\hat{p},\hat{f}\}_{m+1})|\{\hat{s}'\}_{m+1}\rangle \\ &+\theta(l\in\{1,\dots,m\},\hat{f}_l=\hat{f}_{m+1}=g)(\{\hat{s}',\hat{s}\}_{m+1}|\widetilde{\mathcal{W}}(l,l;\{\hat{p}\}_{m+1})|\{s',s\}_m)\Big\}\ ,\end{aligned} \tag{3.122}$$

[18]For the proper definition of $\tilde{W}$ see eq.(8.13)-(8.16) in [1].

while for $i \neq j$ the splitting operator $\mathcal{W}$ can be written as

$$\begin{aligned}(\{\hat{s}', \hat{s}\}_{m+1}|\mathcal{W}(i,j;\{\hat{p}\}_{m+1})|\{s', s\}_m) = \langle\{\hat{s}\}_{m+1}|V_i^{\dagger,\text{soft}}(\{\hat{p},\hat{f}\}_{m+1})|\{s\}_m\rangle \\ \times\langle\{s'\}_m|V_j^{\text{soft}}(\{\hat{p},\hat{f}\}_{m+1})|\{\hat{s}'\}_{m+1}\rangle\end{aligned} \tag{3.123}$$

where the simpler soft splitting operators V^{soft} are used which are mentioned on page (47).

The matrix element $(\{\hat{p},\hat{f}\}_{m+1}|\mathcal{P}_l|\{p,f\}_m)$ is the next factor which must be discussed. It has a delta function which ensures the correct momentum mapping

$$\frac{1}{m!}\int[\mathrm{d}\{p,f\}_m](\{\hat{p},\hat{f}\}_{m+1}|\mathcal{P}_l|\{p,f\}_m)h(\{p,f\}_m) = h(\{p',f'\}_m)\ , \tag{3.124}$$

with h being a test function. The flavors and momenta are given by

$$\{\{p',f'\}_m,\{\zeta_\mathrm{p},\zeta_\mathrm{f}\}\} = Q_l(\{\hat{p},\hat{f}\}_{m+1})\ . \tag{3.125}$$

The flavor and momentum mapping has been explained in section (3.4). Alternatively we can write for $\mathcal{P}_l$

$$\begin{aligned}&\frac{1}{(m+1)!}\int[d\{\hat{p},\hat{f}\}_{m+1}]g(\{\hat{p},\hat{f}\}_{m+1})(\{\hat{p},\hat{f}\}_{m+1}|\mathcal{P}_l|\{p,f\}_m) \\ &= \frac{1}{m+1}\sum_{\zeta_\mathrm{f}\in\Phi_l(f_l)}\int d\zeta_\mathrm{p}\theta(\zeta_\mathrm{p}\in\Gamma_l(\{p\}_m,\zeta_\mathrm{f}))g(\{\hat{p}',\hat{f}'\}_{m+1})\ ,\end{aligned} \tag{3.126}$$

with g being a test function and

$$\{\hat{p}^{'},\hat{f}^{'}\}_{m+1} = R_l(\{\{p,f\}_m,\{\zeta_p,\zeta_f\}\}) \tag{3.127}$$

being the inverse of Q_l. For the derivation of the counting factor $\frac{1}{m+1}$ see Appendix B of [1].
We can now derive the splitting operator $\mathcal{S}$. For the density operator we have

$$|\hat{\rho}) = \mathcal{S}|\rho)\ , \tag{3.128}$$

with

$$\mathcal{S} = \sum_l \mathcal{S}_l\ . \tag{3.129}$$

The terms $\mathcal{S}_l$ are here given by

$$\mathcal{S}_l = \mathcal{S}_{ll}^{(l)} + \sum_{k\neq l}\mathcal{A}_{lk}\left\{\mathcal{S}_{lk}^{(l)} + \mathcal{S}_{kl}^{(l)}\right\}\ . \tag{3.130}$$

The $\mathcal{A}_{lk}$ are operators where each basis vector $|\{p,f,s',c',s,c\}_{m+1})$ is multiplied by the function $A_{lk}(\{\hat{p}\}_{m+1})$. The sum runs over the set $\{\mathrm{a},\mathrm{b},1,\ldots,m\}$. We mention here that a simplification is possible.
We remind, since the quantum amplitudes must be color singlets, we have[19]

$$\sum_l \sum_{\tilde{a}_l} T(f_l)^{a_{m+1}}_{a_l,\tilde{a}_l} \psi^{a_\mathrm{a},a_\mathrm{b},a_1,\ldots,\tilde{a}_l,\ldots,a_m} = 0 \ , \tag{3.131}$$

which can be also written as

$$\sum_l t_l^\dagger(f_l \to f_l + \mathrm{g})|\psi\rangle = 0 \ . \tag{3.132}$$

Thus we can write for the gluon emission operators $\mathcal{G}(l,k;\{\hat{f}\}_{m+1})$ for $\hat{f}_{m+1} = \mathrm{g}$

$$\sum_k \mathcal{G}(l;k;\{\hat{f}\}_{m+1}) = 0 \quad , \quad \sum_k \mathcal{G}(k,l;\{\hat{f}\}_{m+1}) = 0 \ , \tag{3.133}$$

which leads to the following useful relation

$$\mathcal{G}(l;l;\{\hat{f}\}_{m+1}) = -\frac{1}{2}\sum_{k\neq l} \mathcal{G}(l;k;\{\hat{f}\}_{m+1}) - \frac{1}{2}\sum_{k\neq l} \mathcal{G}(k;l;\{\hat{f}\}_{m+1}) \ . \tag{3.134}$$

Now we can write down the splitting operator in an explicit manner. We get for the case $\hat{f}_{m+1} = \mathrm{g}$

$$\begin{aligned}
&\big(\{\hat{p},\hat{f},\hat{s}',\hat{c}',\hat{s},\hat{c}\}_{m+1}\big|\mathcal{S}_l\big|\{p,f,s',c',s,c\}_m\big) \\
&\quad = (m+1)\big(\{\hat{p},\hat{f}\}_{m+1}\big|\mathcal{P}_l\big|\{p,f\}_m\big)\,\frac{n_\mathrm{c}(a)n_\mathrm{c}(b)\,\eta_\mathrm{a}\eta_\mathrm{b}}{n_\mathrm{c}(\hat{a})n_\mathrm{c}(\hat{b})\,\hat{\eta}_\mathrm{a}\hat{\eta}_\mathrm{b}}\,\frac{f_{\hat{a}/A}(\hat{\eta}_\mathrm{a},\mu_F^2)f_{\hat{b}/B}(\hat{\eta}_\mathrm{b},\mu_F^2)}{f_{a/A}(\eta_\mathrm{a},\mu_F^2)f_{b/B}(\eta_\mathrm{b},\mu_F^2)} \\
&\qquad \times \sum_{\substack{k\in\{\mathrm{a},\mathrm{b},1,\ldots,m\}\\ k\neq l}} \Big\{ \big(\{\hat{c}',\hat{c}\}_{m+1}\big|\mathcal{G}(l,k;\{\hat{f}\}_{m+1})\big|\{c',c\}_m\big) \\
&\qquad\qquad \times \Big[A_{lk}(\{\hat{p}\}_{m+1})\big(\{\hat{s}',\hat{s}\}_{m+1}\big|\mathcal{W}(l,k;\{\hat{f},\hat{p}\}_{m+1})\big|\{s',s\}_m\big) \\
&\qquad\qquad\quad - \frac{1}{2}\big(\{\hat{s}',\hat{s}\}_{m+1}\big|\mathcal{W}(l,l;\{\hat{f},\hat{p}\}_{m+1})\big|\{s',s\}_m\big)\Big] \\
&\qquad\quad + \big(\{\hat{c}',\hat{c}\}_{m+1}\big|\mathcal{G}(k,l;\{\hat{f}\}_{m+1})\big|\{c',c\}_m\big) \\
&\qquad\qquad \times \Big[A_{lk}(\{\hat{p}\}_{m+1})\big(\{\hat{s}',\hat{s}\}_{m+1}\big|\mathcal{W}(k,l;\{\hat{f},\hat{p}\}_{m+1})\big|\{s',s\}_m\big) \\
&\qquad\qquad\quad - \frac{1}{2}\big(\{\hat{s}',\hat{s}\}_{m+1}\big|\mathcal{W}(l,l;\{\hat{f},\hat{p}\}_{m+1})\big|\{s',s\}_m\big)\Big]\Big\} \ .
\end{aligned} \tag{3.135}$$

[19] See for that eq.(7.27) and eq.(7.28) of [1].

If $\hat{f}_{m+1} \neq \mathrm{g}$ that means $\{\hat{f}_l, \hat{f}_{m+1}\} = \{q, \bar{q}\}$ we have

$$\begin{aligned}\left(\{\hat{p},\hat{f},\hat{s}',\hat{c}',\hat{s},\hat{c}\}_{m+1}|\mathcal{S}_l|\{p,f,s',c',s,c\}_m\right) = (m+1)(\{\hat{p},\hat{f}\}_{m+1}|\mathcal{P}_l|\{p,f\}_m)\\ \times\frac{n_c(a)n_c(b)\eta_a\eta_b}{n_c(\hat{a})n_c(\hat{b})\hat{\eta}_a\hat{\eta}_b}\frac{f_{\hat{a}/A}(\hat{\eta}_a,\mu_F^2)f_{\hat{b}/B}(\hat{\eta}_b,\mu_F^2)}{f_{a/A}(\eta_a,\mu_F^2)f_{b/B}(\eta_b,\mu_F^2)}\\ \times(\{\hat{c}',\hat{c}\}_{m+1}|\mathcal{G}(l,l;\{\hat{f}\}_{m+1})|\{c',c\}_m)\\ \times(\{\hat{s}',\hat{s}\}_{m+1}|\mathcal{W}(l,l;\{\hat{f},\hat{p}\}_{m+1})|\{s',s\}_m)\ .\end{aligned} \tag{3.136}$$

3.5.4 The real splitting operator $\mathcal{H}(t)$

Our goal is now to set up the evolution equation given in eq.(3.36). The splitting operator $\mathcal{S}$ gives the total probability that a real splitting occurs. In eq.(3.36) the operator $\mathcal{H}(t)$ is supposed to be proportional to the probability that a branching occurs between t and $t + \mathrm{d}t$. It is therefore a probability density that a splitting happens. Thus it is presumed that the following relation holds

$$\int_0^\infty dt\mathcal{H}(t) = \mathcal{S}\ . \tag{3.137}$$

The simplest way to get the real splitting operator $\mathcal{H}(t)$ is just to insert into $\mathcal{S}$ a delta function which defines the shower time t. The choice taken in [1] was

$$t = \log\left(\frac{Q_0^2}{|(\hat{p}_l + (-1)^{\delta_{l,\mathrm{a}}+\delta_{l,\mathrm{b}}}\hat{p}_{m+1})^2 - m^2(f_l)|}\right) \tag{3.138}$$

where Q_0^2 is taken to be the hardness scale of the initial hard scattering which starts the parton shower. Remember from section (3.4) that l is the index of the parton that splits while a and b are the indices of the initial state partons. There are several other possibilities to introduce the shower time. Another choice would be to relate the shower time t to the transverse momentum as it is done in the Catani-Seymour dipole shower[20]

$$t = \log\left(\frac{Q^2}{\mathbf{k}_\perp^2}\right) \tag{3.139}$$

with Q as the hardness scale of the scattering. For our purposes the following definition is used (as it was used in [37] and the results of [37] will be applied

[20] See for that eq.(13.7) of [37].

in the next chapter[21]

$$t = \log\left(\frac{Q^2}{2\hat{p}_{m+1}\cdot\hat{p}_{\rm a}}\right) . \tag{3.140}$$

For the general case we can introduce a function $e(\hat{p})$ which depends on the kinematical momenta of the splitted partons and which defines the shower time. So we define for the real splitting operator

$$\begin{aligned}(\{\hat{p},\hat{f},\hat{c}',\hat{s},\hat{c}\}_{m+1}|\mathcal{H}(t)|(\{p,f,c',s,c\}_m) = \\ \sum_{l\in\{a,b,\ldots,m\}} \{\hat{p},\hat{f},\hat{c}',\hat{s},\hat{c}\}_{m+1}|\mathcal{S}_l|(\{p,f,c',s,c\}_m)) \\ \times\delta(t-e(\hat{p}))\end{aligned} \tag{3.141}$$

With eq.(3.44) it is possible to derive the non splitting operator $\mathcal{V}(t)$.
With eq.(3.36) together with eq.(3.135), eq.(3.136), eq.(3.44) and eq.(3.137) we have now the evolution equation; it was used in [37].
We note that further simplifications are possible. In [45] the evolution was averaged over spins as it is common in Monte Carlo event generators (while soft gluon interference effects remained in [45] in contrast to Monte Carlo event generators). Further the leading color limit was taken.

It is maybe interesting to note that the splitting operator $\mathcal{H}(t)$ has the following structure

$$\left(1\middle|\mathcal{H}(t)\middle|\{p,f,s',c',s,c\}_m\right) = 2\left\langle\{s'\}_m\middle|\{s\}_m\right\rangle\left\langle\{c'\}_m\middle|h(t,\{p,f\}_m)\middle|\{c\}_m\right\rangle \ . \tag{3.142}$$

Thus the splitting operator $\mathcal{H}(t)$ is diagonal in spin but not in color. The full expression for the function h is given in section (12) of [1] and in Appendix[22] A of [37]. In Appendix A of [37] h respective $\mathcal{H}(t)$ has been further simplified. This result will be used in the next chapter.

[21] See for that eq.(3.3) of [37].
[22] Please note that in [37] an error has been corrected.

Chapter 4

Parton shower formalism and the energy fraction in Drell Yan processes

In chapter (3) an analytical formalism for parton showers which takes interference effects into account has been summarized. This formalism was developed in [1]. In [37] this formalism (together with some simplifications) was used in order to calculate the distribution of the transverse momentum $k_\perp$ of the Z^0 boson in Drell Yan processes. It turned out that the result was equivalent to the one given in [46] where the $k_\perp$ distribution was derived by standard resummation techniques.
Our goal in this chapter is now to do the same for the energy fraction[1] in Drell Yan processes. In [2] this problem was already handled, where resummation techniques were used while in [24] the same was considered for a MC generator with color coherence. Here it is our goal to derive the distribution of the energy fraction in Drell Yan with the formalism of [1] together with simplifications given in [37]. We will show that the result is equivalent to the one given in [2] and [24] under certain conditions.

4.1 Review from the literature

In a Drell Yan (DY) process we have two incoming partons (which come out from two incoming hadrons) which form a Z^0 boson that then decays into a lepton-antilepton pair. According to the mass factorization theorem the

[1] For its definition see eq.(4.32).

partonic DY cross section can be written (see for that [47], [48] and [49]) as

$$\tau \frac{d\sigma}{d\tau} = Q^2 \frac{d\sigma}{dQ^2} = \sigma_0 W\left(\tau; Q^2, Q_0^2\right), \tag{4.1}$$

σ_0 stands here for the Born cross section. Q^μ is the four momentum of the lepton pair. The variable $\tau = Q^2/s$ is the (partonic) energy fraction with s as the center of mass energy of the two partons before any parton showering takes place while Q^2 stands for the center of mass energy after the parton shower[2]. The variable Q_0^2 is a kinemetical cut in order to avoid the collinear divergency. Thus only partons with $\mathbf{k}_\perp^2 \geq Q_0^2$ are taken as real emission while the others are considered as unresolved.
The function W can be derived inside the frame of perturbative QCD. This was done for the soft limit in [2] and [24]. In [2] resummation techniques were used for the derivation of W. As it is easier to compare the cross sections of DY and deep inelastic scattering (DIS) in Mellin space the following transformation was used

$$W_N(Q^2; Q_0^2) = \int_0^1 d\tau \tau^{N-1} W\left(\tau; Q^2, Q_0^2\right) \ . \tag{4.2}$$

In [2] it was shown that this function takes the following form in the soft limit[3]

$$\ln W_N(Q^2; Q_0^2) = 2\frac{C_F}{\pi} \int_0^1 d\zeta \frac{\zeta^{N-1} - 1}{1-\zeta} \int_{Q_0^2}^{(1-\zeta)^2 Q^2} \frac{d\mathbf{k}_\perp^2}{\mathbf{k}_\perp^2} \alpha_S\left(\mathbf{k}_\perp^2\right) \ . \tag{4.3}$$

In [24] it was shown that a Monte Carlo event generator which takes into account color coherence can reproduce the result of eq.(4.3).
The question that arises whether the parton shower formalism of [1] can reproduce the expression of eq.(4.3). Our goal in this chapter is to handle this issue. For that we make use of some approximations derived in [37] (see section (4.1.4)). Please note that the energy fraction τ as a purely partonic variable cannot be easily measured. The reason why we consider this variable is that we want to check whether the formalism of [1] can reproduce the results of [2] and [24]. By this we can check the quality of this parton shower formalism.

[2] See for that also section (4.1.2).

[3] We have decided to write instead of z ζ as later in this chapter another variable z will be used.

4.1.1 The differential cross section $d\sigma/d\tau$ and the partonic statistical state

The entity we are interested in is the differential cross section with respect to the energy fraction τ. As τ is a purely partonic variable it makes sense to consider a statistical state $|\rho_{\text{pert}})$ which is defined purely on parton level what means that it is free from PDFs.
The introduction of such a kind of states was already done in [37]. We give here a summary of the consideration there.
It should be reminded that the statistical state $|\rho(t))$ contains a factor[4] which gives the parton-parton luminosity

$$\frac{f_{a/A}(\eta_a, \mu_F^2) f_{b/B}(\eta_b, \mu_F^2)}{4 n_c(a) n_c(b) 2\eta_a \eta_b p_A \cdot p_B} \ . \tag{4.4}$$

The functions $f_{a/A}$ and $f_{b/B}$ are parton distribution functions, $n_c(a)$ and $n_c(b)$ denote the number of colors carried by the partons a and b (3 for quarks and 8 for gluons). Let us introduce an alternative statistical state vector $|\rho_{\text{pert}}(t))$ where this non-pertubative factor is removed

$$\begin{aligned} &(\{p, f, s', c', s, c\}_m|\rho(t)) = \\ &\frac{f_{a/A}\left(\eta_a, Q^2 e^{-t}\right) f_{b/B}(\eta_b, Q^2 e^{-t})}{4 n_c(a) n_c(b) 2\eta_a \eta_b p_A \cdot p_B} (\{p, f, s', c', s, c\}_m|\rho_{\text{pert}}(t)) \ . \end{aligned} \tag{4.5}$$

Thus this density operator ρ_{pert} operates only on parton level. For the scale μ_F inside the PDFs $\mu_F^2 = Q^2 e^{-t}$ was presumed. Q^2 is here the scale of the hard scattering. In our case it is the center of mass energy after the parton shower. For the exact definition of the shower time t see eq.(4.26). We can write for $|\rho_{\text{pert}}(t))$

$$|\rho(t)) = \mathcal{F}(t)|\rho_{\text{pert}}(t)) \, , \tag{4.6}$$

where the operator $\mathcal{F}(t)$ is defined as

$$\mathcal{F}(t)|\{p, f, s', c', s, c\}_m) = \frac{f_{a/A}\left(\eta_a, Q^2 e^{-t}\right) f_{b/B}(\eta_b, Q^2 e^{-t})}{4 n_c(a) n_c(b) 2\eta_a \eta_b p_A \cdot p_B} |\{p, f, s', c', s, c\}_m) \ . \tag{4.7}$$

Now we want to write down an evolution equation for $|\rho_{\text{pert}}(t))$. It should have the same structure as the evolution equation (3.36) that is for the hadronic statistical state; thus we write

$$\frac{d}{dt}|\rho_{\text{pert}}(t)) = [\mathcal{H}^{\text{pert}}(t) - \mathcal{V}^{\text{pert}}(t))]|\rho_{\text{pert}}(t)) \ , \tag{4.8}$$

[4] See for that eq.(3.8), eq.(3.11) and eq.(3.22).

where the objects $\mathcal{H}^{\rm pert}(t)$ and $\mathcal{V}^{\rm pert}(t)$ are supposed to be splitting operators which operate only on parton level which are derived now. If we consider eq.(4.6) and eq.(3.36) we obtain

$$\left[\frac{d}{dt}\mathcal{F}(t)\right]|\rho_{\rm pert}(t)) + \mathcal{F}(t)\frac{d}{dt}|\rho_{\rm pert}(t)) = [\mathcal{H}(t) - \mathcal{V}(t)]\mathcal{F}(t)|\rho_{\rm pert}(t)) \ , \quad (4.9)$$

which leads us to

$$\begin{aligned}\frac{d}{dt}|\rho_{\rm pert}(t)) =& \mathcal{F}(t)^{-1}[\mathcal{H}(t) - \mathcal{V}(t)]\mathcal{F}(t)|\rho_{\rm pert}(t)) \\ &- \mathcal{F}(t)^{-1}\left[\frac{d}{dt}\mathcal{F}(t)\right]|\rho_{\rm pert}(t)) \ .\end{aligned} \quad (4.10)$$

Thus we can write for the partonic splitting operators

$$\begin{aligned}\mathcal{H}^{\rm pert}(t) &= \mathcal{F}(t)^{-1}\mathcal{H}(t)\mathcal{F}(t) \ , \\ \mathcal{V}^{\rm pert}(t) &= \mathcal{F}(t)^{-1}\mathcal{V}(t)\mathcal{F}(t) + \mathcal{F}(t)^{-1}\left[\frac{d}{dt}\mathcal{F}(t)\right] \\ &= \mathcal{V}(t) + \mathcal{F}(t)^{-1}\left[\frac{d}{dt}\mathcal{F}(t)\right] \ ,\end{aligned} \quad (4.11)$$

where we used the fact that $\mathcal{V}(t)$ and $\mathcal{F}(t)$ commute with each other because $\mathcal{V}(t)$ as the virtual splitting operator does not change flavors and momenta. For the real splitting operator the following relation holds[5]

$$\begin{aligned}&(\{\hat{p},\hat{f},\hat{s}',\hat{c}',\hat{s},\hat{c}\}_{m+1}|\mathcal{H}(t)|\{p,f,s',c',s,c\}_m) = \\ &\frac{n_c(a)n_c(b)\eta_a\eta_b}{n_c(\hat{a})n_c(\hat{b})\hat{\eta}_a\hat{\eta}_b}\frac{f_{\hat{a}/A}(\hat{\eta}_a,Q^2e^{-t})f_{\hat{b}/B}(\hat{\eta}_b,Q^2e^{-t})}{f_{a/A}\left(\eta_a,Q^2e^{-t}\right)f_{b/B}(\eta_b,Q^2e^{-t})} \\ &\times(\{\hat{p},\hat{f},\hat{s}',\hat{c}',\hat{s},\hat{c}\}_{m+1}|\mathcal{H}^{\rm pert}(t)|\{p,f,s',c',s,c\}_m) \ .\end{aligned} \quad (4.12)$$

Now we are prepared to define $d\sigma/d\tau$ inside the frame of the parton shower formalism[6]. For that we note that the total cross section on parton

[5]The variables $\hat{\eta}_a$ and $\hat{\eta}_b$ stand for the momentum fraction after the splitting in backward evolution. See for that section (4.1.2).

[6]We note that in the soft limit $d\sigma/d\tau$ is approximately equal to the left side of eq.(4.1) as then τ is close to 1.

level for producing a Z^0 boson can be written[7] as

$$\begin{aligned}\sigma =&\big(1|\rho_{\text{pert}}(t)\big) = \\ &\sum_m \frac{1}{m!}\int [d\{p,f,s',c',s,c\}_m] \\ &\times \big(1|\{p,f,s',c',s,c\}_m\big)\big(\{p,f,s',c',s,c\}_m|\rho_{\text{pert}}(t)\big) = \\ &\sum_m \frac{1}{m!}\int [d\{p,f,s',c',s,c\}_m]\langle\{s'\}_m|\{s\}_m\rangle\langle\{c'\}_m|\{c\}_m\rangle \\ &\times \big(\{p,f,s',c',s,c\}_m|\rho_{\text{pert}}(t)\big)\ .\end{aligned} \tag{4.13}$$

Here eq.(3.40) and the completeness relation given in eq.(3.23) has been used. Thus we define the differential cross section as

$$\begin{aligned}\frac{d\sigma}{d\tau} =& \\ &\sum_m \frac{1}{m!}\int [d\{p,f,s',c',s,c\}_m]\langle\{s'\}_m|\{s\}_m\rangle\langle\{c'\}_m|\{c\}_m\rangle \\ &\times \delta_{a,\tilde{a}}\delta_{b,\tilde{b}}\delta(\eta_a-\tilde{\eta}_a)\delta(\eta_b-\tilde{\eta}_b)\delta\bigg(\tau-\frac{Q^2}{s}\bigg)\big(\{p,f,s',c',s,c\}_m|\rho_{\text{pert}}(t)\big)\ .\end{aligned} \tag{4.14}$$

We have decided to keep track of the momentum fractions η_a and η_b as we will compare our result in section (4.4) with PYTHIA which only yields results on hadron level.
The differential cross section can be also written as[8]

$$\begin{aligned}\frac{d\sigma}{d\tau} &= \big(\tau|\rho_{\text{pert}}(t)\big) \\ &= \big(1|\mathcal{Q}(\tau,\tilde{\eta}_a,\tilde{\eta}_b,\tilde{a},\tilde{b}))|\rho_{\text{pert}}(t)\big)\ ,\end{aligned} \tag{4.15}$$

where the measurement[9] operator $\mathcal{Q}$ is defined as

$$\begin{aligned}&\mathcal{Q}(\tau,\tilde{\eta}_a,\tilde{\eta}_b,\tilde{a},\tilde{b})|\{p,f,s',c',s,c\}_m\big) = \\ &\delta_{a,\tilde{a}}\delta_{b,\tilde{b}}\delta(\eta_a-\tilde{\eta}_a)\delta(\eta_b-\tilde{\eta}_b)\delta\bigg(\tau-\frac{Q^2}{s}\bigg)\big|\{p,f,s',c',s,c\}_m\big)\ .\end{aligned} \tag{4.16}$$

[7] See for that also eq.(2.4) of [37].
[8] This corresponds to eq.(4.1)-(4.3) in [37].
[9] Strictly speaking it is not a measurement function as the variable τ cannot be measured.

On hadron level we write the cross section as

$$\frac{d\sigma_{\text{hadron}}}{d\tau} = \sum_{a,b} \int_0^1 d\eta_a \int_0^1 d\eta_b \frac{f_{a/A}\left(\eta_a, Q^2 e^{-t}\right) f_{b/B}(\eta_b, Q^2 e^{-t})}{4 n_c(a) n_c(b) 2\eta_a \eta_b p_A \cdot p_B} \times \left(1|\mathcal{Q}(\tau, \tilde{\eta}_a, \tilde{\eta}_b, \tilde{a}, \tilde{b}))|\rho_{\text{pert}}(t)\right) . \tag{4.17}$$

The energy fraction τ is in contrast to the transverse momentum an inclusive variable. As discussed in the beginning of this chapter we consider it in order to check whether the formalism of [1] can reproduce the results of [2] and [24]. This is in contrast to the reasoning given in [37] for the transverse momentum of the Z^0 boson. We cannot therefore simply define $d\sigma_{\text{hadron}}/d\tau$ by

$$\left(1|\mathcal{Q}(\tau)|\rho_{\text{pert}}(t)\right) , \tag{4.18}$$

with a hypothetical $\mathcal{Q}(\tau)$ given as

$$\mathcal{Q}(\tau)\big|\{p, f, s', c', s, c\}_m\big) = \delta\left(\tau - \frac{Q^2}{s}\right)\big|\{p, f, s', c', s, c\}_m\big) . \tag{4.19}$$

As discussed in the previous section we must consider the cross section in Mellin space. For the Mellin transform of $d\sigma/d\tau$ we write

$$\sigma_N = \int_0^1 d\tau \tau^{N-1} \frac{d\sigma}{d\tau} . \tag{4.20}$$

Further the Mellin transform of $\mathcal{Q}(\tau, \tilde{\eta}_a, \tilde{\eta}_b, \tilde{a}, \tilde{b})|\{p, f, s', c', s, c\}_m\big)$ is given by

$$\begin{aligned} &\mathcal{Q}(N; \tilde{\eta}_a, \tilde{\eta}_b, \tilde{a}, \tilde{b})|\{p, f, s', c', s, c\}_m) = \\ &\left(\frac{Q^2}{s}\right)^{N-1} \delta_{a,\tilde{a}} \delta_{b,\tilde{b}} \delta(\eta_a - \tilde{\eta}_a) \delta(\eta_b - \tilde{\eta}_b)|\{p, f, s', c', s, c\}_m) . \end{aligned} \tag{4.21}$$

We can therefore write

$$\sigma_N = (1|\mathcal{Q}(N; \tilde{\eta}_a, \tilde{\eta}_b, \tilde{a}, \tilde{b})|\{p, f, s', c', s, c\}_m) . \tag{4.22}$$

On hadron level we can write this as

$$(1|\mathcal{Q}(N)|\rho_{\text{pert}}(t)) = \sum_{a,b} \int_0^1 d\eta_a \int_0^1 d\eta_b \frac{f_{a/A}\left(\eta_a, Q^2 e^{-t}\right) f_{b/B}(\eta_b, Q^2 e^{-t})}{4 n_c(a) n_c(b) 2\eta_a \eta_b p_A \cdot p_B} \times (1|\mathcal{Q}(N; \eta_a, \eta_b, a, b)|\rho_{\text{pert}}(t)) . \tag{4.23}$$

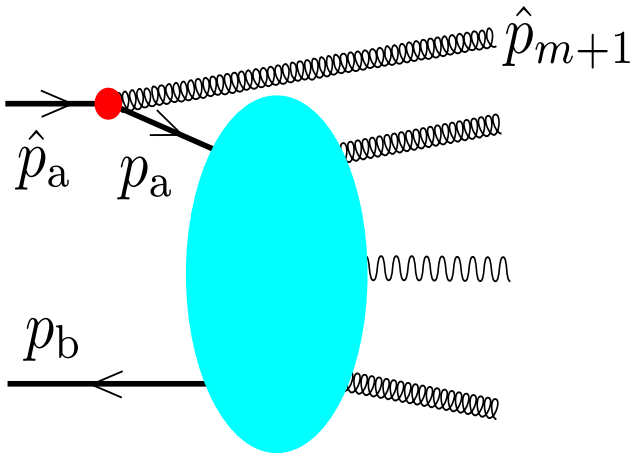

Figure 4.1: Schematic diagram for initial state splitting. This figure was taken from [37].

4.1.2 Kinematics of initial state splitting and definition of the energy fraction

Now we give a review of the kinematics given in [37] for parton splitting in Drell Yan processes[10]. We do this as we will need this in section (4.1.7) for the derivation of the differential cross section of the energy fraction[11].
In [37] the kinematics of the Drell Yan process is given in backward evolution as[12]

$$\begin{aligned} \hat{p}_{m+1} &= \frac{1-z}{z}(1+y)p_a + z\frac{y}{1+y}p_b + k_\perp \ , \\ \hat{p}_a &= \frac{1+y}{z}p_a \ , \\ \hat{p}_b &= p_b \ . \end{aligned} \tag{4.24}$$

Here we require that z must be in the range $0 < z < 1$, and $k_\perp$ is spacelike and orthogonal both to p_a and p_b. *Backward evolution*[13] means that the shower starts with the hard subprocess and the soft emissions in the initial

[10] A summary of this momentum mapping can be also found in section (3.4).
[11] For its definition see eq.(4.32).
[12] See for this also fig.(4.1).
[13] See for that also section (2.2.1).

state are generated after the hard process in shower time. It is presumed that the momenta of the partons are lightlike. With eq.(4.24) we obtain:

$$y = \frac{2\hat{p}_{m+1} \cdot \hat{p}_a}{2p_a \cdot p_b} \ . \tag{4.25}$$

As in [37] we will also use a shower time based on the virtuality

$$t = \log\left(\frac{Q^2}{2\hat{p}_{m+1} \cdot \hat{p}_a}\right) . \tag{4.26}$$

Between y and t we have the following relation

$$y = \frac{Q^2}{2p_a \cdot p_b} e^{-t} \ . \tag{4.27}$$

And for the variable z we have

$$\frac{\hat{p}_{m+1} \cdot p_b}{\hat{p}_a \cdot p_b} = 1 - z \ . \tag{4.28}$$

For the momentum fractions of the partons we may write

$$\begin{aligned} \hat{\eta}_a = \frac{1+y}{z}\eta_a = \frac{1}{z}\left[\eta_a + \frac{Q^2}{\eta_b s_0} e^{-t}\right] , \\ \hat{\eta}_b = \eta_b \ , \end{aligned} \tag{4.29}$$

where we have $s_0 = 2p_A \cdot p_B$ and $2p_a \cdot p_b = \eta_a \eta_b s_0$.
Finally we denote the azimuthal angle of $k_\perp$ with respect to the z axis[14] as ϕ. As all partons are lightlike we may write

$$\begin{aligned} 0 &= \hat{p}_{m+1}^2 \\ &= (1-z) y 2p_a \cdot p_b - \mathbf{k}_\perp^2 \\ &= (1-z) Q^2 e^{-t} - \mathbf{k}_\perp^2 \ , \end{aligned} \tag{4.30}$$

which leads us to

$$\mathbf{k}_\perp^2 = (1-z) Q^2 e^{-t} \ . \tag{4.31}$$

In section (4.1) we have already introduced the energy fraction in Drell Yan processes

$$\tau = \frac{Q^2}{s} \ . \tag{4.32}$$

[14]The z axis is considered to be in the direction of the beam.

We remind here that Q^2 is the center of mass energy of the two quarks at the interaction point (this means after all the soft gluon emission has occurred) where the Z boson is formed.
In fig.(4.1) we see the illustration of one single splitting:

$$Q^2 = (p_a + p_b)^2 = 2p_a \cdot p_b \ . \tag{4.33}$$

On the other hand s is defined as the center of mass energy of the two quarks before any soft gluon emission has occurred. For the case of one single splitting, illustrated in fig.(4.1), it is given as

$$s = (\hat{p}_a + \hat{p}_b)^2 = 2\hat{p}_a \cdot \hat{p}_b \ . \tag{4.34}$$

In section (4.1.4) we must also deal with the rapidity of the emitted gluon. In general it is given by

$$r = \frac{1}{2} \log \left(\frac{E + p_L}{E - p_L} \right) , \tag{4.35}$$

with E as the energy of the gluon and p_L as its longitudinal momentum. In the rest frame of the Z^0 boson this can be written as

$$r = \frac{1}{2} \log \left(\frac{(1-z)(1+y)^2}{z^2 y} \right) . \tag{4.36}$$

4.1.3 Strategy

In section (4.1.1) we have defined by eq.(4.15) the differential cross section for the energy fraction in Mellin space. We can now set up the evolution equation as

$$\begin{aligned} &\frac{d}{dt}(1|\mathcal{Q}(N;\eta_a,\eta_b,a,b)|\rho_{\text{pert}}(t)) = \\ &(1|\mathcal{Q}(N;\eta_a,\eta_b,a,b)[\mathcal{H}^{\text{pert}}(t) - \mathcal{V}^{\text{pert}}(t)]|\rho_{\text{pert}}(t)) \, , \end{aligned} \tag{4.37}$$

where we used the evolution equation (4.8) for $|\rho_{\text{pert}}(t))$. Our goal is now to approximate this evolution equation in order to get an expression of the following form

$$\frac{d}{dt}(1|\mathcal{Q}(N;\eta_a,\eta_b,a,b)|\rho_{\text{pert}}(t)) \approx -K(t,N)(1|\mathcal{Q}(N;\eta_a,\eta_b,a,b)|\rho_{\text{pert}}(t)) \ . \tag{4.38}$$

With such a kind of expression it is possible to write down the solution of eq.(4.37) as

$$\begin{aligned}&(1|\mathcal{Q}(N;\eta_a,\eta_b,a,b)|\rho_{\rm pert}(t_{\rm f}))\approx\\&\exp\left(-\int_0^{t_{\rm f}}dtK(t,N)\right)(1|\mathcal{Q}(N;\eta_a,\eta_b,a,b)|\rho_{\rm pert}(0))\ .\end{aligned}\tag{4.39}$$

$t_{\rm f}$ is here the time when the shower stops[15]. Then we can compare this with the result for the partonic cross section given in [2] where $\ln W_N(Q^2;Q_0^2)$ has been calculated. In order to get an expression like the one given in eq.(4.39) we will use two approximations derived in [37] in section (4.1.7). These will be given in the next section.

4.1.4 Approximations

Here we summarize the equations that will be later used in section (4.1.7). The operators $\mathcal{V}_a^{\rm pert}(t;z,\phi,f')$ and $\mathcal{H}_a(t;z,\phi,f')$ will be defined on page 66. The first one is eq.(8.12) of [37]

$$\begin{aligned}&(1|\mathcal{V}_a^{\rm pert}(t;z,\phi,f')|\{p,f,s',c',s,c\}_m)\approx\\&\frac{n_c(a)f_{(a+f')/A}\left(\frac{1+y}{z}\eta_a,Q^2e^{-t}\right)}{n_c(a+f')f_{a/A}\left(\eta_a,Q^2e^{-t}\right)}\frac{1}{1+y}(1|z\mathcal{H}_a^{\rm pert}(t;z,\phi,f')|\{p,f,s',c',s,c\}_m)\\&-\frac{\alpha_S(\mu_R^2)}{2\pi}\left(P_{a,a+f'}(z)\frac{f_{(a+f')/A}\left(\eta_a/z,Q^2e^{-t}\right)}{zf_{a/A}\left(\eta_a,Q^2e^{-t}\right)}-\delta_{f',g}\left[\frac{2C_a}{1-z}-\gamma_a\right]\right)\\&\times(1|\{p,f,s',c',s,c\}_m)\ ,\end{aligned}\tag{4.40}$$

with C_a given as

$$C_a=\begin{cases}C_F\ , & a\neq{\rm g}\\ C_A\ , & a={\rm g}\end{cases}\ .\tag{4.41}$$

For the derivation of eq.(8.12) in [37] eq.(8.5) and eq.(4.15)[16] of [37] has been used where $\hat{\eta}_a\approx\eta_a/z$ was taken. Instead of this it appears to us better to

[15] In section (4.4.1) we will call it also t_c for reasons that will become clear there.
[16] which corresponds to eq.(4.12).

retain $\hat{\eta}_a = \frac{1+y}{z}\eta_a$ and thus we obtain using eq.(4.12)

$$(1|\mathcal{H}_a(t;z,\phi,f')|\{p,f,s',c',s,c\}_m) = \frac{1}{1+y}\frac{n_c(a)f_{(a+f')/A}\left(\frac{1+y}{z}\eta_a, Q^2e^{-t}\right)}{n_c(a+f')f_{a/A}\left(\eta_a, Q^2e^{-t}\right)}$$
$$\times (1|z\mathcal{H}_a^{\text{pert}}(t;z,\phi,f')|\{p,f,s',c',s,c\}_m) \ . \tag{4.42}$$

That is the reason why we have in eq.(4.63) the additional factor $\frac{1}{1+y}$ in front of $(1|z\mathcal{H}_a^{\text{pert}}(t;z,\phi,f')|\{p,f,s',c',s,c\}_m)$.
The second one is eq.(7.13) of [37]:

$$\begin{aligned}&(1|z\mathcal{H}_a^{\text{pert}}(t;z,\phi,f')|\{p,f,s',c',s,c\}_m) \approx \\ &\delta_{f',g}\frac{\alpha_S(\mu_R^2)}{2\pi}C_a\frac{2}{1-z+y}(1|\{p,f,s',c',s,c\}_m) \ .\end{aligned} \tag{4.43}$$

For the derivation of eq.(7.13) of [37] it was presumed that the following relation holds

$$e^{2r} \gg e^{2r_k} \ . \tag{4.44}$$

Here r stands for the rapdity of the emitted gluon while r_k stands for the rapidity of the previously emitted gluon in the rest frame of the Z^0 boson. The consideration of [37] was conducted however in $\mathbf{b}$ space[17]. As we work here in Mellin space we must check whether this approximation is also valid in our case. We rewrite eq.(4.36) as

$$r = \frac{1}{2}\log\left[e^t\frac{\mathbf{k}_\perp^2}{Q^2}\frac{(1+y)^2}{z^2y}\right] \ . \tag{4.45}$$

As we will discuss in section (4.1.6) y must be in the soft limit close to zero. Further z must be close to 1 so we have for the rapiditiy of the emitted gluon

$$r \approx \frac{1}{2}\log\left[e^{2t}\frac{\mathbf{k}_\perp^2}{Q^2}\frac{2p_a\cdot p_b}{Q^2}\right] , \tag{4.46}$$

where eq. (4.27) has been used. We can therefore write

$$r \approx t + \frac{1}{2}\log\left(\frac{\mathbf{k}_\perp^2}{Q^2}\right) + \frac{1}{2}\log\left(\frac{2p_a\cdot p_b}{Q^2}\right) \ . \tag{4.47}$$

[17] $\mathbf{b}$ is the Fourier transform of $\mathbf{k}_\perp$.

By the same reasoning we have for the previously emitted gluon

$$r_k \approx t_k + \frac{1}{2}\log\left(\frac{\mathbf{k}_{\perp,k}^2}{Q^2}\right) + \frac{1}{2}\log\left(\frac{2p_a \cdot p_b}{Q^2}\right) \ . \tag{4.48}$$

Because of eq.(4.27) we conclude that emissions with large t are favored. This implies that we can presume for soft emissions

$$e^{2t} \gg e^{2t_k} \ . \tag{4.49}$$

And this implies that also for our case eq.(4.44) holds. Thus we can also apply eq.(4.43).

4.1.5 Final state splitting

In section (4.1.2) we have introduced momentum mapping for initial state splitting. Now we are forced to consider also final state splitting. Though in Drell Yan the outgoing leptons do not participate in the parton shower it is still possible that outgoing gluons from the incoming quarks can undergo further branching. Thus we can still have final state splitting. In [1] a mapping was chosen where the momenta of the final state splitting were taken to remain unchanged: $\hat{p}_a = p_a, \quad \hat{p}_b = p_b$.
In order to preserve both momentum conservation and keeping all partons on shell it was chosen to change all the momenta of the final state spectator partons by a Lorentz transformation

$$\hat{p}_j^\mu = \Lambda^\mu{}_\nu p_j^\nu \ , \quad j \neq \{l, m+1\} \ . \tag{4.50}$$

As the momenta of the initial state remain unchanged we conclude that final state splitting has no effect on the energy fraction at all. Thus we can for our purposes completely ignore final state splitting.

4.1.6 Initial state splitting

A little more complicated is the case for initial state splitting. For that we must first of all consider the effect of initial state splitting on Q^2 and s and by that on the energy fraction $\tau = \dfrac{Q^2}{s}$.

The center of mass energy after soft gluon emission: Q^2

Here we want to obtain the relation between Q^2 and $\hat{Q}^2$. Q^2 is defined as the center of mass energy at the interaction point this means where the Z^0

boson is formed:

$$Q^2 = 2p_a \cdot p_b \ . \tag{4.51}$$

If we look at fig.(4.1) we see that the parton momenta at the interaction point are not changed by parton splitting due to backward evolution. Thus we have

$$\hat{Q}^2 = 2p_a \cdot p_b = Q^2 \ . \tag{4.52}$$

The center of mass energy before soft gluon emission: s

With s being the center of mass energy of the two incoming partons before any splitting, we have at the beginning of the parton evolution

$$s = 2p_a \cdot p_b \ . \tag{4.53}$$

This means that we have for the energy fraction at the beginning of the evolution

$$\tau = \frac{Q^2}{s} = 1 \ . \tag{4.54}$$

After the splitting we have

$$\hat{s} = 2\hat{p}_a \cdot \hat{p}_b \ . \tag{4.55}$$

This is according to eq.(4.24)

$$\begin{aligned} \hat{s} &= 2\frac{1+y}{z} p_a \cdot p_b \\ &= \frac{1+y}{z} s \ . \end{aligned} \tag{4.56}$$

With that we obtain for the energy fraction

$$\hat{\tau} = \frac{z}{1+y}\tau \ . \tag{4.57}$$

In the high N limit which corresponds to soft gluon emission both τ and $\hat{\tau}$ are close[18] to 1. Thus y must be close to 0 and z close to 1.

[18] See for that eq.(4.2).

The evolution equation

Now we want to consider the evolution equation for the energy fraction distribution. For that let us return to equation (4.37). The operators $\mathcal{Q}$ and $\mathcal{V}^{\text{pert}}$ commute with each other. The reason for this lies in the fact that the non-splitting operator $\mathcal{V}^{\text{pert}}$ does not change the momenta and flavors of a partonic basis state $|\{p, f, s', c', s, c\}_m)$. Further it does not add a new parton. We can therefore write

$$\begin{aligned}\frac{d}{dt}(1|\mathcal{Q}(N;\eta_a,\eta_b,a,b)|\rho_{\text{pert}}(t)) =&(1|\mathcal{Q}(N;\eta_a,\eta_b,a,b)\mathcal{H}^{\text{pert}}(t)\\ &-\mathcal{V}^{\text{pert}}(t)\mathcal{Q}(N;\eta_a,\eta_b,a,b)|\rho_{\text{pert}}(t))\ .\end{aligned} \tag{4.58}$$

In order to proceed further we take the decompostion of $\mathcal{H}^{\text{pert}}(t)$ and $\mathcal{V}^{\text{pert}}(t)$ given in eq.(6.2) and eq.(6.3) of [37]

$$\begin{aligned}\mathcal{H}^{\text{pert}}(t) = \mathcal{H}_{\text{FS}}(t) &+ \int_0^1 dz \int_{-\pi}^{\pi} \frac{d\phi}{2\pi} \sum_{f'} \mathcal{H}_a^{\text{pert}}(t;z,\phi,f')\\ &+ \int_0^1 dz \int_{-\pi}^{\pi} \frac{d\phi}{2\pi} \sum_{f'} \mathcal{H}_b^{\text{pert}}(t;z,\phi,f')\ ,\\ \mathcal{V}^{\text{pert}}(t) = \mathcal{V}_{\text{FS}}(t) &+ \int_0^1 dz \int_{-\pi}^{\pi} \frac{d\phi}{2\pi} \sum_{f'} \mathcal{V}_a^{\text{pert}}(t;z,\phi,f')\\ &+ \int_0^1 dz \int_{-\pi}^{\pi} \frac{d\phi}{2\pi} \sum_{f'} \mathcal{V}_b^{\text{pert}}(t;z,\phi,f')\ .\end{aligned} \tag{4.59}$$

The entities $\mathcal{H}_{\text{FS}}$ and $\mathcal{V}_{\text{FS}}$ stand for final state splitting. As we are dealing with initial splitting they both commute with $\mathcal{Q}$ and yield therefore no contribution to the evolution. f' stands for the flavor of the emitted parton. For the commutator relation between $\mathcal{Q}(N;\eta_a,\eta_b,a,b)$ and $\mathcal{H}_a^{\text{pert}}(t;z,\phi,f')$ we must consider eq.(4.21) and eq.(4.29). The operator $\mathcal{Q}$ before splitting yields a factor $\left(\frac{Q^2}{s}\right)^{N-1}$ while after splitting a factor $\left(\frac{\hat{Q}^2}{\hat{s}^2}\right)^{N-1}$.

Thus we may write[19]

$$\begin{aligned}
&\mathcal{Q}(N;\eta_a,\eta_b,\eta_b,a,b)\mathcal{H}_a^{\rm pert}(t;z,\phi,f') = \\
&\frac{z}{1+y}\left(\frac{s}{\hat{s}}\right)^{N-1}\mathcal{H}_a^{\rm pert}(t;z,\phi,f')\mathcal{Q}\left(N;\frac{z}{1+y}\eta_a,\eta_b,a-f',b\right) = \\
&\left(\frac{z}{1+y}\right)^{N}\mathcal{H}_a^{\rm pert}(t;z,\phi,f')\mathcal{Q}\left(N;\frac{z}{1+y}\eta_a,\eta_b,a-f',b\right) \ .
\end{aligned} \tag{4.60}$$

The additional factor $\frac{z}{1+y}$ comes from a delta distribution given in eq.(4.21). Regarding the expression $a-f'$ we note that it stands for the flavor of parton a before the splitting $a = a - f'$. For the flavor mapping we write $u - \mathrm{g} = u$ or $\mathrm{g} - \bar{u} = u$ etc.

Thus we can write the evolution equation as

$$\begin{aligned}
&\frac{d}{dt}(1|\mathcal{Q}(N;\eta_a,\eta_b,a,b)|\rho_{per}(t)) = \\
&\int_0^1 dz \int_{-\pi}^{\pi}\frac{d\phi}{2\pi}\sum_{f'}(1|\mathcal{K}_a(t;z,\phi,f';N;\eta_a,\eta_b,a,b)|\rho_{\rm pert}(t)) \\
&+\int_0^1 dz \int_{-\pi}^{\pi}\frac{d\phi}{2\pi}\sum_{f'}(1|\mathcal{K}_b(t;z,\phi,f';N;\eta_a\eta_b,a,b)|\rho_{\rm pert}(t)) \ .
\end{aligned} \tag{4.61}$$

The operator $\mathcal{K}_a$ is here given by

$$\begin{aligned}
&(1|\mathcal{K}_a(t;z,\phi,f';N;\eta_a,\eta_b,a,b)|\rho_{\rm pert}(t)) = \\
&\left(1\left|\left[\mathcal{H}_a^{\rm pert}(t;z,\phi,f')\left(\frac{z}{1+y}\right)^{N}\mathcal{Q}(N;\frac{z}{1+y}\eta_a,\eta_b,a-f',b)\right.\right.\right. \\
&\left.\left.\left.-\mathcal{V}_a^{\rm pert}(t;z,\phi,f')\mathcal{Q}(N;\eta_a,\eta_b,a,b)\right]\right|\rho_{\rm pert}(t)\right) \ .
\end{aligned} \tag{4.62}$$

The expression for $\mathcal{K}_b$ is corresponding to that of $\mathcal{K}_a$.

4.1.7 Evolution up to the shower final time $t_{\rm f}$

In this section we are interested in the evolution of the energy fraction distribution up to a shower final time $t_{\rm f}$. What will be the proper value of $t_{\rm f}$ will be discussed in section (4.4.1) and (4.4.2). It is our goal to achieve a

[19] We remind here that $Q^2 = \hat{Q}^2$ holds.

factorization as it is written in eq.(4.38) and eq.(4.39). First of all we focus on the second term in $\mathcal{K}_a$ (see for that eq.(4.62)). Using eq.(4.40)[20] leads to

$$\begin{aligned}
&\left(1|\mathcal{V}_a^{\rm pert}(t;z,\phi,f')\mathcal{Q}(N;\eta_a,\eta_b,a,b)|\rho_{\rm pert}(t)\right) \approx \\
&\sum_m \frac{1}{m!}\int [d\{p,f,s',c',s,c\}_m] \\
&\Bigg\{ \frac{n_c(a) f_{(a+f')/A}\left(\frac{1+y}{z}\eta_a, Q^2 e^{-t}\right)}{n_c(a+f') f_{a/A}\left(\eta_a, Q^2 e^{-t}\right)} \frac{1}{1+y} \left(1|z\mathcal{H}_a^{\rm pert}(t;z,\phi,f')|\{p,f,s',c',s,c\}_m\right) \\
&- \frac{\alpha_S(\mu_R^2)}{2\pi}\left(P_{a,a+f'}(z) \frac{f_{(a+f')/A}\left(\eta_a/z, Q^2 e^{-t}\right)}{z f_{a/A}\left(\eta_a, Q^2 e^{-t}\right)} - \delta_{f',g}\left[\frac{2C_a}{1-z} - \gamma_a\right]\right) \\
&\times \left(1|\{p,f,s',c',s,c\}_m\right)\Bigg\} \left(\{p,f,s',c',s,c\}_m|\mathcal{Q}(N;\eta_a,\eta_b,a,b)|\rho_{\rm pert}(t)\right) \ .
\end{aligned} \tag{4.63}$$

Here we made use of the completeness relation given by eq.(3.23).
By using the completeness relation again eq.(4.63) can be rewritten as

$$\begin{aligned}
&\left(1|\mathcal{V}_a^{\rm pert}(t;z,\phi,f')\mathcal{Q}(N;\eta_a,\eta_b,a,b)|\rho_{\rm pert}(t)\right) \approx \\
&\frac{1}{1+y} \frac{n_c(a) f_{(a+f')/A}\left(\frac{1+y}{z}\eta_a, Q^2 e^{-t}\right)}{n_c(a+f') f_{a/A}\left(\eta_a, Q^2 e^{-t}\right)} \\
&\times \left(1|z\mathcal{H}_a^{\rm pert}(t;z,\phi,f')\mathcal{Q}(N;\tilde{\eta}_a,\tilde{\eta}_b,\tilde{a},\tilde{b})|\rho_{\rm pert}(t)\right) \\
&- \frac{\alpha_S(\mu_R^2)}{2\pi}\left(P_{a,a+f'}(z) \frac{f_{(a+f')/A}\left(\eta_a/z, Q^2 e^{-t}\right)}{z f_{a/A}\left(\eta_a, Q^2 e^{-t}\right)} - \delta_{f',g}\left[\frac{2C_a}{1-z} - \gamma_a\right]\right) \\
&\times \left(1|\mathcal{Q}(N;\eta_a,\eta_b,a,b)|\rho_{\rm pert}(t)\right) \ .
\end{aligned} \tag{4.64}$$

We remind that in [2] and [24] the case of soft gluon emission was considered. Thus it seems important to us to consider the case of soft gluon emission for the evolution of the energy fraction as well. According to eq.(4.28) the following relation holds

$$\frac{\hat{p}_{m+1}\cdot p_b}{\hat{p}_a \cdot p_b} = 1 - z \ . \tag{4.65}$$

The situation where $\hat{p}_{m+1}$ becomes small compared to $\hat{p}_a$ therefore corresponds to

$$(1-z) \ll 1 \ . \tag{4.66}$$

[20] which corresponds to eq.(8.12) of [37]

Then we have according to eq.(4.43)[21]

$$
\begin{aligned}
&(1|z\mathcal{H}_a^{\rm pert}(t;z,\phi;f^{'})|\{p,f,s',c',s,c\}_m) \approx \\
&\delta_{f',g}\frac{\alpha_S(\mu_R^2)}{2\pi}C_a\frac{2}{1-z+y}(1|\{p,f,s',c',s,c\}_m)
\end{aligned}
\tag{4.67}
$$

As we deal only with gluon emission (which is further only soft) we obtain the following approximation for $\mathcal{K}_a$

$$
\begin{aligned}
&(1|\mathcal{K}_a(t;z,\phi,f';N;\tilde{\eta}_a,\tilde{\eta}_b,\tilde{a},\tilde{b})|\rho_{\rm pert}(t)) \approx \\
&\Bigg\{\delta_{f',g}\frac{\alpha_S(\mu_R^2)}{2\pi}C_a\frac{2}{1-z+y} \\
&\times\left(\frac{z^{N-1}}{(1+y)^N}-\frac{1}{1+y}\frac{n_c(a)f_{(a+f')/A}\left(\frac{1+y}{z}\eta_a,Q^2e^{-t}\right)}{n_c(a+f')f_{a/A}\left(\eta_a,Q^2e^{-t}\right)}\right) \\
&+\frac{\alpha_S(\mu_R^2)}{2\pi}\left(P_{a,a+f'}(z)\frac{f_{(a+f')/A}\left(\eta_a/z,Q^2e^{-t}\right)}{zf_{a/A}\left(\eta_a,Q^2e^{-t}\right)}-\delta_{f',g}\left[\frac{2C_a}{1-z}-\gamma_a\right]\right)\Bigg\} \\
&\times(1|\mathcal{Q}(N;\eta_a,\eta_b,a,b)|\rho_{\rm pert}(t))\ .
\end{aligned}
\tag{4.68}
$$

So we have the desired factorization formulation[22]. Let us take now a look at eq.(4.61). The integration over ϕ is simple as we have no ϕ dependent term; so this yields only a trivial factor.
According to eq.(4.61), eq.(4.38) and eq.(4.39) we must perform for $\mathcal{K}_a$ an integration over the shower time t and an integration over the variable z. Let us substitute t by $\mathbf{k}_\perp^2$. Then we define the following entity

$$
\begin{aligned}
S:=&\int_0^1 dz\int_{(1-z)Q^2e^{-t_{\rm f}}}^{(1-z)Q^2}\frac{d\mathbf{k}_\perp^2}{\mathbf{k}_\perp^2}C_a\frac{\alpha_S(\mu_R^2)}{2\pi}\frac{2}{1-z+y} \\
&\times\left(\frac{z^{N-1}}{(1+y)^N}-\frac{1}{1+y}\frac{n_c(a)f_{(a+f')/A}\left(\frac{1+y}{z}\eta_a,Q^2e^{-t}\right)}{n_c(a+f')f_{a/A}\left(\eta_a,Q^2e^{-t}\right)}\right)\ .
\end{aligned}
\tag{4.69}
$$

S stands here for the first term in $\mathcal{K}_a$ integrated over ϕ, z and t.
We can perform a further approximation. According to section (4.1.6) y

[21] which corresponds to eq.(7.13) of [37]
[22] See for that eq.(4.62) and eq.(4.61).

must be close to 0 while z must be close to 1. Further gluon emission does not change the flavor of a quark. Thus we can set

$$\frac{1}{1+y}\frac{n_c(a)f_{(a+f')/A}\left(\frac{1+y}{z}\eta_a, Q^2e^{-t}\right)}{n_c(a+f')f_{a/A}(\eta_a, Q^2e^{-t})} \approx 1 \ . \tag{4.70}$$

We must be however careful as $f_{a/A}$ is in some areas of η_a a steeply falling function. By using a Taylor expansion around η_a for $f_{a/A}$ we can write

$$\begin{aligned} f_{a/A}\left(\frac{1+y}{z}\eta_a, Q^2e^{-t}\right) &\approx f_{a/A}\left(\eta_a, Q^2e^{-t}\right) \\ &+ \left(\frac{1+y}{z}-1\right)\eta_a\frac{\partial f_{a/A}\left(\eta_a, Q^2e^{-t}\right)}{\partial\eta_a} \ . \end{aligned} \tag{4.71}$$

Thus eq.(4.70) holds for

$$\left(\frac{1+y}{z}-1\right)\eta_a\frac{\partial f_{a/A}\left(\eta_a, Q^2e^{-t}\right)}{\partial\eta_A} \approx 0 \ . \tag{4.72}$$

But as $f_{a/A}$ is in some areas of η_a a steeply falling function this presupposes that $\dfrac{1+y}{z}$ is extremely close to 1. Thus the approximation given in eq.(4.70) must be considered with caution.
So we have

$$\begin{aligned} S \approx \int_0^1 dz \int_{(1-z)Q^2e^{-t_{\rm f}}}^{(1-z)Q^2} \frac{d\mathbf{k}_\perp^2}{\mathbf{k}_\perp^2}C_a\frac{\alpha_S\left(\mu_R^2\right)}{2\pi}\frac{2}{1-z+y} \\ \times\left(\frac{z^{N-1}}{(1+y)^N}-1\right) \ . \end{aligned} \tag{4.73}$$

For the second term in $\mathcal{K}_a$ we consider now the following expression

$$\begin{aligned} B := \sum_{f'}\int_0^{t_{\rm f}} dt \int_0^1 dz \frac{\alpha_S(\mu_R^2)}{2\pi} \\ \times\left(P_{a,a+f'}(z)\frac{f_{(a+f')/A}\left(\eta_a/z, Q^2e^{-t}\right)}{zf_{a/A}\left(\eta_a, Q^2e^{-t}\right)} - \delta_{f',g}\left[\frac{2C_a}{1-z}-\gamma_a\right]\right) \ . \end{aligned} \tag{4.74}$$

We can make now use of the DGLAP equations in order to solve this integral. They are given by[23]

$$\frac{d}{dt}f_{a/A}\left(\eta_a, Q^2e^{-t}\right) = -\int_0^1 dz \sum_{f'} \frac{\alpha_S(\mu_R^2)}{2\pi}$$
$$\times \left\{ \frac{1}{z} P_{a,a+f'}(z) f_{(a+f')/A}\left(\eta_a/z, Q^2e^{-t}\right) - \delta_{f',g}\left[\frac{2C_a}{1-z} - \gamma_a\right] f_{a/A}\left(\eta_a, Q^2e^{-t}\right)\right\}$$
$$+ \mathcal{O}(\alpha_S^2) \ . \tag{4.75}$$

So this leads to

$$\begin{aligned} B = &\sum_{f'} \int_0^{t_\mathrm{f}} dt \int_0^1 dz \frac{\alpha_S\left(\mu_R^2\right)}{2\pi} \left\{ \frac{1}{z} P_{a,a+f'}(z) f_{(a+f')/A}\left(\eta_a/z, Q^2e^{-t}\right) \right. \\ &\left. - \delta_{f',g}\left[\frac{2C_a}{1-z} - \gamma_a\right] f_{a/A}\left(\eta_a, Q^2e^{-t}\right) \right\} \frac{1}{f_{a/A}\left(\eta_a, Q^2e^{-t}\right)} = \\ &- \int_0^{t_\mathrm{f}} dt \left(\frac{d}{dt} f_{a/A}\left(\eta_a, Q^2e^{-t}\right) \right) \frac{1}{f_{a/A}\left(\eta_a, Q^2e^{-t}\right)} = \\ &- \int_0^{t_\mathrm{f}} dt \frac{d}{dt} \ln(f_{a/A}\left(\eta_a, Q^2e^{-t}\right)) = \\ &- \left\{ \ln\left[f_{a/A}\left(\eta_a, Q^2e^{-t_\mathrm{f}}\right)\right] - \ln\left[f_{a/A}\left(\eta_a, Q^2\right)\right] \right\} . \end{aligned} \tag{4.76}$$

We take this together with the result of eq.(4.73).
This yields[24]

$$\begin{aligned} &\int_0^{t_\mathrm{f}} dt \int_0^1 dz \sum_{f'} (1|\mathcal{K}_a(t; z, f'; N; \tilde{\eta}_a, \tilde{\eta}_b, \tilde{a}, \tilde{b})|\rho_{\mathrm{pert}}(t)) = \\ &\left(\int_0^1 dz \int_{(1-z)Q^2e^{-t_\mathrm{f}}}^{(1-z)Q^2} \frac{d\mathbf{k}_\perp^2}{\mathbf{k}_\perp^2} C_a \frac{\alpha_S(\mu_R^2)}{2\pi} \frac{2}{1-z+y} \left(\frac{z^{N-1}}{(1+y)^N} - 1 \right) \right. \\ &\left. - \frac{\ln\left[f_{a/A}(\eta_a, Q^2e^{-t_\mathrm{f}})\right]}{\ln[f_{a/A}(\eta_a, Q^2)]} \right) \left(1|\mathcal{Q}(N; \eta_a, \eta_b, a, b)|\rho_{\mathrm{pert}}(t_\mathrm{f})\right) \ . \end{aligned} \tag{4.77}$$

By taking a look at eq.(4.39) and eq.(4.61) we get[25]

$$\begin{aligned} (1|\mathcal{Q}(N; \eta_a, \eta_b, a, b)|\rho_{\mathrm{pert}}(t_\mathrm{f})) = (1|\mathcal{Q}(N; \eta_a, \eta_b, a, b)|\rho_{\mathrm{pert}}(0)) \\ \times W_{N,\,\mathrm{PS}} \end{aligned} \tag{4.78}$$

[23] See for that eq.(8.9) of [37].
[24] Where the variable ϕ as integration over it $\frac{d\phi}{2\pi}$ only yields a trivial one factor.
[25] Where we used $\tilde{\eta}_a \approx \eta_a$ which is valid for the soft case.

with

$$\ln W_{N,\,\mathrm{PS}} = \int_0^1 dz \int_{(1-z)Q^2 e^{-t_\mathrm{f}}}^{(1-z)Q^2} \frac{d\mathbf{k}_\perp^2}{\mathbf{k}_\perp^2} C_a \frac{\alpha_S\left(\mu_R^2\right)}{2\pi} \frac{2}{1-z+y} \times \left(\frac{z^{N-1}}{(1+y)^N} - 1\right) - \ln\left[\frac{f_{a/A}(\eta_a, Q^2 e^{-t_\mathrm{f}})}{f_{a/A}(\eta_a, Q^2)}\right] + b \longleftrightarrow a \ . \tag{4.79}$$

The second term in $\ln W_{N,\,\mathrm{PS}}$ contains no dependence on N. Thus we can neglect it with respect to the first term in the high N limit:

$$\ln\left[\frac{f_{a/A}\left(\eta_a, Q^2 e^{-t_\mathrm{f}}\right)}{f_{a/A}(\eta_a, Q^2)}\right] \approx 0 \ . \tag{4.80}$$

We obtain therefore

$$\ln W_{N,\,\mathrm{PS}} = 2\int_0^1 dz \int_{(1-z)Q^2 e^{-t_\mathrm{f}}}^{(1-z)Q^2} \frac{d\mathbf{k}_\perp^2}{\mathbf{k}_\perp^2} C_a \frac{\alpha_S\left(\mu_R^2\right)}{2\pi} \frac{2}{1-z+y} \times \left(\frac{z^{N-1}}{(1+y)^N} - 1\right) . \tag{4.81}$$

The factor 2 comes from quark b.
On hadron level the solution can be written as

$$(1|\mathcal{Q}(N)|\rho(t_\mathrm{f})) = \sum_{a,b} \int_0^1 d\eta_a \int_0^1 d\eta_b \frac{f_{a/A}\left(\eta_a, Q^2 e^{-t_\mathrm{f}}\right) f_{b/B}\left(\eta_b, Q^2 e^{-t_\mathrm{f}}\right)}{4 n_c(a) n_c(b) 2\eta_a \eta_b p_A \cdot p_B} \times (1|\mathcal{Q}(N;\eta_a,\eta_b,a,b)|\rho_{\mathrm{pert}}(t_\mathrm{f})) \ . \tag{4.82}$$

4.2 Comparison with published results

The next step is to compare the result we have derived with that of [2] and [24]. In [2] resummation techniques have been used in order to obtain the differential cross section of the energy fraction in Drell Yan processes. In [24] it was shown that the same result can be obtained inside the frame of a Monte Carlo event generator with angular ordering. The result is given by[26]

$$\ln W_{N,\,\mathrm{res}} = 2\frac{C_F}{\pi} \int_0^1 d\zeta \frac{\zeta^{N-1} - 1}{1-\zeta} \int_{Q_0^2}^{(1-\zeta)^2 Q^2} \frac{d\mathbf{k}_\perp^2}{\mathbf{k}_\perp^2} \alpha_S(\mathbf{k}_\perp^2) \ . \tag{4.83}$$

[26] See eq.(2.14) of [2] and eq.(36) of [24]. The variable z of [2] and [24] has been relabeled into ζ as the z used here is another variable. See for that also eq.(4.91). Please note that $\alpha_S(\mu_R^2)$ is indirectly dependent on $\mathbf{k}_\perp^2$ via the scale μ_R^2.

Here we have

$$1 - \zeta = \omega_q / E \ . \tag{4.84}$$

Here is E is the energy of the two partons in the center of mass frame before the shower takes place

$$p_1^0 = p_2^0 = E \ , \tag{4.85}$$

and ω_q is the energy of the emitted gluon. Now it is our goal to see whether the same result can be obtained inside the frame of the parton shower formalism. In order to understand the relation between the two expressions we must find a relation between the two splitting variables: z and ζ. The z is defined by the momentum mapping given in eq.(4.24). We remind that for z we have

$$\frac{\hat{p}_{m+1} \cdot p_b}{\hat{p}_a \cdot p_b} = 1 - z \ . \tag{4.86}$$

By application of eq.(4.24) we may write

$$\begin{aligned} p_b &= (E, 0, 0, -E) \\ \hat{p}_{m+1} &= \left(\omega_q, \mathbf{k}_\perp, \frac{1-z}{z}(1+y)E - z\frac{y}{1+y}E \right) \\ \hat{p}_a &= \frac{1+y}{z}(E, 0, 0, E) \ . \end{aligned} \tag{4.87}$$

With that we can derive a relation between z and ζ. So we have

$$\hat{p}_{m+1} \cdot p_b = \left\{ E^2(1-\zeta) + E^2 \left[\frac{1-z}{z}(1+y) - z\frac{y}{1+y} \right] \right\} \tag{4.88}$$

and

$$\hat{p}_a \cdot p_b = \frac{1+y}{z}(E^2 + E^2) = 2\frac{1+y}{z}E^2 \ . \tag{4.89}$$

This leads to

$$\frac{\hat{p}_{m+1} \cdot p_b}{\hat{p}_a \cdot p_b} = \frac{(1-\zeta) + \frac{1-z}{z}(1+y) - z\frac{y}{1+y}}{2\frac{1+y}{z}} \stackrel{!}{=} 1 - z \ . \tag{4.90}$$

From this relation follows

$$\begin{aligned} 2\frac{1+y}{z}(1-z) &= 1 - \zeta + \frac{1-z}{z}(1+y) - z\frac{y}{1+y} \\ \Rightarrow \frac{1+y}{z}(1-z) &= 1 - \zeta - z\frac{y}{1+y} \\ \Rightarrow \zeta &= 1 - \frac{1+y}{z}(1-z) - z\frac{y}{1+y} \ . \end{aligned} \tag{4.91}$$

The last line is the exact relation between ζ and z. Obviously both entities are not identical.
We derive now an expression for ζ in the semi-inclusive limit. Here z is close to 1 (see for that section (4.1.6)) so that we can write

$$z = 1 - \alpha \ , \tag{4.92}$$

where α must be treated as a small number. As we mentioned in section (4.1.6) also y must be small compared to 1 for soft gluon emission. So we can make the following approximation

$$\begin{aligned} \zeta &\approx 1 - (1+y)(1+\alpha)\alpha - (1-\alpha)y(1-y) \\ &\approx 1 - (1+\alpha+y)\alpha - y(1-y) \\ &\approx 1 - \alpha - y = z - y \ . \end{aligned} \tag{4.93}$$

Now we focus on the expression

$$\frac{\zeta^{N-1} - 1}{1 - \zeta} \ , \tag{4.94}$$

which we find in eq.(4.83). We have

$$1 - \zeta \approx 1 - z + y \ . \tag{4.95}$$

So the denominator is the same as the corresponding expression $1 - z + y$ we find in eq.(4.81). Then let us investigate the numerator. We have (for a sufficiently small y so that terms which are of order N^2y^2 or smaller can be neglected)

$$\frac{z^{N-1}}{(1+y)^N} \approx (z(1-y))^{N-1} = ((1-\alpha)(1-y))^{N-1} \tag{4.96}$$

so

$$\begin{aligned} ((1-\alpha)(1-y))^{N-1} &\approx (1-y-\alpha)^{N-1} = (z-y)^{N-1} \\ &= \zeta^{N-1} \ . \end{aligned} \tag{4.97}$$

As we deal with incoming quarks which emit soft gluons we have according to eq.(4.41) $C_a = C_F$.
Up to now we have no fixed value for t_f. We[27] can identify the lower integration boundary $(1-z)Q^2e^{-t_\mathrm{f}}$ in eq.(4.81) with Q_0^2 in eq.(4.83).

[27]The proper value of t_f will be later discussed in section (4.4.1) and (4.4.2).

A bit more tricky is the case of the upper integration boundary. We must compare the expression

$$(1-z+y)^2Q^2 \tag{4.98}$$

with

$$(1-z)Q^2 \ . \tag{4.99}$$

Obviously the two expressions are not identical. In order to proceed further we note that the following manipulation is possible

$$\int_{Q_0^2}^{(1-\zeta)^2Q^2} \frac{d\mathbf{k}_\perp^2}{\mathbf{k}_\perp^2}\alpha_S(\mathbf{k}_\perp^2) = \int_{Q_0^2}^{Q^2} \frac{d\mathbf{k}_\perp^2}{\mathbf{k}_\perp^2}\alpha_S\left(\mathbf{k}_\perp^2\right)\theta\left(\mathbf{k}_\perp^2 \leq (1-\zeta)^2Q^2\right) \ . \tag{4.100}$$

Now we can switch the θ function to the ζ integration inside $\ln W_{N,\,\mathrm{res}}$. The result is

$$\begin{aligned}\ln W_{N,\,\mathrm{res}} =& 2\frac{C_F}{\pi}\int_{Q_0^2}^{Q^2} \frac{d\mathbf{k}_\perp^2}{\mathbf{k}_\perp^2}\alpha_S\left(\mathbf{k}_\perp^2\right) \\ & \times \int_0^{1-\sqrt{\mathbf{k}_\perp^2/Q^2}} d\zeta \frac{\zeta^{N-1}-1}{1-\zeta} \ .\end{aligned} \tag{4.101}$$

According to the same reasoning we may write

$$\begin{aligned}\ln W_{N,\,\mathrm{PS}} =& 2\frac{C_F}{\pi}\int_{Q_0^2}^{Q^2} \frac{d\mathbf{k}_\perp^2}{\mathbf{k}_\perp^2}\alpha_S\left(\mathbf{k}_\perp^2\right) \\ & \times \int_0^{1-\mathbf{k}_\perp^2/Q^2} dz \frac{1}{1-z+y}\left(\frac{z^{N-1}}{(1+y)^N}-1\right) \ .\end{aligned} \tag{4.102}$$

We see that for the $\mathbf{k}_\perp^2$ integration the boundaries of the two expressions are now identical. (However for the z and the ζ integration the upper boundary is not identical anymore). As y is small we must compare the two relations[28]

$$z \leq 1-\sqrt{\mathbf{k}_\perp^2/Q^2}+y \approx 1-\sqrt{\mathbf{k}_\perp^2/Q^2} \tag{4.103}$$

with

$$z \leq 1-\mathbf{k}_\perp^2/Q^2 \ . \tag{4.104}$$

Later in section (4.4.2) we will see that (in the large N limit) for $\ln W_N$ those $z's$ that fullfill eq.(4.143)

$$z \geq 1-e^{-\gamma_E}/N \tag{4.105}$$

[28] because of $z \approx \zeta + y$. See for that eq.(4.93).

can be neglected. When $\mathbf{k}_\perp^2$ is sufficiently small we have

$$\begin{aligned} &1 - \mathbf{k}_\perp^2/Q^2 \geq 1 - e^{-\gamma_E}/N \\ &\text{and} \\ &1 - \sqrt{\mathbf{k}_\perp^2/Q^2} \geq 1 - e^{-\gamma_E}/N \ . \end{aligned} \tag{4.106}$$

Now in the $\mathbf{k}_\perp^2$ integration the small $\mathbf{k}_\perp^2$ is strongly favored because of the factor $\mathbf{k}_\perp^{-2}$. So the two results are approximately equal if $\sqrt{\frac{Q_0^2}{Q^2}} \leq e^{-\gamma_E}/N$.

We can compute the difference between $\ln W_{N,\,\mathrm{res}}$ and $\ln W_{N,\,\mathrm{PS}}$. Let us first of all focus on the case where α_S is constant. We take further the approximation that y is small compared to $1-z$ and can be treated inside $\frac{z^{N-1}}{(1+y)^N}$ as zero. This is justified for the high t limit (see for that eq.(4.27)). In that case we may write

$$\ln W_{N,\,\mathrm{PS}} = 2\frac{\alpha_S}{\pi} C_F \int_0^1 dz \ln\left[\frac{(1-z)Q^2}{Q_0^2}\right] \frac{z^{N-1}-1}{1-z} \tag{4.107}$$

and

$$\ln W_{N,\,\mathrm{res}} = 2\frac{\alpha_S}{\pi} C_F \int_0^1 d\zeta \frac{\zeta^{N-1}-1}{1-\zeta} \ln\left[\frac{(1-\zeta)^2Q^2}{Q_0^2}\right] \ . \tag{4.108}$$

As ζ has now just the role of an integral parameter we can relabel it into z. Thus we can write for the difference

$$\ln W_{N,\,\mathrm{res}} - \ln W_{N,\,\mathrm{PS}} = 2\frac{\alpha_S}{\pi} C_F \int_0^1 dz \frac{z^{N-1}-1}{1-z} \ln(1-z) \ . \tag{4.109}$$

What does this result[29] actually mean? It is written in terms of $\ln(1-z)$. This implies that our parton shower algorithm (which uses virtual ordering) does not resum completely terms of $\ln(1-z)$ as standard resummation techniques. According to [24] a Monte Carlo algorithm that uses angular ordering can also reproduce $\ln W_{N,\,\mathrm{res}}$ given in eq.(4.83). The difference comes from different upper boundaries for the $\mathbf{k}_\perp^2$ integration (which corresponds to $t = 0$). They are the result of two different ordering variables: in our formalism virtuality is taken as an ordering variable; in [24] effectively angular ordering is used. As the upper boundary of the integration is $(1-z)^2Q^2$ this corresponds effectively to transverse momentum ordering. Now the ordering

[29] This integral can be analytically calculated. The result can be found in the appendix.

variable is not just for the parton shower relevant but also for the pdf. The usual $\overline{\text{MS}}$ scheme actually presupposes a $\mathbf{k}_\perp^2$ ordering. Absorbing the pole into the pdfs means at one loop to make a cut on the transverse momentum. This implies that any parton splitting with $\mathbf{k}_\perp^2 < \mu_0^2$ is[30] integrated into the pdf while splittings with higher transverse momentum are part of the parton shower. Thus it is appropriate to use a $\mathbf{k}_\perp^2$ ordered shower together with $\overline{\text{MS}}$ pdfs.
How is now the situation in a virtuality ordered shower? For that we recall that the scale μ_F^2 inside the pdfs[31] is given by $Q^2 e^{-t}$. Thus we have inside the pdfs as a[32] scale $\mathbf{k}_\perp^2/(1-z)$ and not $\mathbf{k}_\perp^2$. This kind of mismatch inside the pdfs must be taken into account. A possibility are new pdfs which are based on a virtuality ordered renormalization scheme. A new renormalization scheme actually means that the finite part (inside the contribution to the structure function F_2) is distributed between the pdfs and the shower in a different way[33].

4.3 Integration

The next step is to compare the previous analytical result for the Drell Yan process with results from a Monte Carlo event generator. This will be done in section (4.4). For that we need explicit numerical expressions from the analytical result given in eq.(4.83). Thus we perform the integration explicitly. For that we will make use of MATHEMATICA[34]. Further we relabel ζ to z and write instead of $\ln W_{N,\,\text{res}}$ just $\ln W_N$. Now we describe our strategy to deal with $\ln W_N$ for the general case when α_S is not constant. Then only a numerical integration is possible. For the z integration inside $\ln W_N$ we must deal with the following expression[35]

$$\int_0^{1-\sqrt{\mathbf{k}_\perp^2/Q^2}} dz \frac{z^{N-1}-1}{1-z} \ . \tag{4.110}$$

This integration can be performed analytically. The result is given by

$$\int_0^{1-\sqrt{\mathbf{k}_\perp^2/Q^2}} dz \frac{z^{N-1}-1}{1-z} = B_\varepsilon(N,0) + \frac{1}{2}\ln\left[\mathbf{k}_\perp^2/Q^2\right] \tag{4.111}$$

[30] where μ_0^2 is the factorization scale.

[31] which is related to the virtuality y by $y = \frac{\mu_F^2}{2p_a\cdot p_b}$

[32] See for that eq.(4.31).

[33] See for that section (4.3.2) in [3].

[34] For a description see [50].

[35] See for that eq.(4.101).

with

$$\varepsilon = 1 - \sqrt{\frac{\mathbf{k}_\perp^2}{Q^2}} \ . \tag{4.112}$$

$B_\varepsilon(N,0)$ is here the Betafunction. With that we can write now

$$\ln W_N = 2C_F \int_{Q_0^2}^{Q^2} \frac{d\mathbf{k}_\perp^2}{\mathbf{k}_\perp^2} \left(B_\varepsilon(N,0) + \ln\left[\sqrt{\mathbf{k}_\perp^2/Q^2}\right] \right) \frac{\alpha_S\left(\mathbf{k}_\perp^2\right)}{\pi} \ . \tag{4.113}$$

For this expression a numerical integration can be performed. Examples for this can be seen in fig.(A.3) and fig.(A.4) which can be found in the appendix. In the appendix we will see that for the case that α_S is constant it is possible to perform for $\ln W_N$ an analytical integration. However it will be shown that this result is numerically unstable. Thus even for constant α_S it is meaningful to use eq.(4.113).

4.4 Comparison of the analytical result with a Monte Carlo event generator

In the previous sections we derived an expression for the energy fraction distribution τ in Drell Yan processes[36]. We applied the analytical formalism that had been developed in [1] together with simplifications of it given in [37]. We showed that this result (see eq.(4.78) and (4.81)) is equivalent under special conditions to another result that was derived with resummation techniques in [2] in the soft limit. However in general we have a disagreement with respect to an integration boundary due to the usage of different ordering variables. In [24] it was shown that this result (the one given by eq.(4.83)) should be reproduced in a Monte Carlo event generator that uses angular ordering[37].
In this section it is our goal to confirm this result. At first we must fix the value[38] of the final shower time t_f which will be done in the following section. Then we will compare the analytical result with a simulation from PYTHIA.

[36] For its definition see eq.(4.32).

[37] For leading soft and collinear logarithms only the angular ordered region of phase space plays a significant role. Outside of this region we have destructive interference. This is called *color coherence*. See for that section (3) of [24]. HERWIG has angular ordering by construction while PYTHIA is supposed to have it effectively.

[38] See for that section (4.1.7).

4.4.1 Consideration for the shower time t_{f}

For the derivation of the shower time t_{f} we consider now the evolution of the energy fraction on hadron level. Strictly speaking there is not one "right" value for t_{f}. However we would like to reflect what is the most natural choice. The evolution equation for that is written as

$$\frac{d}{dt}(1|\mathcal{Q}(N)|\rho(t)) = (1|\mathcal{Q}(N)[\mathcal{H}(t) - \mathcal{V}(t)]|\rho(t)) \ . \tag{4.114}$$

This is in correspondence to eq.(10.1) of [37] where in the hadronic differential cross section $(1|\mathcal{Q}(\mathbf{b}, Y)|\rho(t))$ for the transverse momentum the evolution stops above some critcal time t_c. Please note that this is the evolution equation for the hadronic cross section $(1|\mathcal{Q}(N)|\rho(t))$ and not $(1|\mathcal{Q}(N; \eta_a, \eta_b, a, b|\rho(t))$ for the differential cross section of the energy fraction on parton level. We are interested in the question whether evolution for the energy fraction stops for the high t case in a similar way as for the transverse momentum[39].
For that we rewrite the splitting operators as

$$\begin{aligned} \mathcal{H}(t) &= \int_0^1 dz \mathcal{H}(t, z) \\ \mathcal{V}(t) &= \int_0^1 dz \mathcal{V}(t, z) \ . \end{aligned} \tag{4.115}$$

Then we can rewrite eq.(4.114) as[40]

$$\begin{aligned} \frac{d}{dt}(1|\mathcal{Q}(N)|\rho(t)) &= \int_0^1 dz (1|\mathcal{Q}(N)[\mathcal{H}(t, z) - \mathcal{V}(t, z)]|\rho(t)) \\ &= (1|\mathcal{Q}(N)\mathcal{H}(t, z) - \mathcal{V}(t, z)\mathcal{Q}(N)|\rho(t)) \ . \end{aligned} \tag{4.116}$$

Now we focus on the term $\mathcal{Q}(N)\mathcal{H}(t, z)$. The following relation holds

$$\mathcal{Q}(N)\mathcal{H}(t, z)|\rho(t)) = \left(\frac{\hat{Q}^2}{\hat{s}}\right)^{N-1} \left(\frac{s}{Q^2}\right)^{N-1} \mathcal{H}(t, z)\mathcal{Q}(N)|\rho(t)) \ . \tag{4.117}$$

We have (see for that fig.(4.1) and eq.(4.24))

$$Q^2 = \hat{Q}^2 \tag{4.118}$$

[39] See for that section (9) and (10) of [37].
[40] As the measurement operator $\mathcal{Q}$ and the non splitting operator $\mathcal{V}$ commute with each other.

and

$$\begin{aligned} \hat{s} &= 2\hat{p}_a \cdot \hat{p}_b \\ s &= 2p_a \cdot p_b \ . \end{aligned} \tag{4.119}$$

Thus we get

$$\begin{aligned} \mathcal{Q}(N)\mathcal{H}(t,z) &= \left(\frac{p_a \cdot p_b}{\hat{p}_a \cdot \hat{p}_b}\right)^{N-1} \mathcal{H}(t,z)\mathcal{Q}(N) \\ \Rightarrow \mathcal{Q}(N)\mathcal{H}(t,z) &= \left(\frac{z}{1+y}\right)^{N-1} \mathcal{H}(t,z)\mathcal{Q}(N) \ . \end{aligned} \tag{4.120}$$

In the high t case we can use (see for that also eq.(4.27))

$$y = \frac{Q^2}{2p_a \cdot p_b} e^{-t} \approx 0 \ . \tag{4.121}$$

Thus the commutator only vanishes (and hadronic evolution stops, see eq.(4.116) and eq.(3.42)) if eq.(4.121) and

$$(z)^{N-1} \approx 1 \tag{4.122}$$

holds.
Now we must look at the variable y. From eq.(4.120) it follows that the evolution stops when the following condition holds

$$\begin{aligned} Ny &\approx 0 \\ \Rightarrow N\frac{Q^2}{2p_a \cdot p_b} e^{-t} &\approx 0 \ . \end{aligned} \tag{4.123}$$

This is the case when we have

$$t \gg \ln\left(\frac{Q^2}{2p_a \cdot p_b} N\right) \ . \tag{4.124}$$

So we can define a critical time as[41]

$$t_c = \ln\left(\lambda N \frac{Q^2}{2p_a \cdot p_b}\right). \tag{4.125}$$

Here is λ a factor which is similar to $e^{2\gamma_E}/4$ in [37]. The choice of the proper value of this will be considered in the next section. This critical time

[41] Only above this value it is possible for evolution to stop.

is supposed to be identical to the final shower time t_f. A further point that must be considered is the scale μ_F^2 the parton density functions $f_{a/A}(\eta_a, \mu_F^2)$ and $f_{b/B}(\eta_b, \mu_F^2)$ depend on. We can set[42]:

$$\mu_F^2 = Q^2 e^{-t} \ . \tag{4.126}$$

Thus

$$\mu_F^2(t = t_\mathrm{f}) = \frac{2p_a \cdot p_b}{\lambda N} \ , \tag{4.127}$$

which leads us to

$$(1|\mathcal{Q}(N)|\rho(t_\mathrm{f})) = \sum_{a,b} \int_0^1 d\eta_a \int_0^1 d\eta_b \frac{f_{a/A}\left(\eta_a, \frac{2p_a \cdot p_b}{\lambda N}\right) f_{b/B}\left(\eta_b, \frac{2p_a \cdot p_b}{\lambda N}\right)}{4n_c(a)n_c(b)2\eta_a\eta_b p_A \cdot p_B} \times (1|\mathcal{Q}(N; \eta_a, \eta_b, a, b)|\rho_\mathrm{pert}(t_\mathrm{f})) \ . \tag{4.128}$$

4.4.2 Derivation of the critical time t_c

Now we want to consider what would be the proper value for λ. For that we must go back to eq.(4.122). Practically we want to consider the z region where the parton shower evolution stops. Thus we want to make an approximation like

$$z^{N-1} - 1 \approx -\theta(z \leq z_0) \tag{4.129}$$

for large N. Here we must take into account that we have to deal with an integral of the following form[43]

$$C := \int_0^1 dz \frac{\alpha_S(\mu_R^2)}{1 - z + y} \left(\left(\frac{z}{1+y} \right)^{N-1} - 1 \right) \ . \tag{4.130}$$

Here α_S is indirectly dependent on z via the scale μ_R. We can simplify this expression by introducing a new variable

$$\sigma := \frac{z}{1+y} \ . \tag{4.131}$$

As we have

$$\frac{dz}{d\sigma} = 1 + y \ , \tag{4.132}$$

[42] See for that eq.(4.7) in [37].

[43] See for that for example eq.(4.81).

eq.(4.130) results in

$$\begin{aligned} C &= \int_0^{\frac{1}{1+y}} d\sigma \frac{(1+y)\alpha_S(\mu_R^2)}{1+y-(1+y)\sigma}(\sigma^{N-1}-1) \\ &= \int_0^{\frac{1}{1+y}} d\sigma \frac{\alpha_S(\mu_R^2)}{1-\sigma}(\sigma^{N-1}-1) \ . \end{aligned} \tag{4.133}$$

For the scale μ_R there are several possible choices. In [37] the following choice was taken

$$\mu_{\rm R}^2 = \lambda_{\rm R}(1-z+y)Q^2 e^{-t} \tag{4.134}$$

with

$$\lambda_{\rm R} = \exp\left(-\frac{C_{\rm A}[67-3\pi^2]-10n_{\rm f}}{3(33-2n_{\rm f})} \right) . \tag{4.135}$$

According to [37] we could in principle also take the simpler form

$$\mu_{\rm R}^2 = \lambda_{\rm R}(1-z)Q^2 e^{-t} \ , \tag{4.136}$$

though according to [37] the form for $\mu_{\rm R}$ taken in eq.(4.134) is preferable[44]. The question that arises now is how does the expression given in eq.(4.133) behave in the high N limit? For that we must consider an integral like

$$\int_0^1 d\sigma \frac{f(\log(1-\sigma))}{1-\sigma}\left\{\sigma^{N-1}-1\right\} . \tag{4.137}$$

According to [2] the following relation holds[45] for large N

$$\begin{aligned} I_n(N) &= \int_0^1 d\sigma \frac{\sigma^{N-1}-1}{1-\sigma}\ln^n(1-\sigma) \\ &= \frac{(-1)^n}{n+1}(\gamma_E+\ln N)^{n+1} + \mathcal{O}((\ln N)^{n-1}) \ . \end{aligned} \tag{4.138}$$

This expression can be also written according to eq.(5.2) of [2] as

$$I_n(N) = -\int_0^{1-N_0/N} \frac{d\sigma}{1-\sigma}\ln^n(1-\sigma) + \mathcal{O}\left((\ln N)^{n-1}\right) \tag{4.139}$$

with $N_0 = e^{-\gamma_E}$. The upper integration limit means that we can neglect those σ which fullfill

$$\sigma \geq 1 - e^{-\gamma_E}/N \ . \tag{4.140}$$

[44] We note that we later make usage of the $\alpha_S = \text{const.}$ case.

[45] See eq.(5.1) of [2] which is proven in Appendix A of that paper.

This means that the evolution stops for those σ. What are the implications of eq.(4.140) for $\mathbf{k}_\perp^2$ and t? For that we rewrite eq.(4.140) with respect to the "old" variables z and y:

$$\frac{z}{1+y} \geq 1 - e^{-\gamma_E}/N \ . \tag{4.141}$$

We consider it meaningful to further simplify this relation. From eq.(4.27) it is clear that we have in the high t limit

$$y \approx 0 \ . \tag{4.142}$$

Thus we can set

$$z \geq 1 - e^{-\gamma_E}/N \ . \tag{4.143}$$

This means that for all $z's$ which fullfill eq.(4.143) the evolution can stop[46]. Now we recall that the following relation holds for $\mathbf{k}_\perp^2$

$$\mathbf{k}_\perp^2 = Q^2(1-z)e^{-t} \ . \tag{4.144}$$

By using eq.(4.143) we come to

$$\mathbf{k}_\perp^2 \leq \frac{Q^2}{N} e^{-\gamma_E} e^{-t} \ . \tag{4.145}$$

We define a new variable

$$\mathbf{k}_{\perp\,\min}^2 = \frac{Q^2}{N} e^{-\gamma_E} \ . \tag{4.146}$$

The meaning of this variable is the following:
when $\mathbf{k}_\perp^2$ takes values above $\mathbf{k}_{\perp\,\min}^2$ the evolution will never stop. On the contrary the evolution can stop for all $\mathbf{k}_\perp^2$ values which are below $\mathbf{k}_{\perp\,\min}^2$. Thus $\mathbf{k}_{\perp\,\min}^2$ constitutes a boundary where the nature of parton evolution changes.
Which implications does that have for the shower time t? For that we must write t as a function of $\mathbf{k}_\perp^2$. Eq.(4.144) yields

$$\begin{aligned} t = &- \log\left(\frac{\mathbf{k}_\perp^2}{Q^2(1-z)}\right) = \\ &\log\left(\frac{Q^2}{\mathbf{k}_\perp^2}\right) + \log(1-z) \ . \end{aligned} \tag{4.147}$$

[46]See for that the discussion of the previous section.

Because of

$$\log(1-z) \leq 0 \tag{4.148}$$

we have for the biggest possible value $t_{\max}$ of t

$$t_{\max} = \log\left(\frac{Q^2}{\mathbf{k}_\perp^2}\right) . \tag{4.149}$$

The application of eq.(4.146) leads us to

$$t_{\max} \geq \gamma_E + \log N . \tag{4.150}$$

Thus we define a critical time by

$$t_c := \gamma_E + \log N . \tag{4.151}$$

Only above this value it is possible for the evolution to stop. As already discussed we take this value as the final shower time. Thus we can write in analogy to eq.(12.1) of [37]

$$(1|\mathcal{Q}(N)|\rho(t_{\mathrm{f}})) = \sum_{a,b}\int_0^1 d\eta_a \int_0^1 d\eta_b \frac{f_{a/A}\left(\eta_a, \frac{Q^2}{N}e^{-\gamma_E}\right) f_{b/B}\left(\eta_b, \frac{Q^2}{N}e^{-\gamma_E}\right)}{4n_c(a)n_c(b)2\eta_a\eta_b p_A\cdot p_B} \times(1|\mathcal{Q}(N;\eta_a,\eta_b,a,b)|\rho_{\mathrm{pert}}(t_{\mathrm{f}})) . \tag{4.152}$$

4.4.3 Analytical integration on hadron level

Now we want to derive the cross section in Mellin space on hadron level. However it is not possible to perform the integral given in eq.(4.152) analytically as there is no analytical expression for the parton density functions (PDFs). Thus we must perform the integral numerically. We recall further that the partonic cross section factorizes into a parton shower part and the Born cross section σ_0. The decay widths of the W and Z boson are small ($\Gamma_W = 2.08$ GeV and $\Gamma_Z = 2.50$ GeV) in comparison to their masses. We take therefore the following expression as the Born cross section of the Z^0 resonance[47] at leading order (see for that section (9.4) of [3] especially eq.(9.32))

$$\hat{\sigma}^{q\bar{q}\to Z} = \frac{\pi}{3}\sqrt{2}G_F M_Z^2\big(V_q^2 + A_q^2\big)\delta\big(s_{\mathrm{part}} - M_Z^2\big) . \tag{4.153}$$

[47]Strictly speaking we could also consider a situation beyond the Z^0 resonance. This choice is just by default.

Here is G_F the Fermi constant, M_Z the mass of the Z^0 resonance. s_{part} is the center of mass energy on parton level that means the center of mass energy of the two incoming partons that form the Z^0 boson.
The advantage of this approximation for the Born cross section is due to the δ function. By that we must only integrate over one variable (we choose here η_a) instead of two variables η_a and η_b. Further we have $Q^2 = M_Z^2$. V_f and A_f are given by

$$V_f = T_f^3 - 2Q_f \sin^2\theta_W, \;\; A_f = T_f^3 \;, \tag{4.154}$$

θ_W is here the Weinberg angle, Q_f the charge of the particle. For T_f^3 we have $+\frac{1}{2}$ for $f = \nu, u, \ldots$ and $T_f^3 = -\frac{1}{2}$ for $f = e, d, \ldots$ (see for that page 55 of [3]).
We want to integrate this expression over the PDFs. We obtain

$$\begin{aligned} &\int_0^1 d\eta_a \int_0^1 d\eta_b q_f\left(\eta_a, \mu_F^2\right) \bar{q}_f\left(\eta_b, \mu_F^2\right) \hat{\sigma}^{q\bar{q}\to Z} = \\ &\frac{\pi}{3}\sqrt{2} G_F M_Z^2 \left(V_q^2 + A_q^2\right) \int_{\frac{M_Z^2}{s}}^1 d\eta_a \frac{q_f\left(\eta_a, \mu_F^2\right) \bar{q}_f\left(\frac{M_Z^2}{\eta_a s}, \mu_F^2\right)}{s\eta_a} \;. \end{aligned} \tag{4.155}$$

With this expression we can obtain the Born cross section. A cross check shows that this analytical expression is identical within the uncertainty to the Born cross section obtained by the MC generator PYTHIA.
For the scale μ_F^2 inside the PDFs we take $\frac{M_Z^2}{N} e^{-\gamma_E}$. We recall that for $\mathbf{k}_{\perp\,\min}^2$ eq.(4.146) holds. Thus we take for Q_0^2 also $\frac{M_Z^2}{N} e^{-\gamma_E}$. Thus we use as the analytical cross section on hadron level in Mellin space

$$\begin{aligned} &(1|\mathcal{Q}(N)|\rho(t)) = 2\frac{\pi}{3}\sqrt{2} G_F M_Z^2 \left(V_q^2 + A_q^2\right) \\ &\times \int_{\frac{M_Z^2}{s}}^1 d\eta_a \frac{q_f\left(\eta_a, \frac{M_Z^2}{N} e^{-\gamma_E}\right) \bar{q}_f\left(\frac{M_Z^2}{\eta_a s}, \frac{M_Z^2}{N} e^{-\gamma_E}\right)}{s\eta_a} W_N\left(M_Z^2; \frac{M_Z^2}{N} e^{-\gamma_E}\right) \;. \end{aligned} \tag{4.156}$$

This function is plotted in fig.(4.2).

The next step is to compare the analytical result with the one obtained from PYTHIA. PYTHIA has effectively angular ordering due to color coherence. According to eq.(36) of [24] such a Monte Carlo event generator is supposed to reproduce the same distribution as the analytical approach in

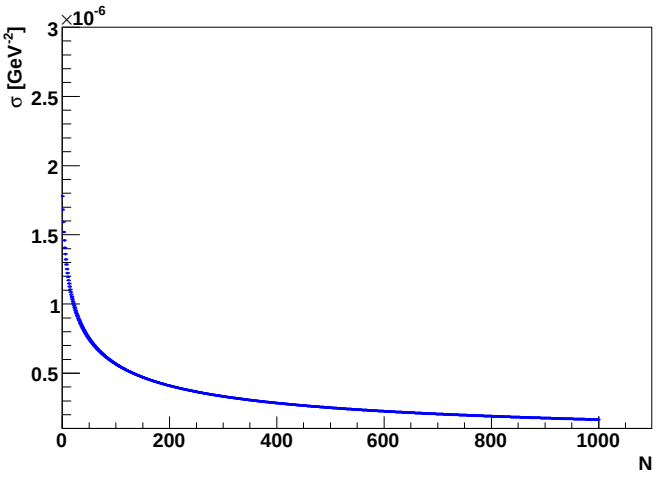

Figure 4.2: Hadron level cross section distribution for $pp \to Z + X$ at $\sqrt{s} = 10^4\,\text{GeV}$ in Mellin space; the lower boundary Q_0^2 of $\mathbf{k}_\perp^2$ is running as $\frac{M_Z^2}{N} e^{-\gamma_E}$.

the soft limit[48].

A comparison between PYTHIA and the analytical one can be seen in fig.(4.3). For the analytical curve we made the condition that both the μ_F^2 inside the pdfs and the minimal value of $\mathbf{k}_\perp^2$ never go below the value Q_0^2. We do this as in PYTHIA the scale for real emission can also never fall below Q_0^2. We see that there is a huge difference between the two (up to two orders of magnitude). The next step is to investigate the reason for this discrepancy. For that we make the situation as simple as possible. We choose to have only one quark flavor (the s quark) and use instead of realistic pdfs simplified ones in order to fix the source of the problem[49]. The result of this can be seen in fig.(4.4). In this plot the analytical result is compared to two simulations done within PYTHIA: one where we have set MSTP(65) = 0 which means that the emitted soft gluons are entirely neglected while in the other we have set MSTP(65) = 1 which means that the emission of the

[48]For simplicity we first of all focus on the $\alpha_S = \text{const}$ case. For that reason we apply the virtuality ordered algorithm PYSSPA as the transverse momentum ordered algorithm PYPTIS does not have the option $\alpha_S = \text{const}$.

[49]This means that the pdf function of the s and $\bar{s}$ quark is set to 1. The pdfs of the other flavors are set to zero.

soft gluons is effectively resummed as a z shift[50]. As we see there is still a discrepancy between the analytical result and that of PYTHIA. This plot gives us however a hint that the reason for the discrepancy lies in the way the z variable is generated.
This is backed up in fig.(4.5). As we see the reason for the discrepancy lies in the parameter XEC in PYSSPA which works as an effective cut on $1-z$ in order to avoid the divergencies inside the splitting functions. A good value for XEC seems to be $3*10^{-6}$ for the z generation while it remained on default for the Sudakov factor. We note when the lower boundary Q_0^2 is changed, PYTHIA and the analytical generation do not agree anymore. This can be seen in fig.(4.6) where Q_0^2 has been set to $5\,\mathrm{GeV}^2$. This problem can be solved by changing the XEC value as we see in fig.(4.7). We conclude that XEC $= 10^{-8}$ is in that case the best value. In order to understand this we take a look at eq.(4.31). From that it follows that a change on the cut of $\mathbf{k}_\perp^2$ implies also a new cut on $1-z$. Thus we must also change the value of XEC. After this has been fixed we can show the final result in fig.(4.8). In the first plot from above the scale μ_F^2 inside the PDFs has been fixed to $1\,\mathrm{GeV}^2$. We see a good agreement between PYTHIA and the analytical generation for large N. The same applies to the second plot in fig.(4.8) where we have fixed the scale μ_F^2 to M_Z^2. What is interesting to note is that we see in the third plot where the scale inside the PDFs is not fixed anymore both for the analytical generation and for PYTHIA (that means we have evolution also for the scale inside the PDF) the two approaches do not agree anymore. In order to understand this discrepancy we note that for the analytical generation the value of Q_0^2 (the under boundary of the integral inside W_N) was fixed to 1 GeV^2. On the other hand we have in the upper plot of fig.(4.9) for Q_0^2 inside the analaytical integration taken the value $e^{-\gamma_E}\frac{M_Z^2}{N}$. As we see it agrees now better with the PYTHIA result. In the lower plot of fig.(4.9) we compare a PYTHIA simulation with fixed $\mu_F^2 = 1\mathrm{GeV}^2$ inside the PDFs with an analytical result where we have $\mu_F^2 = 1\mathrm{GeV}^2$ inside the PDFs and the lower boundary of the integral inside W_N is running. This corresponds to the upper plot of fig.(4.8). We see that the two result do not agree anymore.
The last step is to consider running coupling. This can be seen in fig.(4.10). We see that PYTHIA and the analytical generation do not agree anymore. In order to understand this we switch back to the previous case where we have only one quark flavor and its PDF is simplified. The result of this can be seen in fig.(4.11). It seems that XEC $= 10^{-13}$ is a better value than

[50] See for that page 321 of [13].

$3. * 10^{-6}$. We conclude that the cutoff XEC plays inside the Monte Carlo simulation an important role. After adjusting it properly the simulation agrees nicley with the analytical result.

4.5 Summary

In section (4.1.7) we have derived the distribution of the energy fraction τ in Drell Yan (its definition is given by eq.(4.32)). The result is given in the equations (4.78), (4.81) and (4.82). We made use of an analytical formalism for parton showers which takes interference effects into account. This formalism was developed in [1]. Further we applied simplifications of this formalism from [37].
In section (4.2) we saw that this result is equivalent (under special conditions) to a result given in [2] where standard resummmation techniques were applied. However while the integrand is approximately the same the different choice of the ordering variable leads in the general case to different integration boundaries. In section (4.3)[51] we discussed how to solve the integral given in eq.(4.81) respective eq.(4.83). This is important as in section (4.4) the analytical result is compared with one obtained from PYTHIA. According to [24] the two results are supposed to be equivalent. While it is possible for constant α_S to perform the integration exactly for first order running α_S only a numerical integration is possible. We showed however that even for α_S = const. the numerical integration is suitable due to a numerical instability in the exact solution.
In section (4.4) we have further considered the differential cross section of the energy fraction τ in Drell Yan processes[52]. We compared the analytical result derived in section (4.1) on hadron level with a result obtained by the Monte Carlo event generator PYTHIA. At first it turned out that there was a discrepancy between the two approaches which contradicts a result given in [24]. According to [24] a Monte Carlo event generator should reproduce the distribution derived from analytical resummation techniques. This discrepancy however could be traced back to a z cut (the variable XEC) in PYTHIA. After adjustment the two approaches agree well.

[51] See further the appendix.
[52] For a proper definition of this variable see eq.(4.32).

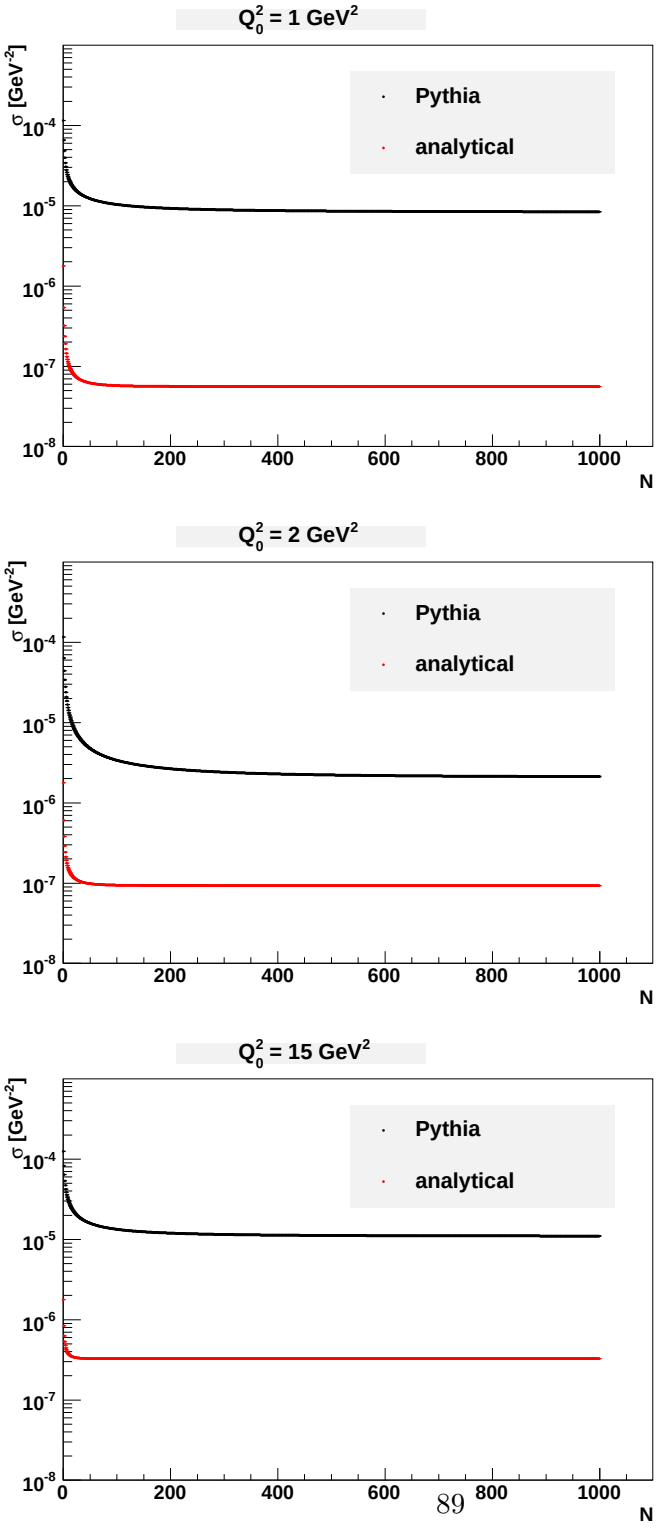

Figure 4.3: Hadron level cross section distribution for $pp \to Z + X$ at $\sqrt{s} = 10^4$ GeV in Mellin space; PYTHIA and the analytical result are compared; Q_0^2 (the minimal value of $\mathbf{k}_\perp^2$) is varied.

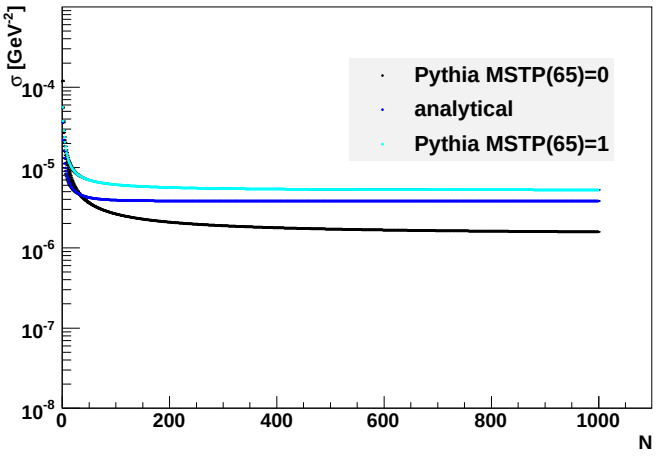

Figure 4.4: Hadron level cross section distribution for $pp \to Z + X$ at $\sqrt{s} = 10^4$ GeV in Mellin space; PYTHIA and the analytical result are compared; Q_0^2 (the minimal value of $\mathbf{k}_\perp^2$) was set to 1 GeV^2. Only a simplified PDF of the s and $\bar{s}$ quark was used. For the other flavors the PDFs were set to zero. XEC was set to default value. The analytical distribution is compared to two distributions obtained in PYTHIA: MSTP(65) = 0 means that soft gluon emission is entirely neglected while MSTP(65) = 1 means that it is effectively resummed as a z shift. The analytical curve is different from the one given in fig.(4.2) because of the different PDFs.

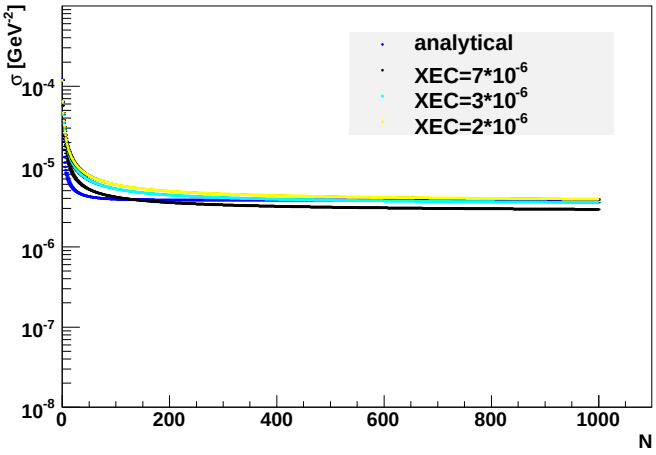

Figure 4.5: Hadron level cross section distribution for $pp \to Z + X$ at $\sqrt{s} = 10^4$ GeV in Mellin space; PYTHIA and the analytical result are compared; Q_0^2 (the minimal value of $\mathbf{k}_\perp^2$) was set to 1 GeV^2. Only a simplified PDF of the s and $\bar{s}$ quark was used. For the other flavors the PDFs were set to zero. For the Sudakov factor XEC remains on default value while it it is varied in the realm of 10^{-6} for the z generation.

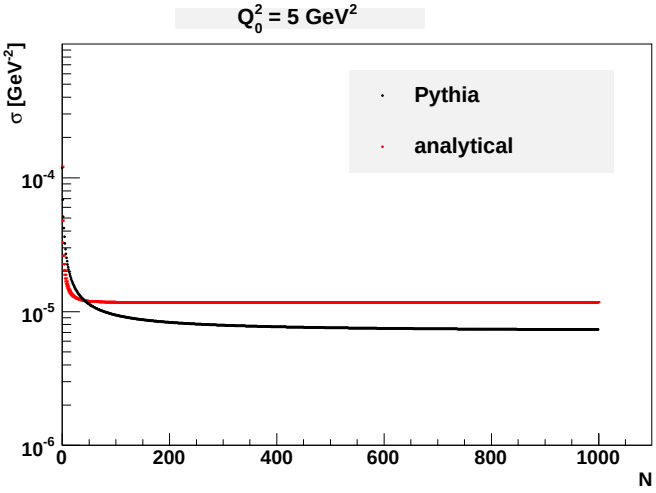

Figure 4.6: Comparison of the hadronic cross section in Mellin space between PYTHIA and the analytical result. Q_0^2 (the minimal value of $\mathbf{k}_\perp^2$) was set to 5 GeV^2. Only a simplified PDF of the s and $\bar{s}$ quark was used. For the other flavors the PDFs were set to zero. XEC was set on default value for the Sudakov factor while it was set to $3 * 10^{-6}$ for the z generation.

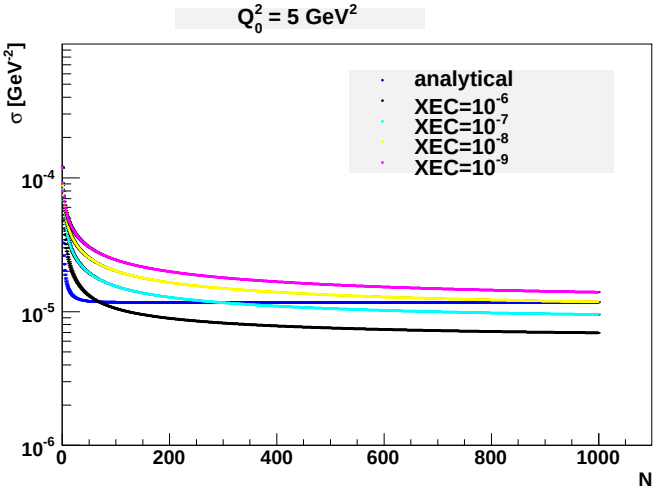

Figure 4.7: Comparison of the hadronic cross section in Mellin space between PYTHIA and the analytical result; Only a simplified PDF of the s and $\bar{s}$ quark was used. For the other flavors the PDFs were set to zero. For $Q_0^2 = 5\,\mathrm{GeV}^2$ the XEC value is varied.

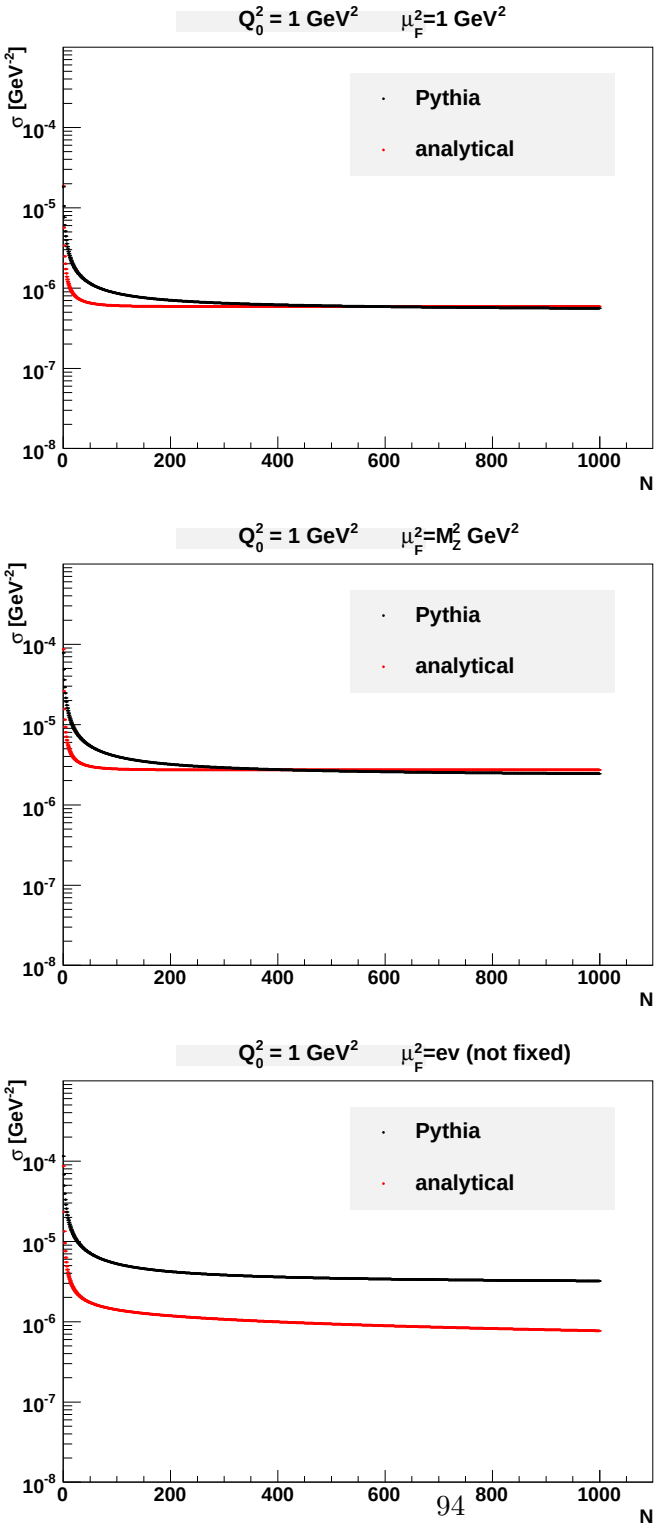

Figure 4.8: Hadron level cross section distribution for $pp \to Z + X$ at $\sqrt{s} = 10^4$ GeV in Mellin space; PYTHIA and the analytical result are compared. For all quark flavors realistic PDFs have been used. In the first plot from above the scale μ_F^2 inside the PDFs has been set to 1 GeV^2 both for PYTHIA and the analytical generation. In the second plot the scale μ_F^2 inside the PDFs has been set to M_Z^2. In the third plot the scale μ_F^2 inside the PDFs is not fixed any more.

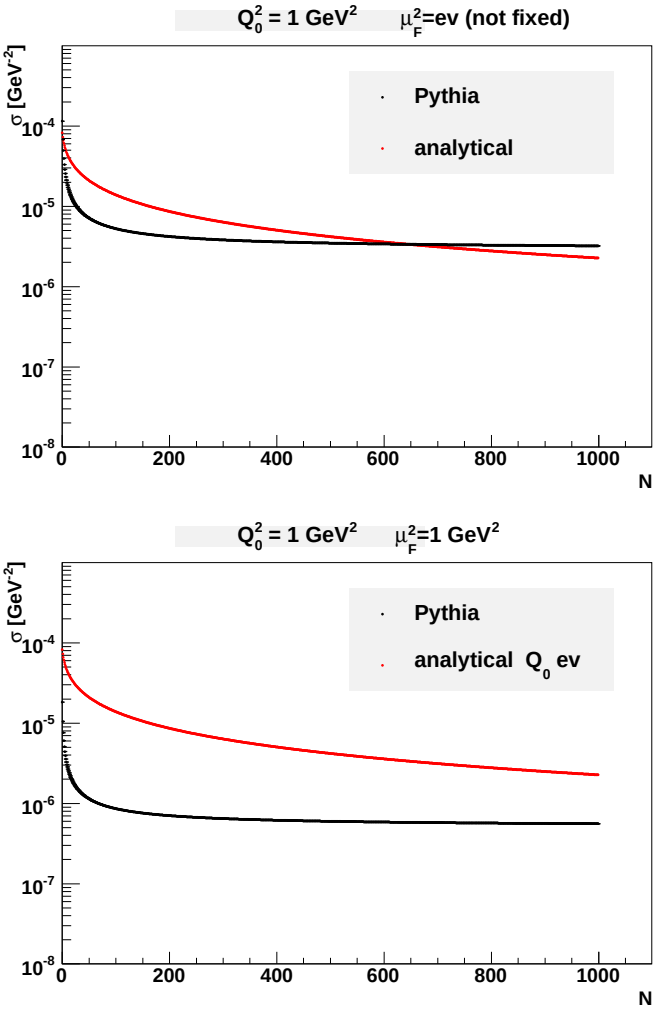

Figure 4.9: Hadron level cross section distribution for $pp \to Z + X$ at $\sqrt{s} = 10^4$ GeV in Mellin space; PYTHIA and the analytical result are compared. For all quark flavors realistic PDFs have been used. In the first plot from above the scale μ_F^2 inside the PDFs is not fixed any more. In the lower plot the scale μ_F^2 inside the PDFs is fixed to 1 GeV^2. For the analytical result the lower boundary inside the integration $\frac{M_Z^2}{N} e^{-\gamma_E}$ in W_N has been set.

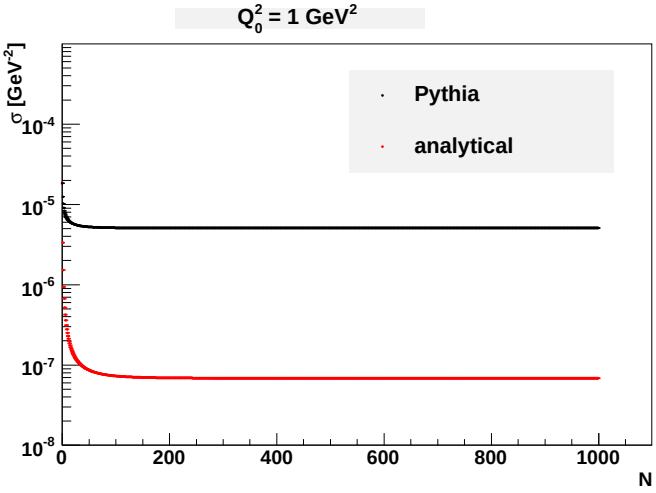

Figure 4.10: Hadron level cross section distribution for $pp \to Z + X$ at $\sqrt{s} = 10^4$ GeV in Mellin space; PYTHIA and the analytical result are compared. Here we have running coupling. For all quark flavors realistic PDFs have been used. For PYTHIA and the analytical generation the scale μ_F^2 inside the PDFs has been set to $1\,\mathrm{GeV}^2$.

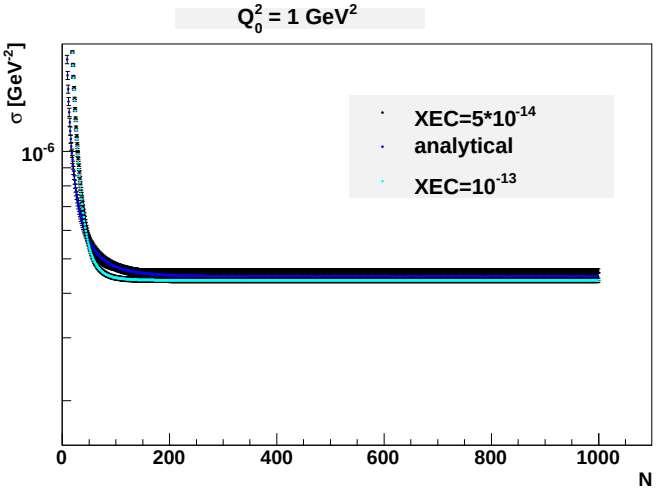

Figure 4.11: Hadron level cross section distribution for $pp \to Z + X$ at $\sqrt{s} = 10^4$ GeV in Mellin space; PYTHIA and the analytical result are compared. Here we have running coupling. Only a simplified PDF of the s and $\bar{s}$ quark was used. For the other flavors the PDFs were set to zero.

Chapter 5

The $k_{\perp}^{++}$ jet algorithm

5.1 Introduction

In this chapter we will investigate a modified version of the k_T algorithm in order to identify multi parton interaction (MPI). In this algorithm we have two parameters: R (already known from the standard k_T algorithm) and ε. We will show that it can detect multi parton interaction in an idealised case (parton showers and fragmentation switched off) under the condition that an unusual low R value ($R = 0.1$) is taken. It will be shown however that this algorithm is not suitable for detecting multi parton interaction for a realistic scenario.

Although jets are supposed to give insight into scattering processes we must be aware that there is no *unique* correlation between a jet and a single initial quark or gluon. The reason for this lies in the fact that hadrons carry no color in contrast to gluons and quarks. Despite this, the goal remains to reduce the effects of long distance physics and to come to a more or less precise view of the hard scattering.
First of all we must note that there is a crucial difference between e^+e^- scattering and hadron-hadron collision. In the first case we have a purely electromagnetic initial state. Then we have afterwards a virtual photon which decays into a quark antiquark pair that evolves via parton radiation and after that is transformed into hadrons. Thus we can say that all hadrons emerge from the hard scattering process.
Different is the case in hadron-hadron scattering. Here we have only one 'active parton' from each hadron that participates in the hard interaction. Thus only a fraction of the final state hadrons can be considered to be associ-

ated with the hard scattering while the rest comes from the soft interactions of the remaining partons. In a first approximation this can be treated as uncorrelated with the hard interaction.
A further point that must be taken into account is that the natural variables are different in both cases. In the case of e^+e^- scattering a natural choice would be (because of rotational invariance) the energies E and the polar angles θ, ϕ. In the case of hadron-hadron scattering we would like to have boost invariance along the beam axis as the c.m frame of the hard scattering usually moves in the frame of the hadron-hadron c.m. frame. Thus we consider as natural variables the transverse momentum p_T or the corresponding "transverse energy" $E_T = E \sin\theta$, azimuthal angle ϕ and pseudo-rapidity $\eta = -\ln(\tan(\theta/2))$.

5.2 A jet algorithm

We present here the k_T jet algorithm which was introduced in [19]. We look at hadron-hadron collisions in the center of mass frame with the z-axis taken in the beam direction. The final state of the collision is considered to be a set of protojets i with momenta p_i. The momentum of a protojet can be the momentum of an individual particle or the total momentum of a bunch of particles that are contained in a small angle around the leading particle. The masses of the protojets are considered to be small compared to the transverse momentum so that the protojets are more or less lightlike. For each protojet we have an azimuthal angle ϕ, a pseudorapidity $\eta_i = -\ln(\tan(\theta_i/2))$ and a transverse energy $E_{T,i} = |\vec{p}_{T,i}|$.
We start with a full list of protojets and an empty list of jets. We demand that protojets with nearly parallel transverse momentum should be joined. We have a parameter R which is considered to be a radius and is of order 1. The steps of the jet algorithm are as follows:

1. For each protojet define:
$$d_i = E_{T,i}^2 \ . \tag{5.1}$$
For each pair of protojets introduce the following definition
$$d_{ij} = \min(E_{T,i}^2, E_{T,j}^2)[(\eta_i - \eta_j)^2 + (\phi_i - \phi_j)^2]/R^2 \ . \tag{5.2}$$

2. Search for the smallest of all the d_i and d_{ij} and call it $d_{\min}$.

3. For the case that $d_{\min}$ is a d_{ij}, protojets i and j are merged into a new protojet k with

$$E_{T,k} = E_{T,i} + E_{T,j} \tag{5.3}$$

and

$$\begin{aligned} \eta_k &= [E_{T,i}\eta_i + E_{T,j}\eta_j]/E_{T,k} \ , \\ \phi_k &= [E_{T,i}\phi_i + E_{T,j}\phi_j]/E_{T,k} \ . \end{aligned} \tag{5.4}$$

4. If $d_{\min}$ is a d_i, call the corresponding protojet not "mergable", remove it from the list of protojets and add it to the list of jets.

5. Repeat from step 1 until all protojets are assigned to jets.

The whole process continues until there are no more protojets. While applying the above procedure to all particles we obtain a list of jets with successively increasing values of $d_i = E_{T,i}^2$.
This algorithm attempts to seperate jets based on angle. Protojets that have nearly parallel momenta should be joined so that they are part of the same jet. If, however, a protojet i is isolated from other protojets it should be considered its own jet.
It is interesting to note the relation of the jets obtained from the k_T algorithm to partons generated in a parton shower. A parton shower starts with relatively hard splitting (and this implies large d_{ij}) and then goes to splittings which are softer and softer. The k_T algorithm does this in the reversed order as the d_i values become larger and larger. A problem with the application of the algorithm lies in the fact that it is not possible to say where a specific parton comes from: some partons might come from initial state splitting while others might come from final splitting. The algorithm tries to make a distinction between those partons that are the result of final state splittings and those that come either from initial state or directly from the hard interaction. We note that this is relevant only in collinear factorisation where the hardest p_t comes from the matrix element. The procedure is based on angle so that final state splittings do not create new jets. In order to make a further distinction between those jets that are the result of initial state splitting and those jets that are the result of the hard interaction we are introducing a cut on transverse momentum P_{cut}: jets with high transverse momentum (this means $p_T^2 \geq P_{cut}^2$) are considered to emerge from the hard interaction while jets with low transverse momentum (this means ${p_T}^2 < P_{cut}^2$) are considered to emerge from initial or final state splitting.

5.3 Application of the jet algorithm without multi-parton interaction

Now we want to apply this algorithm to the case of proton proton collision where a Z^0 is produced which is set stable. The Z^0 boson itself is not included in the list of protojets. For the simulation PYTHIA (6.4) (see [13]) is used.

We investigate Z^0 production at a center of mass energy of 7 TeV. We require $|\eta| \leq 3$. In fig.(5.1) we show the jet multiplicities for different values of the minimum p_T of the jets. We observe less jets for higher p_T cuts.

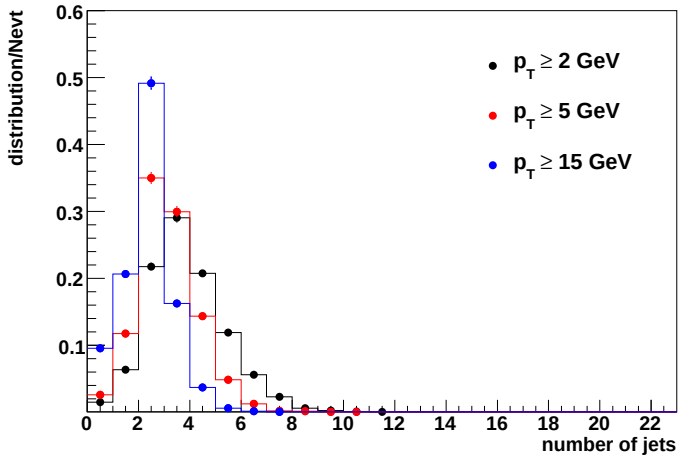

Figure 5.1: Number of jets without MPI in pp collisions for the case of the production of a stable Z at $\sqrt{s} = 7\,\text{GeV}$. The distributions for the number of jets are shown for several p_T cuts. The distributions themselves were normalized with respect to the number of events Nevt.

5.4 Influence of multi parton interaction

The next step is to consider the influence of multi parton interaction (MPI) on jets. We expect that with MPI we see more jets. For that we can compare the jet multiplicity obtained from a simulation where MPI is switched on and off. This is shown in fig.(5.2). The number of jets, the average and the width of the distribution increases significantly when MPI is included. In

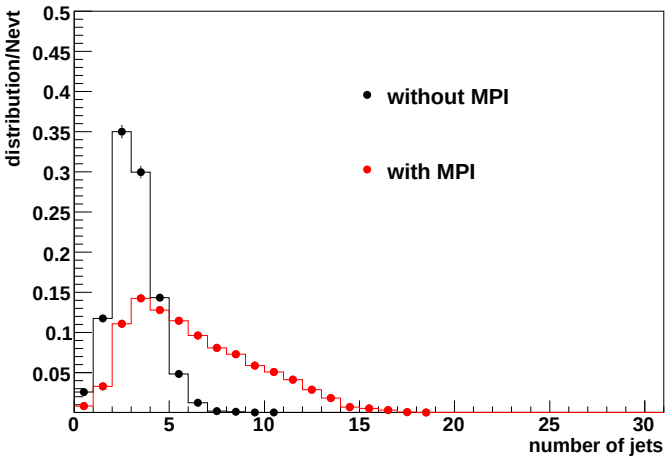

Figure 5.2: Number of jets with and without MPI. The p_T cut was set to 5 GeV. The distributions themselves were normalized with respect to the number of events Nevt.

figure (5.3) the jet multiplicity is compared for different values of the p_T cut for a Monte Carlo (MC) simulation of MPI. By comparing it to fig.(5.1) it is seen that the MPI contribution becomes much smaller at larger p_T while at lower p_T we observe a siginificant increase. The p_T spectrum of the jets with and without MPI is shown in fig.(5.4) and in fig.(5.5).

We see that the MPI contribution at large p_T is small while at small p_T it is significant. The reason for this lies in the fact that MPI processes have by definiton less energy than the main interaction[1]. This means that we classify the process with the highest p_t as the direct process. Therefore jets that originate from MPI interactions must themselves be at lower energy. In fig.(5.6), fig.(5.7) and fig.(5.8) we see the changes on the η distribution. In the area where $|\eta|$ is about 7 the jet cross section is very small. Here we reach the kinematical border.

[1]see section (2.3)

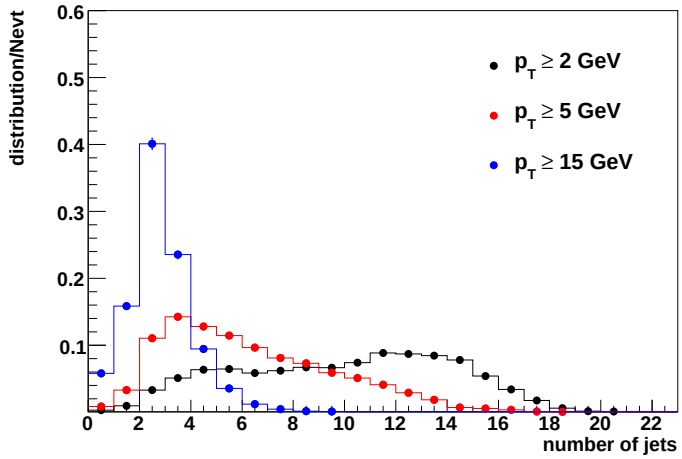

Figure 5.3: Number of jets with MPI for several p_T cuts in pp collisions. The distributions for the number of jets are shown for several p_T cuts. The distributions themselves were normalized with respect to the number of events Nevt.

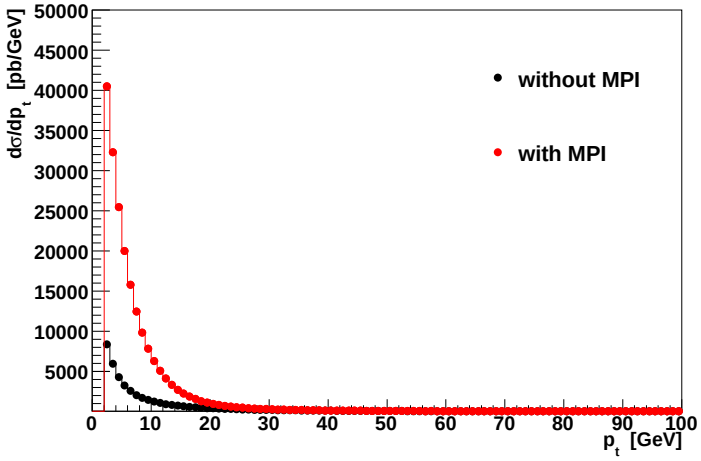

Figure 5.4: p_T distribution of the jets. The p_T cut was set to 2 GeV.

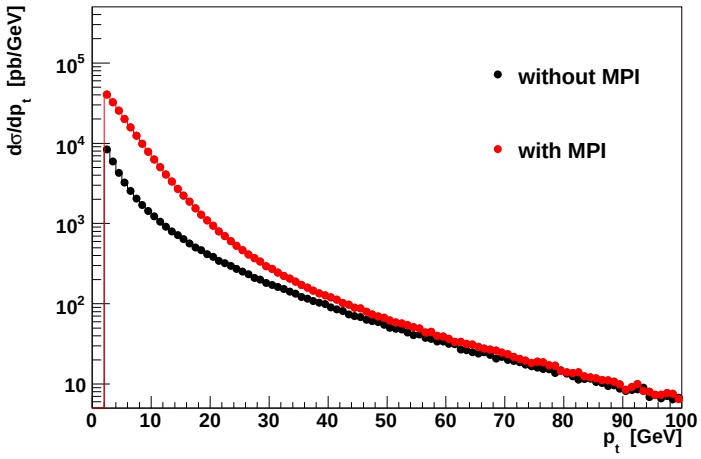

Figure 5.5: p_T distribution of the jets. The p_T cut was set to 2 GeV. Same as fig.(5.4) but with log scale.

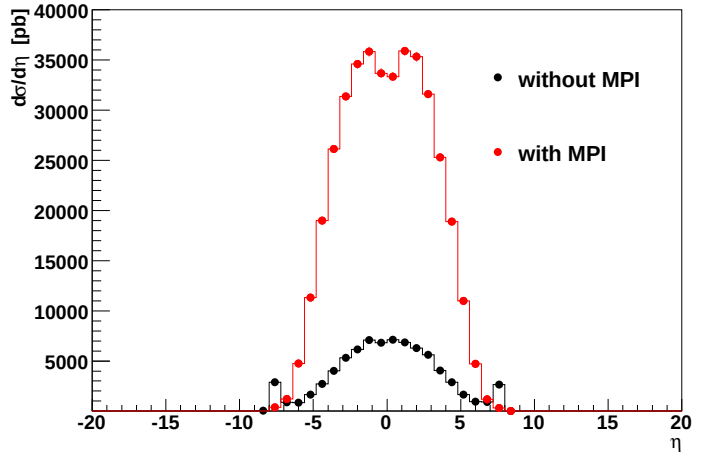

Figure 5.6: η distribution of the jets with $p_T > 2$ GeV.

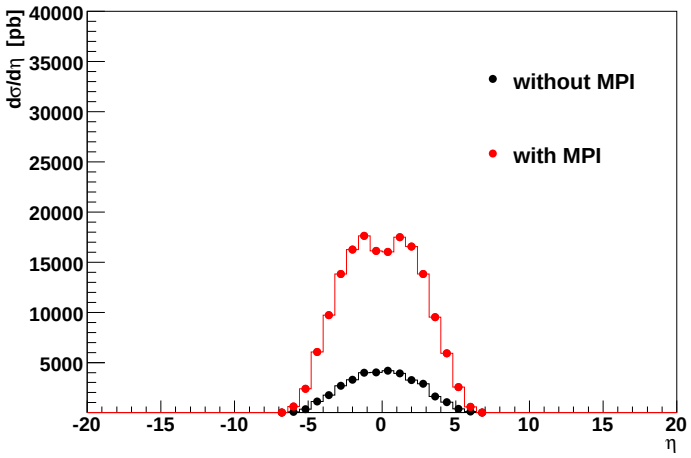

Figure 5.7: η distribution of the jets with $p_T > 5$ GeV.

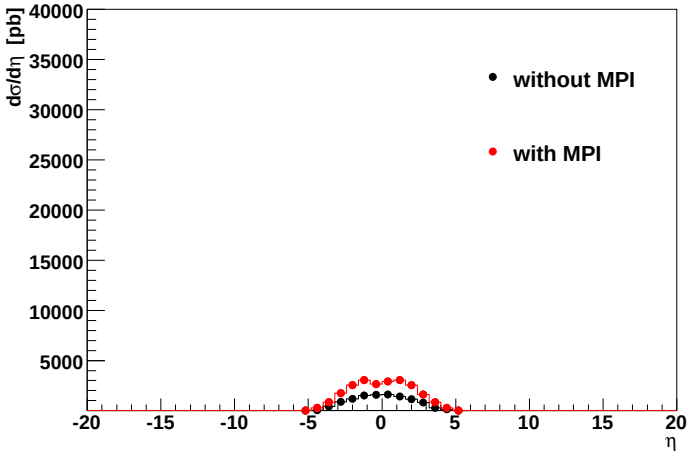

Figure 5.8: η distribution of the jets with $p_T > 15$ GeV.

5.5 The MPI jet algorithm

5.5.1 A new algorithm

In this section we describe a modification of the inclusive k_T algorithm of [19] in order to seperate the MPI contribution from the primary hard interaction. We start again with a list of protojets. Then we define R_{ij} for every pair of protojets

$$R_{ij}^2 = (\eta_i - \eta_j)^2 + (\phi_i - \phi_j)^2 \ . \tag{5.5}$$

Here is η_i the pseudorapidity of protojet i and ϕ_i its azimuthal angle while i and j denote any of the protojets. Further we have a parameter Λ.

After the application of the algorithm we have two types of objects:

- The first type are "NON-MPI jets".
- The second type are the "MPI jets".

The algorithm works as follows:

1. (a) For each protojet we define

$$d_i = \mathbf{p}_i^2 \ . \tag{5.6}$$

   $\mathbf{p}_i$ denotes here the transverse momentum of protojet i.

   (b) Every pair of protojets has

$$d_{ij} = \min\{\mathbf{p}_i^2, \mathbf{p}_j^2\} \frac{R_{ij}}{R^2} \ . \tag{5.7}$$

   (c) For every pair of protojets that fullfills the condition

$$(\mathbf{p}_i + \mathbf{p}_j)^2 < \Lambda^2 \ , \tag{5.8}$$

   we calculate

$$\tilde{d}_{ij} = \min\{\mathbf{p}_i^2, \mathbf{p}_j^2\} \ . \tag{5.9}$$

2. We derive the minimal value of $\tilde{d}_{ij}$ and call it $\mathrm{t_{min}}$. We also derive the minimal value of d_{ij} and call it $\mathrm{d_{min}}$. If $\mathrm{t_{min}} < \mathrm{d_{min}}$ holds then:

   (a) Remove the two protojets i and j which correspond to $\mathrm{t_{min}}$ from the list of protojets and add them to the list of MPI jets.

   (b) Go to 1.

3. We derive the minimal value of d_i and call it δ. If $\mathrm{d_{min}} < \delta$ then

   (a) Merge the two protojets i and j which correspond to $\mathrm{d_{min}}$ into a new protojet k

   $$p_k = p_i + p_j \ . \tag{5.10}$$

   (b) Go to 1.

4. If $\delta < \mathrm{d_{min}}$ then:

   (a) Remove the protojet i which corresponds to δ from the list of protojets and add it to the list of jets.

   (b) Go to 1.

Without step 2 this is just the k_T algorithm (see section (5.2)) with the merging condition

$$p_k = p_i + p_j \ . \tag{5.11}$$

In order to seperate MPI from the hard interaction we have introduced a new measure $\tilde{d}_{ij}$ together with the condition

$$(\mathbf{p}_i + \mathbf{p}_j)^2 < \Lambda^2 \ . \tag{5.12}$$

If this condition is fullfilled and the smallest of $\tilde{d}_{ij}$ is smaller than the smallest of the d_{ij} we have a pair which is balanced in p_T and which we consider as a candidate for an MPI jet pair. The hardness scale for the scattering is $\tilde{H}_{ij} = \tilde{d}_{ij}$ and the hardness scale for the final state splitting is $H_{ij} = R^2 d_{ij}$. In PYTHIA the MPI scattering happens (with hardness scale $\tilde{H}_{ij}$) after the hard scattering with hardness scale H_{ij}. For the case that R is small compared to 1 we seperate the MPI jets too "early" in reversed shower time[2].

5.6 Application of the algorithm

5.6.1 Validation of the algorithm

For a cross check of the implementation we skip step 2 from our algorithm. Then our algorithm is supposed to be the same as the k_T algorithm. The result of this can be seen in the upper plots of figure (5.9) where the p_T distribution of the jets is shown at $\sqrt{s} = 7000$ GeV similar to what is shown in (5.10). As we see there are tiny differences between the two. The reason

[2] concerning shower time see chapter (3) and section (2.2)

for this lies in the fact that in the original routine the kinematical relations are written in a different way. This leads to different rounding errors. After rewriting the expressions identical results are obtained as can be seen in the lower plots of the figures (5.9) and (5.10). A check of the number of jets and the kinematical variables of the jets (like pseudorapidity, transverse momentum) showed that the two k_T algorithms are now completely identical.

5.6.2 k_T++ algorithm: First attempt to identify MPI jets - the Λ case

After we have seen that our implementation of the k_T algorithm is correct we switch on step 2 of the jet algorithm. We call this modified k_t algorithm $k_\perp^{++}$ algorithm. If we have only the hard interaction in the Monte Carlo event generator (this means no PS and no MPI) we should see no jets since the Z is not included in the jet finding and we have $|\eta_{\text{jet}}| < 3$. In fig. (5.11) we see the comparison of the p_t distribution for the case that the parton showers are switched off respectively switched on. We see that there are a few non MPI jets even for PS being off. The reason for this is traced back to the fact that the primordial $k_\perp$ inside the two protons was still switched on. This is shown in fig.(5.12). As we see we obtain no jets at all when primordial $k_\perp$ is switched off.
Now we start investigating the value of Λ (see eq.(5.8)) to seperate MPI jets from the other jets. We require that without multi parton interaction no MPI jets should be seen. The result of this can be seen in the plots (5.13) to (5.15). There we see the p_t distribution of the MPI jets both for the case that multi parton interaction is switched on and off. Though the distribution has a tail to higher values of p_T when multi parton interaction is switched on we see no clear distinction between the two cases when MPI is switched on and MPI is switched off. This problem does not depend on the concrete Λ value. What we see further is that the $p_\perp$ spectrum for the MPI jets becomes harder when Λ is increased.
Further we note that the shape of the $p_\perp$ distribution does not depend significantly on an η cut as shown in fig.(5.15). There are only minor changes[3]. The same applies to fig.(5.16) where we show the distribution of the non MPI jets with and without an η cut. Thus removing the η cut does not solve the problem.
The reason of this problem can be traced back to the condition given in

[3]for the small p_T area

eq.(5.8). When the transverse momenta of two protojets are sufficiently small they are considered as potential candidates for MPI jets no matter how uncorrelated they are. Thus we must search for a better condition to identify MPI jets.

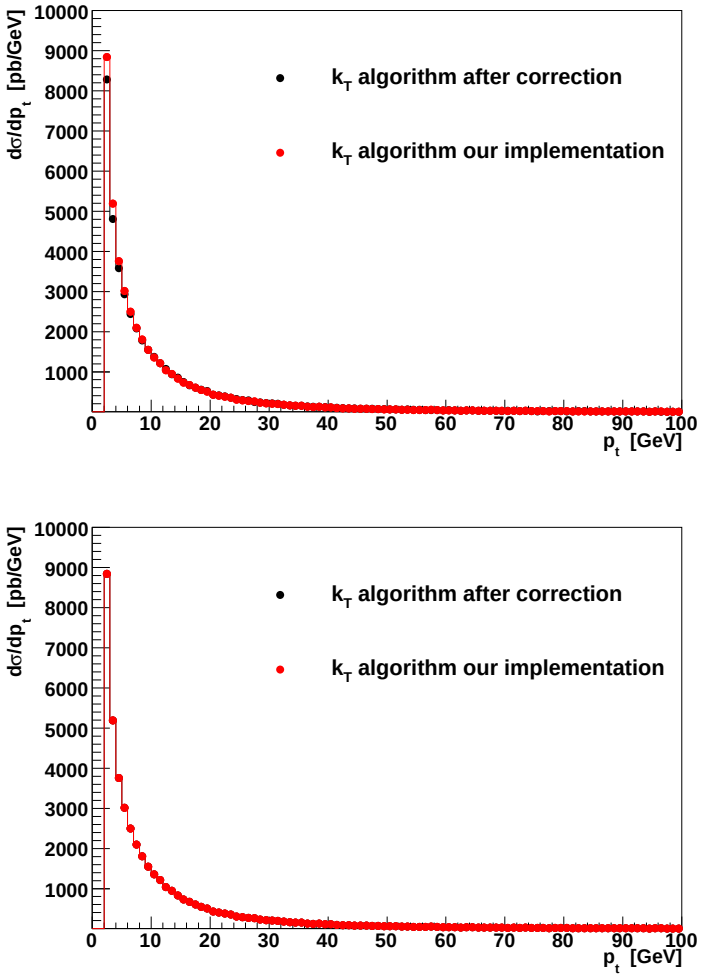

Figure 5.9: Comparison of the k_T algorithm with our new algorithm. Here we deleted step 2 of the new algorithm. The plot above shows the distribution before the correction while the plot beneath stands for the distribution after the correction.

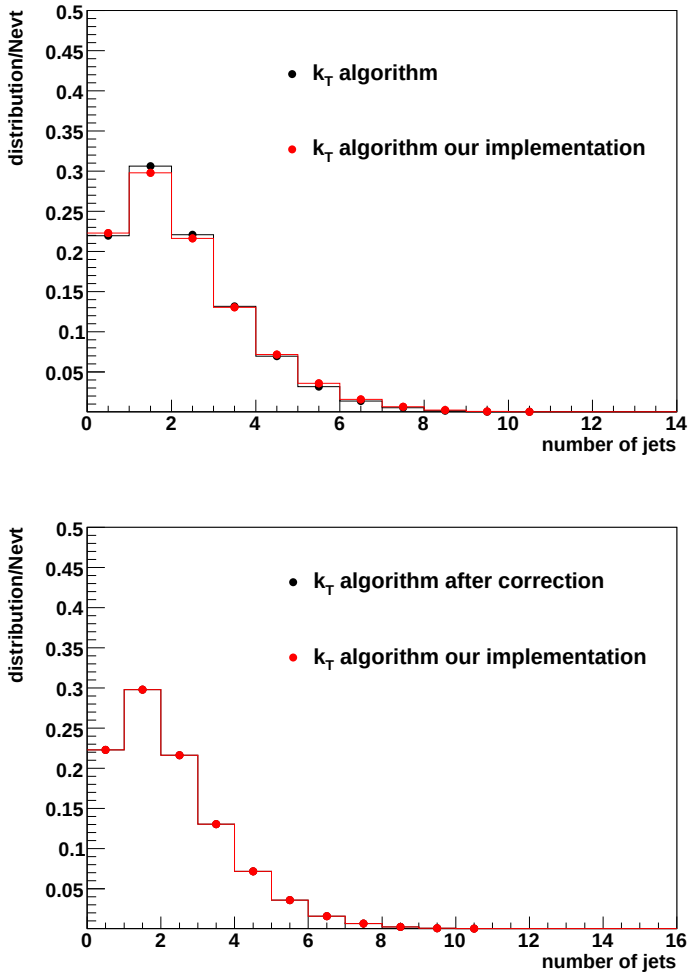

Figure 5.10: Comparison of the k_T algorithm with our new algorithm. Here we deleted step 2 of the new algorithm. The plot above shows the distribution before the correction while the plot beneath shows the distribution after the correction.

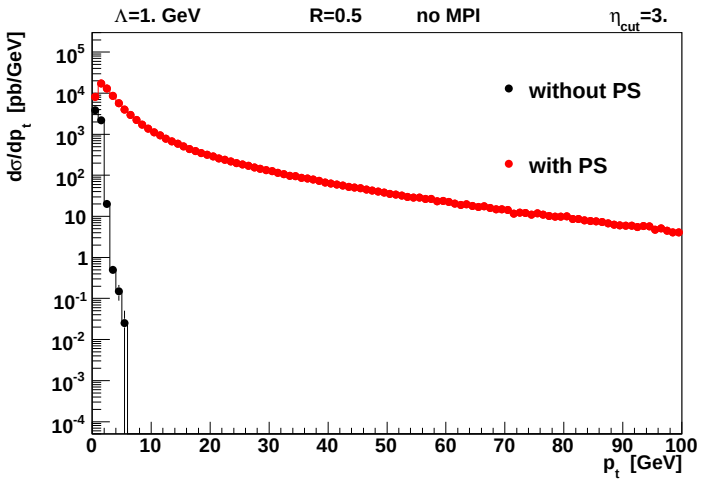

Figure 5.11: Comparison of the p_T distribution of the non MPI jets with and without PS. We had no p_T cut. Fragmentation was switched off.

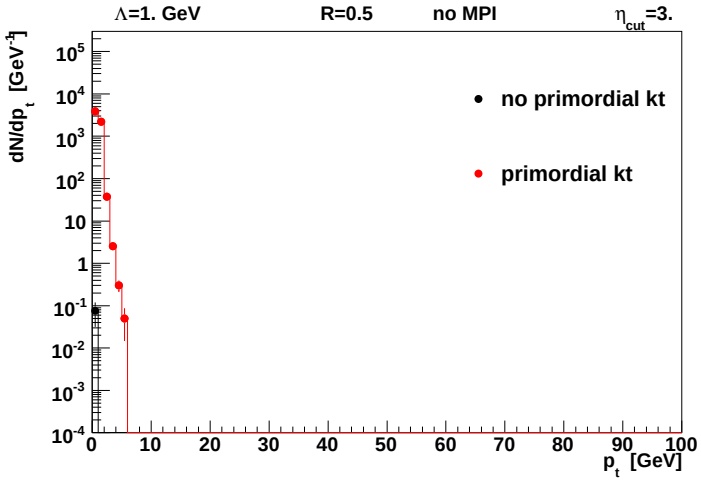

Figure 5.12: Comparison of the p_T distribution of the non MPI jets with and without primordial $k_\perp$. We had no p_T cut. Fragmentation was switched off.

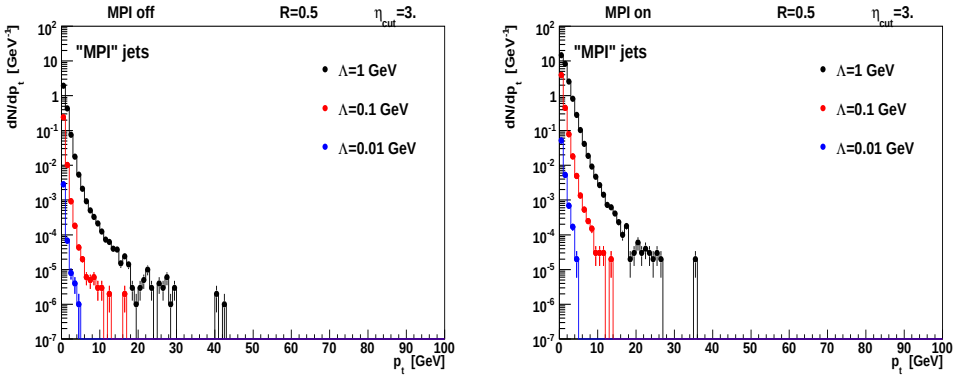

Figure 5.13: p_T distribution of the MPI jets. The distributions for several Λ values are compared. In the left plot multi parton interaction is switched off while in the right plot multi parton interaction is switched on. The distribution in each plot has been normalized with respect to the number of events.

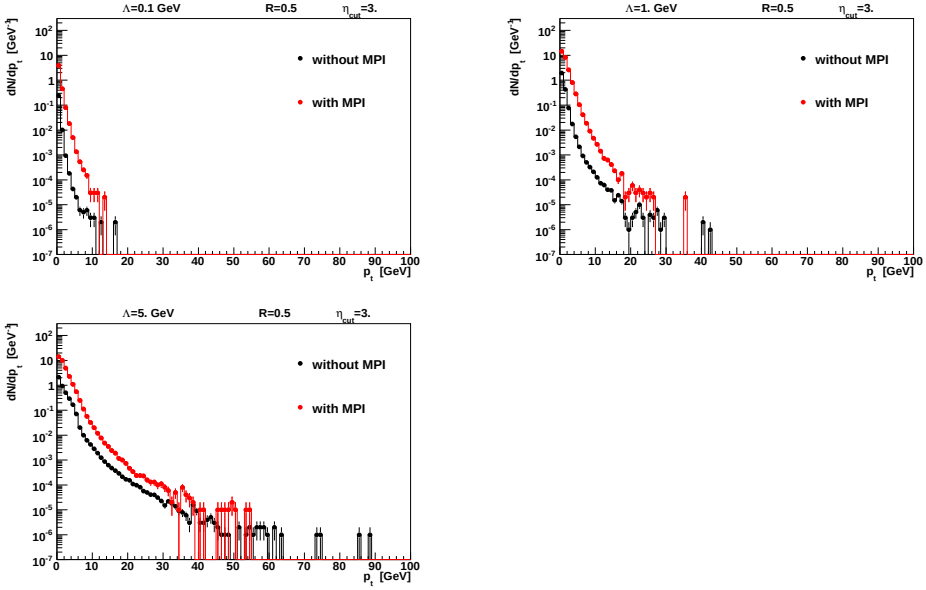

Figure 5.14: p_T distribution of the MPI jets. In these plots we compare the distribution for several Λ values. The distributions have been normalized with respect to the number of events.

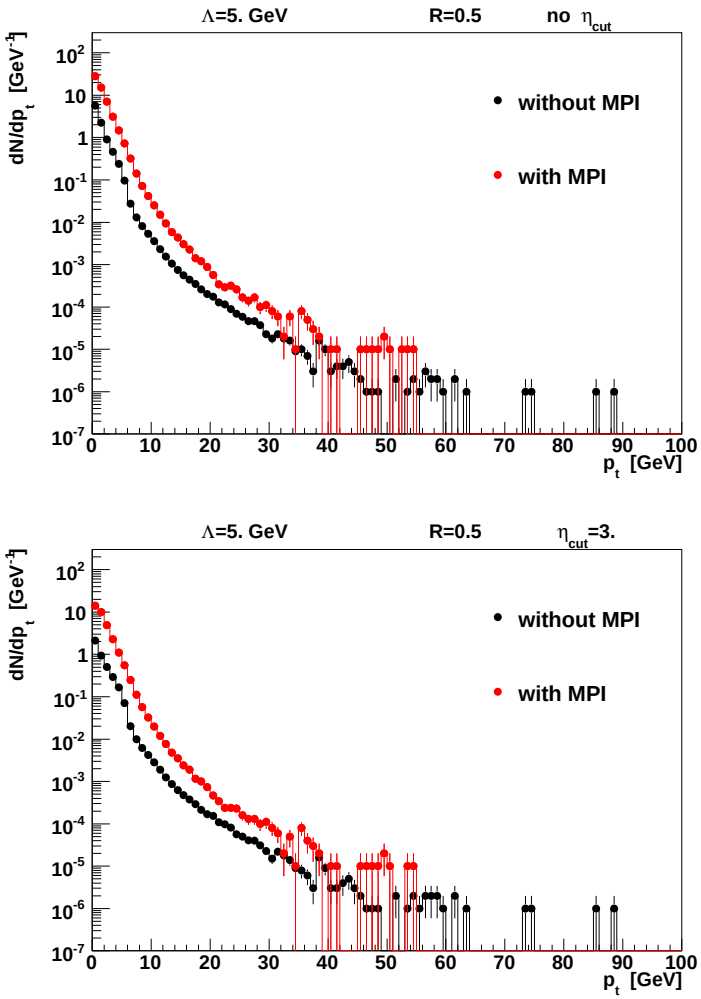

Figure 5.15: Comparison of the p_T distribution of the MPI jets. In the plot above we have no η cut while in the plot beneath we have an η cut. The distributions have been normalized with respect to the number of events. Please note that the two distributions are distinct for small p_T values only.

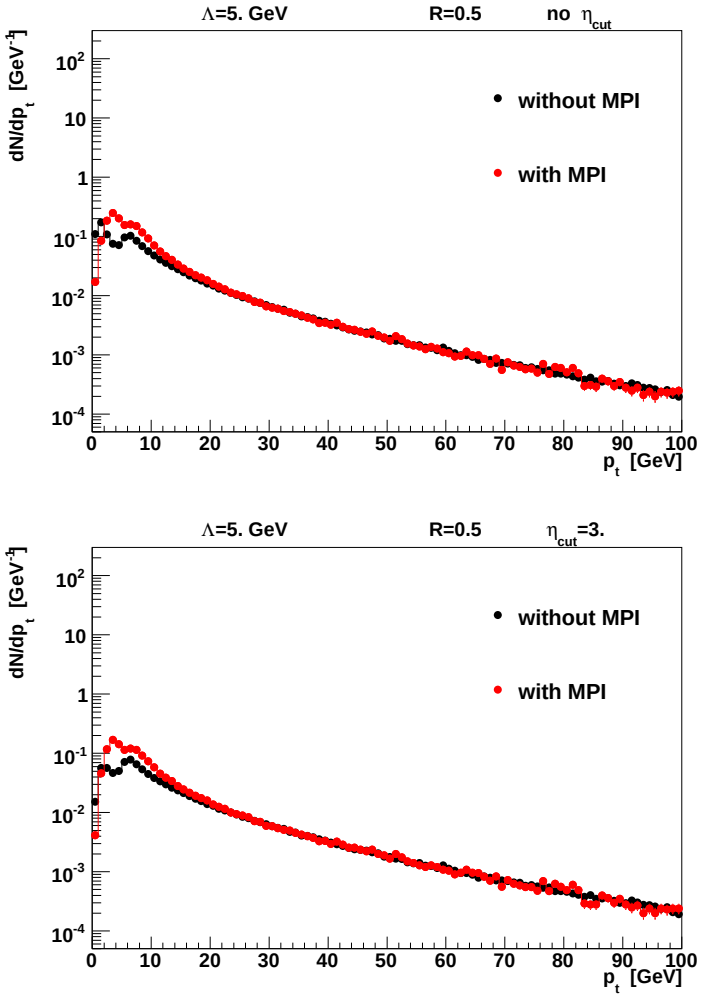

Figure 5.16: Comparison of the distribution of the transverse momentum for the non MPI jets. In the plot above we have no η cut while in the plot beneath we have an η cut. The distributions have been normalized with respect to the number of events. Please note that the two distributions are distinct for small p_T values only.

5.6.3 $k_\perp^{++}$ algorithm: further condition- ε value

As we have seen the condition given in eq.(5.8) is inappropriate as in the low p_T region all protojet pairs fullfill the condition no matter how uncorrelated they are. Thus we replace eq.(5.8) by the following condition for $\tilde{d}_{ij}$

$$\frac{|\mathbf{p}_i + \mathbf{p}_j|}{|\mathbf{p}_i| + |\mathbf{p}_j|} < \varepsilon \ . \tag{5.13}$$

We investigate the effects of this condition. It seems reasonable that ε should not exceed 0.1 or 0.2, as otherwise protojet pairs ought not to be considered as back-to-back. Higher values (like for example 0.3 or 0.4) would mean that the correlation is too weak so we cannot say that such pairs are back-to-back.
In fig.(5.17) we see two plots[4] for $\varepsilon = 0.1$ and with an η cut less than 3 and without an η cut which corresponds to fig.(5.16) in the Λ case. We observe that the distribution of the "non" MPI jets changes depending whether MPI is switched on or off. This is not what we expect. In the ideal case the algorithm would recognize all the additional jets produced by multi parton interaction as MPI jets and not as non MPI jets. Then no change in the distribution of non MPI jets would be seen when MPI is switched on. This is however not the case in fig.(5.17). What we see further in fig.(5.17) is that removing the η cut does not solve the problem. However removing the η cut increases the distribution but not its shape. This corresponds to the situation in fig.(5.16) for the Λ case. In fig.(5.18) we see the p_T distributions for $\varepsilon = 0.03$ and $\varepsilon = 0.07$. We see that the problem cannot be solved by changing the ε value. This should not surprise us as lower ε values imply that the condition to identify MPI jets given in eq.(5.13) becomes stricter. We note that in this ε region there is almost no change in the distribution. In principle it is possible to obtain the desired distribution by going to higher ε values. Examples of that can be seen in fig.(5.19). However we consider those ε values as too high as discussed before.

In order to investigate why the algorithm does not find all MPI jets we perform a systematic study using the following simplifications:

1. We switch off for initial state radiation further branching.

2. We switch off primordial $k_\perp$.

The result of this can be seen in fig.(5.20) (and fig.(5.21) where parton showers have been switched off). In both plots we have no η cut. This was

[4] In the following we have set $R = 1$ instead of $R = 0.5$ in the previous section.

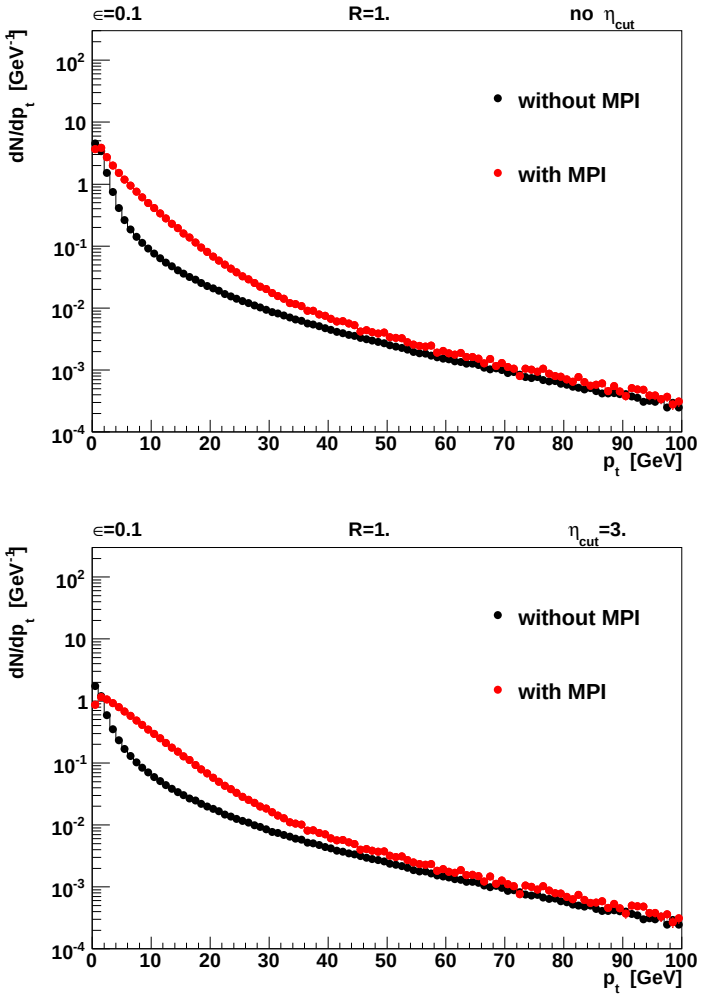

Figure 5.17: Comparison of the p_T distribution of the non MPI jets both for MPI being switched off and on. The distributions have been normalized with respect to the number of events. We see that the η cut changes the size of the distribution but not its shape.

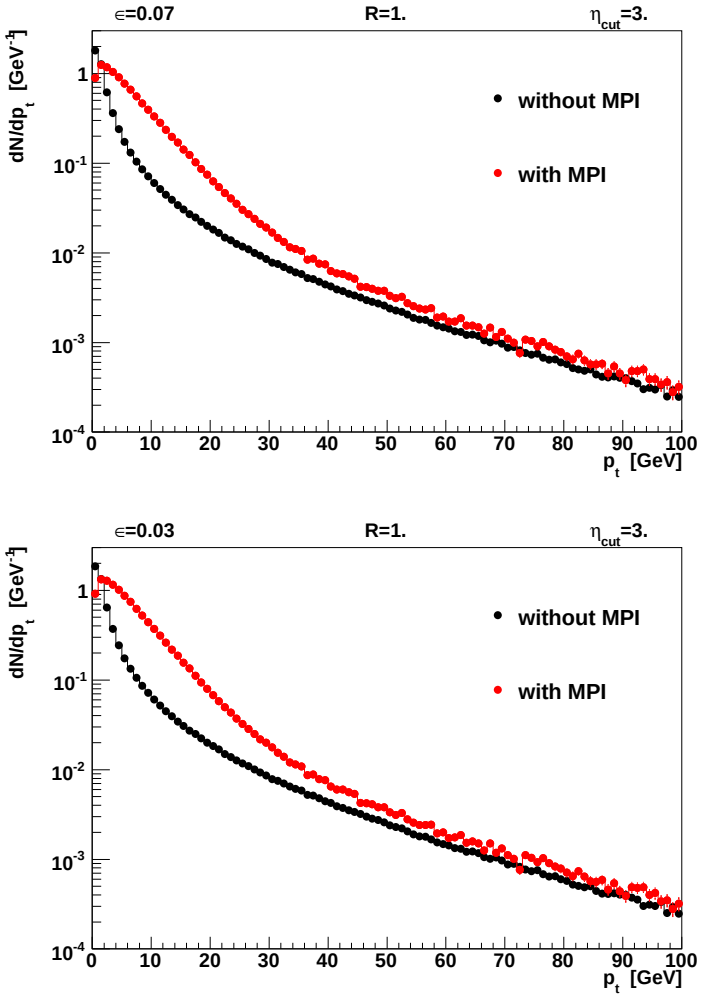

Figure 5.18: Comparison of the p_T distribution of the non MPI jets both for MPI being switched off and on. The distributions have been normalized with respect to the number of events.

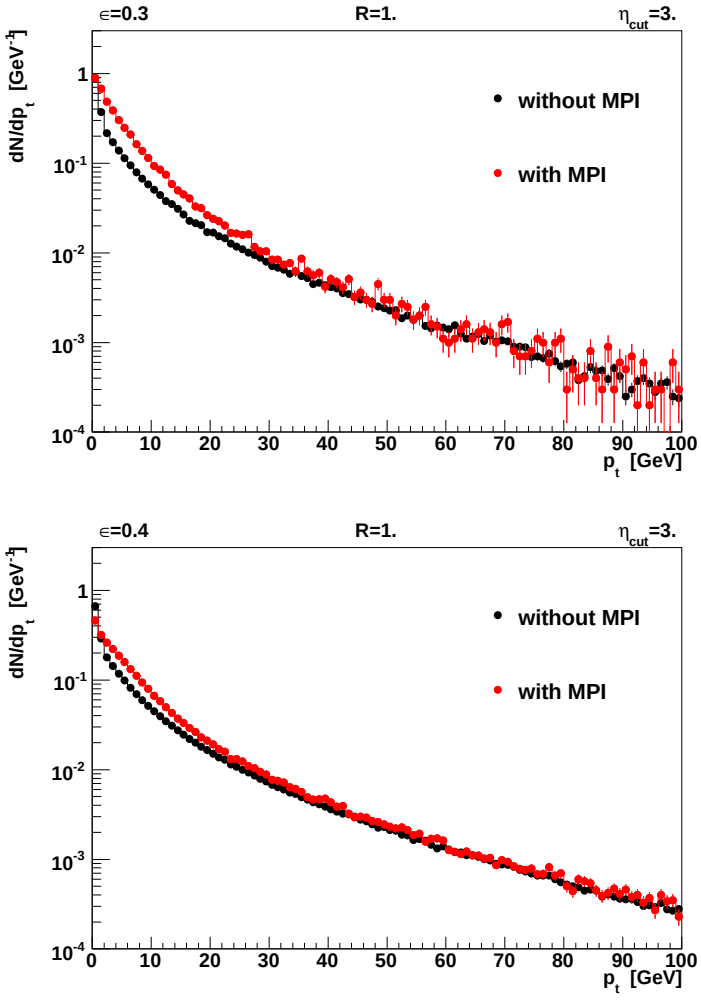

Figure 5.19: Comparison of the p_T distribution of the non MPI jets both for MPI being switched off and on. The distributions have been normalized with respect to the number of events.

done in order to eliminate one possible source of the problem. In the following we will renounce an η cut. It is possible that multi parton interaction radiates along the beam axis. However we want to reconstruct all multi parton interactions. Thus we skip an η cut[5]. We see no real improvement in both figures. This corresponds to the situation in fig.(5.15) and (5.16) for the Λ case.

In order to understand the reason why the algorithm cannot recognize all multi parton interactions we focus on one single event. After switching off parton showers we see in the event record parton pairs which are exactly back-to-back. This should not surprise us as only MPI is on and there is nothing that could smear the back-to-back relation. It is possible to obtain the true number of multi parton interactions[6].

Because of the fact that the pairs are exactly back-to-back the ε parameter can be set as near as possible to zero (however not exactly equal to zero). One possible choice would be $\varepsilon = 0.00000001$. The R value remains unchanged that means $R = 1$. The algorithm does not detect all MPI jet pairs. Many are dismissed as non MPI jets. For simplification we only allow two back-to-back pairs as input for the algorithm. The result is that the algorithm yields 3 non MPI jets and no MPI jet.
By looking directly into the algorithm we see that the d_{ij} are systematically too low compared to the $\tilde{d}_{ij}$. This leads to the merging of two protojets where each of them comes from a different pair. Thus protojets are dismissed as non MPI jets. An illustration of this misidentification can be seen in fig.(5.22).

As the problem lies in the d_{ij} values which are too low we conclude that it can be solved by a different scaling which means we must go to lower R values. By that procedure the d_{ij} will become bigger. We switch to lower R values. The desired result is obtained with $R = 0.1$.
The next step is to investigate whether this works now for a whole simulation. The result of this can be seen in fig.(5.23). In the ideal case we should see no non MPI jets no matter whether multi parton interaction is switched on or off. This is not the case in fig. (5.23). What we see however is that the agreement between the case of MPI being switched off and MPI being switched on becomes better and better the lower the R value is taken. The best value seems to be $R = 0.01$. However for practical applications the best value seems to be $R = 0.1$ because with lower values we resolve single partons which is in a realistic application inappropriate as we deal here with

[5]Later in fig.(5.31) we will see that removing the η cut is justified.
[6]see for that page 275 of [13] (variable MINT(351))

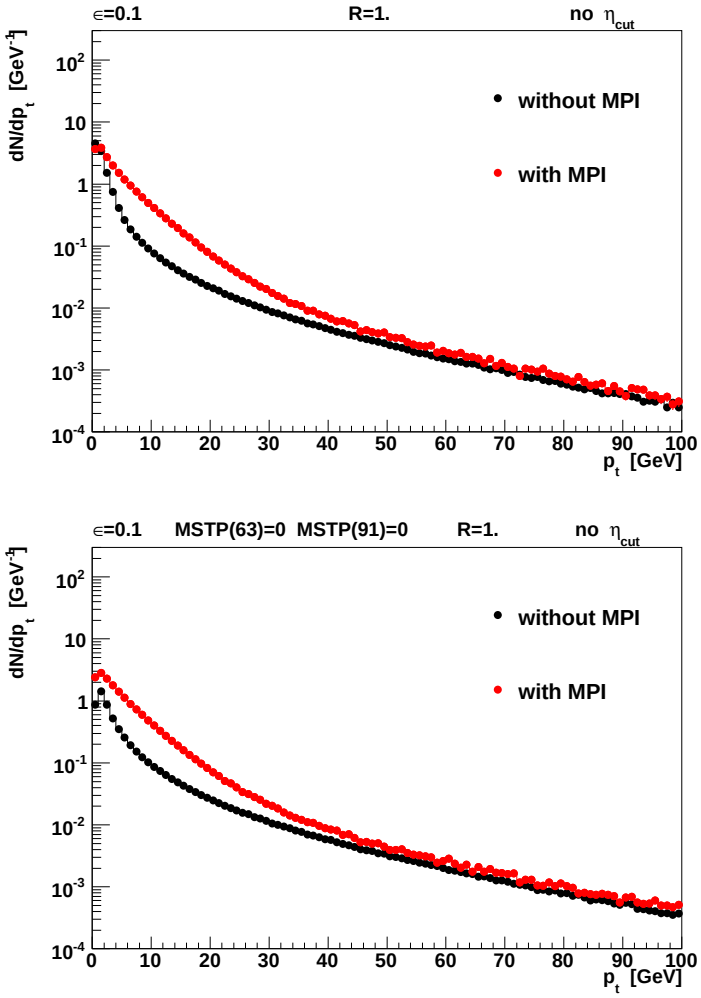

Figure 5.20: Comparison of the p_T distribution of the non MPI jets both for MPI being switched off and on. In the plot above we have standard parton showers on. In the plot beneath we have no primordial k_t and no further branching after initial state radiation. The distributions have been normalized with respect to the number of events.

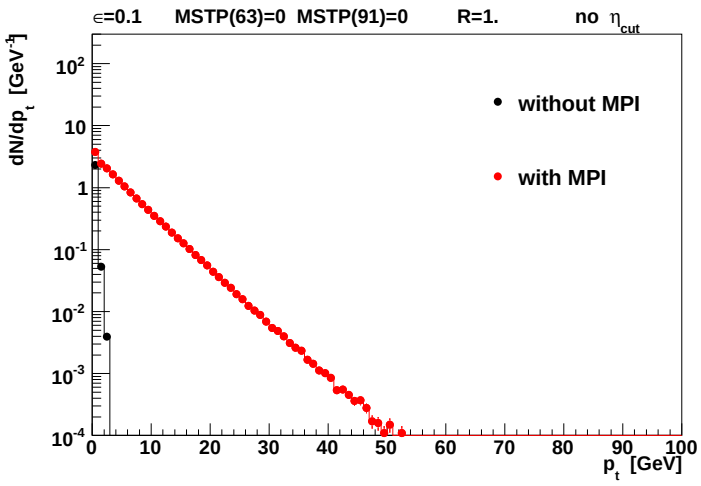

Figure 5.21: Comparison of the p_T distribution of the non MPI jets both for MPI being switched off and on. Parton showers were switched off. We have no primordial k_t. The distributions have been normalized with respect to the number of events. Please note that for the case that MPI is switched off not the whole distribution vanishes due to the absence of an η cut. This is in contrast to fig.(5.12) where we have an η cut.

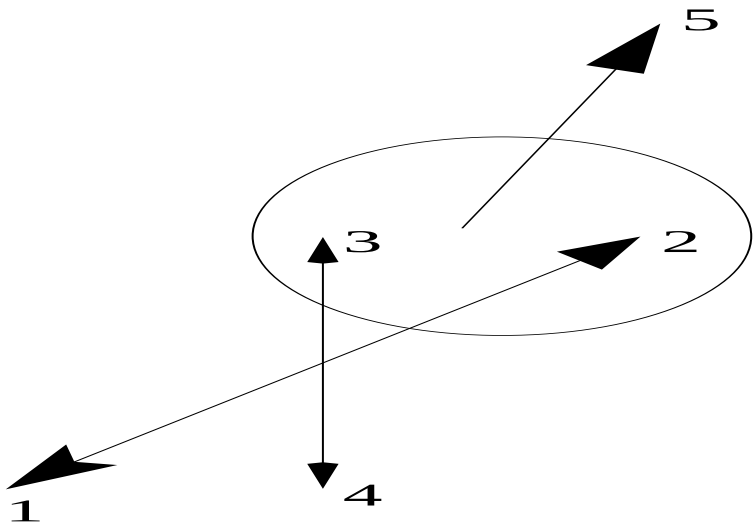

Figure 5.22: An illustration of the merging of two protojets inside the MPI jet algorithm. The protojets 2 and 3 are merged to the new protojet 5. After that we have no back-to-back pair. The three protojets 1, 4 and 5 are regarded as non MPI jets.

jets consisting of hadrons.

As a next step we want to ensure that the number of reconstructed multi parton interactions and the true number of multi parton interactions are similar. The result is given in fig.(5.24) where we compare the true number of multi parton interactions with the number of reconstructed MPI jets. These plots correspond to fig.(5.23) where the p_t distribution is shown. As we see the choice $R = 0.3$ yields a really bad result while already the choice $R = 0.1$ yields a rather good aggreement. The best result is given by $R = 0.01$. However as discussed above we consider R values less than 0.1 as too small. We conclude therefore that for our purpose the most appropriate R value is 0.1.

In case of only one multi parton interaction the distribution of the reconstructed MPI tends to be too low as can be seen in fig.(5.24)[7]. The reason for this is a preclustering of partons in case of small parton-parton mass.

As a next step we focus on a realistic scenario. The result of this can be seen in fig.(5.25). We see that we have no longer agreement. The reason for this is that we have in a realistic scenario smearing effects: MPI jets are no longer exactly back to back.

[7]This can be seen in the first bin of every plot.

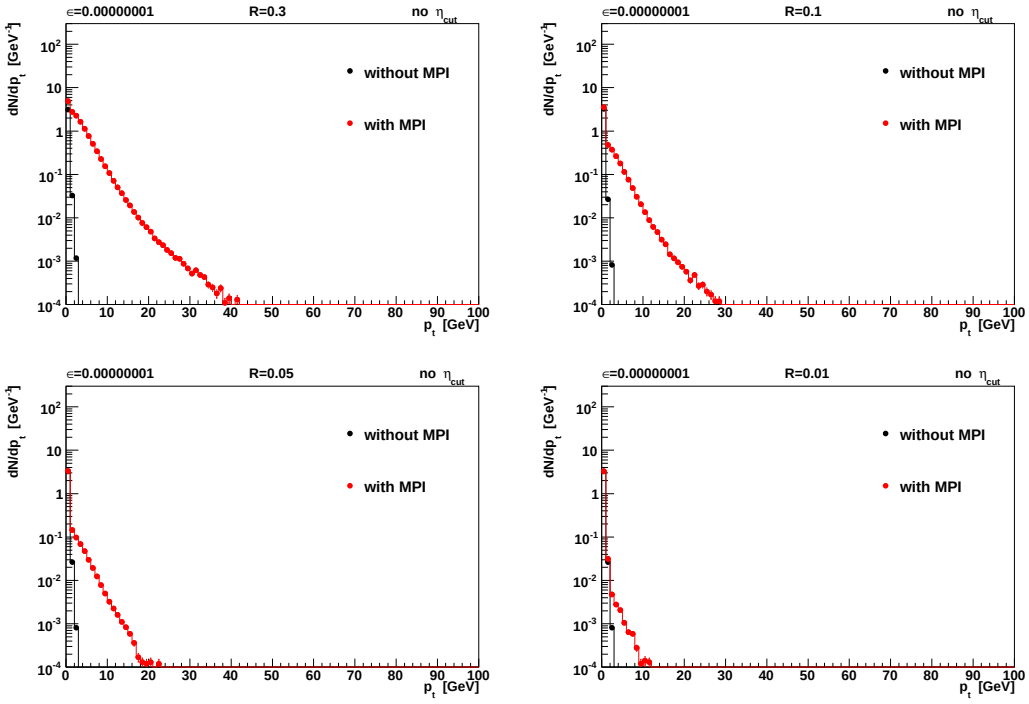

Figure 5.23: Comparison of the p_T distribution of the non MPI jets both for MPI being switched off and on. The distributions are compared for several R values. Parton showers were switched off. The distributions have been normalized with respect to the number of events.

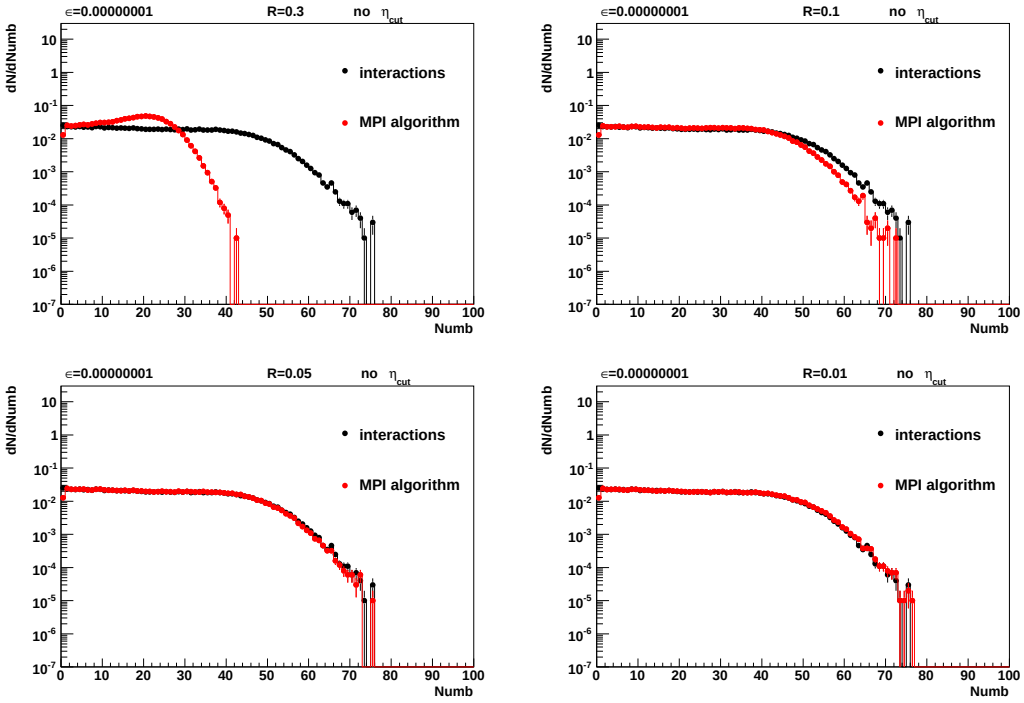

Figure 5.24: Comparison for several R values. The true distribution for the number of MPI interactions ("interactions") versus the number of reconstructed MPI interactions ("MPI alogorithm") is plotted. Here we have no PS and no hadrionization switched on.

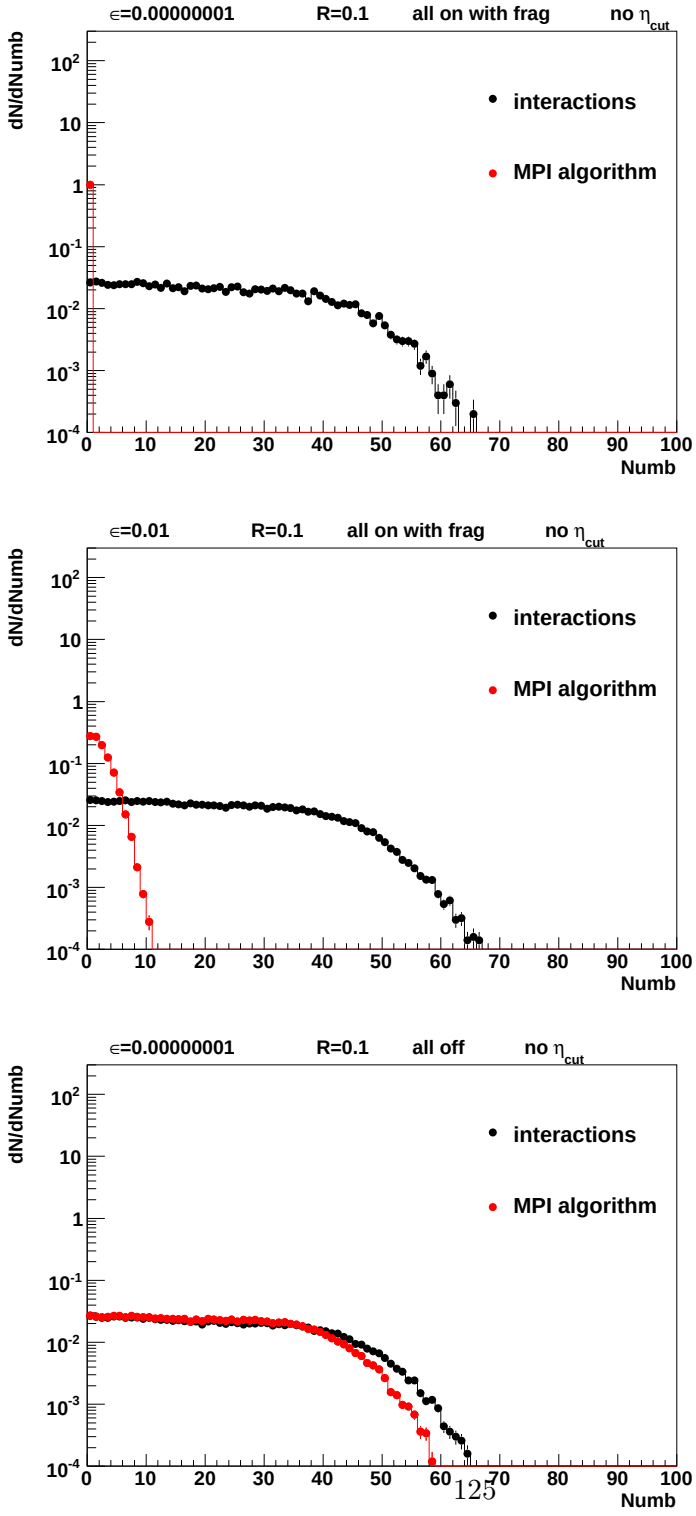

Figure 5.25: Comparison of the number of MPI interactions ("interactions") versus the number of reconstructed MPI interactions ("MPI alogorithm"). In the lowest plot everything is switched off (with the exception of MPI itself) while in the two upper plots everything is switched on.

Thus we must switch to higher ε values. However it is a priori not clear which value is the proper one. We must therefore tune the value.

The result can be seen in fig.(5.26). We see that while $\varepsilon = 0.043$ yields a rather good agreement the value $\varepsilon = 0.035$ yields a rather bad result. Thus we conclude that the algorithm works for a parameter set $R = 0.1$ and $\varepsilon = 0.043$.

In order to verify this statement we check the p_t distributions for the non MPI jets. The result can be seen in (5.27). As expected the agreement is rather good.

On the other hand we observe in the first two plots in fig.(5.26) (with $\varepsilon = 0.043$ and $\varepsilon = 0.045$) that the algorithm has in the region of only a few interactions (about 1 to 5 interactions) the tendency not to reconstruct the correct number of interactions as seen by the red curve which is systematically too low. This means that in this region the algorithm reconstructs too many interactions. The reason for this lies in the rather high ε value. Too many potential back-to-back pairs are included in the $\tilde{d}_{ij}$ array what leads to the reconstruction of too many interactions. That this is true can be checked by going to lower ε values. The result of this can be seen in fig.(5.28). We see that with lower ε values this problem more and more dissapears. However the agreement as a whole between the true number of multi parton interactions and the number of reconstructed multi parton interactions becomes worse and worse. Thus we conclude that the value $\varepsilon = 0.043$ is still a reasonable compromise.

Then we can compare further the distributions of the non MPI jets, the MPI jets and the sum of them. This can be seen in fig.(5.29). We see that the program detects clearly more MPI jets when multi parton interaction is switched on.

Further in fig.(5.30) we see the distribution of the MPI jets compared both for the case that MPI is switched off and on. We see that the distribution has a tail to large values when MPI is switched on as it is supposed to be.

Then we investigate the influence of an η cut. This can be seen in fig.(5.31). We see that the reconstructed number of multi parton interactions is no longer in such a good agreement.

As a final remark it would be good to take a look at fig.(5.32). Here we see a comparison between the Λ and the ε case. We see that the algorithm with ε performs better. The difference however is not big.

Until now we had investigated MPI in a model where the multi parton interaction did not undergo any parton shower (old model in PYTHIA). We

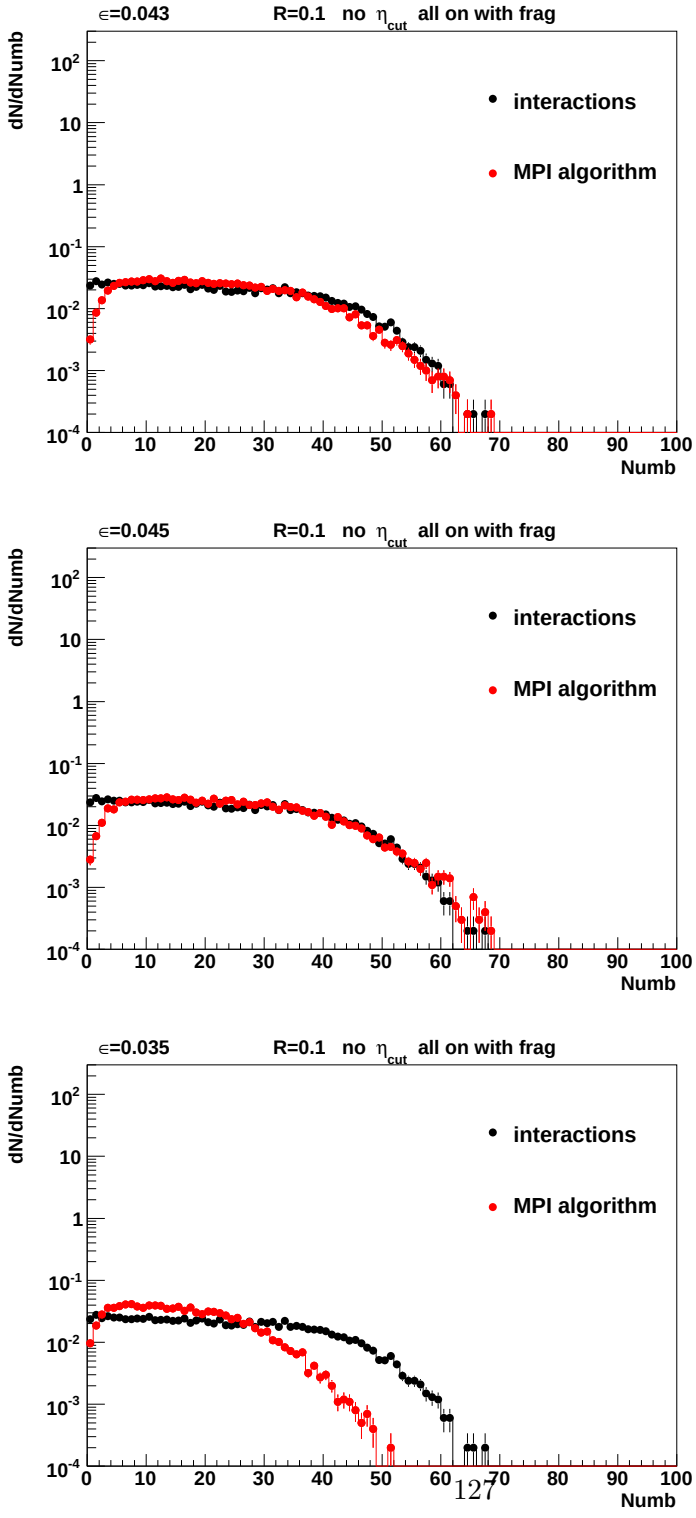

Figure 5.26: Comparison for several ε values. The true distribution for the number of MPI interactions ("interactions") versus the number of reconstructed MPI interactions ("MPI alogortihm") is plotted. The distributions have been normalized with respect to the number of events.

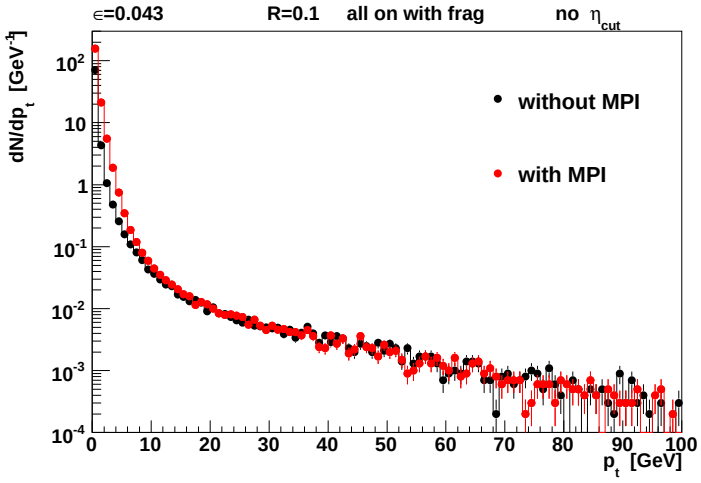

Figure 5.27: Comparison of the p_T distribution of the non MPI jets both for MPI being switched off and on. The distributions have been normalized with respect to the number of events.

now investigate the 'new' model, where MPI can also have initial and final state parton showers.
As a first step we use the parameter set from above, $R = 0.1$ and $\varepsilon = 0.043$. The comparison for the number of multi parton interactions can be seen in fig.(5.33). As we see there is a clear disagreement. We investigate this by switching off both primoridial $k_\perp$ and associated time-like branching of the initial state parton shower[8]. The result of this can be seen in fig.(5.34). We see that this does not solve the problem (compare in contrast to that as an example fig.(5.26) where we see the distribution for the true number of multi parton interactions in the old model). It is on the other hand possible in PYTHIA to switch off the extra PS for the MPI. Then we have, as in the old MPI model, only PS for the main interaction. The result can be seen in fig.(5.35). We see that the disagreement is rather big. From the plots (5.33) to (5.35) we see that that in the new model the distribution for the real number of multi parton interactions is not so extended as in the old model even when parton showers are switched off. Further we see that the proper value for ε is dependent on the real number of MPI. The reason for this must be traced back to the fact that the new model uses a different parameter set as a tune. A way to address this would be to tune again the ε

[8]See for that page 321 of [13]

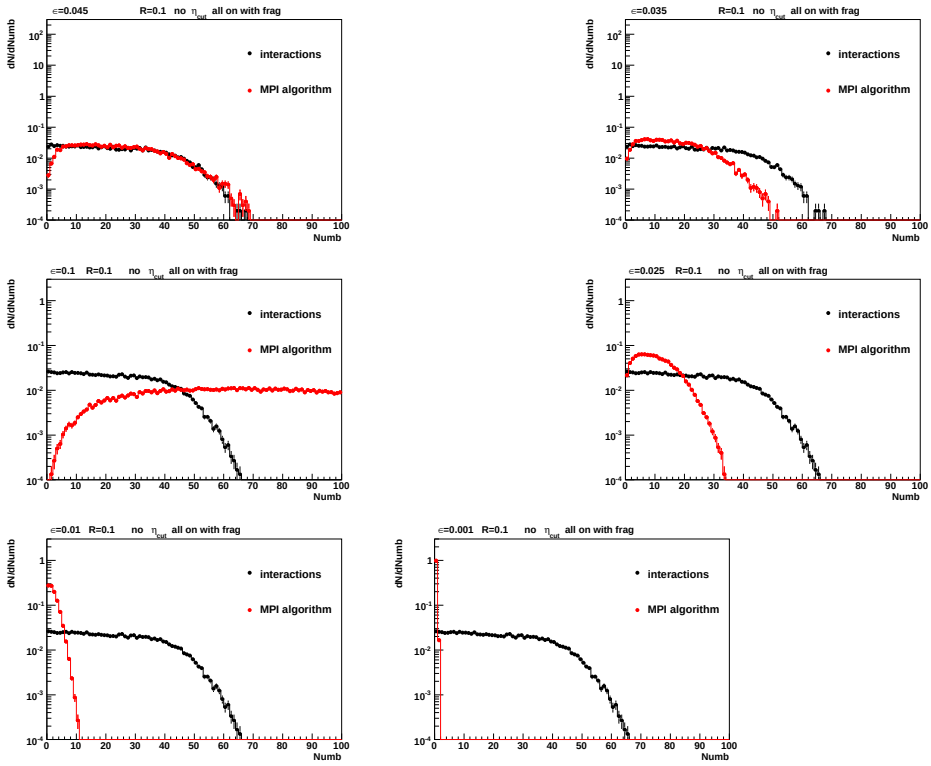

Figure 5.28: Comparison for several ε values. The true distribution for the number of MPI interactions ("interactions") versus the number of reconstructed MPI interactions ("MPI algorithm") is plotted. The distributions have been normalized with respect to the number of events.

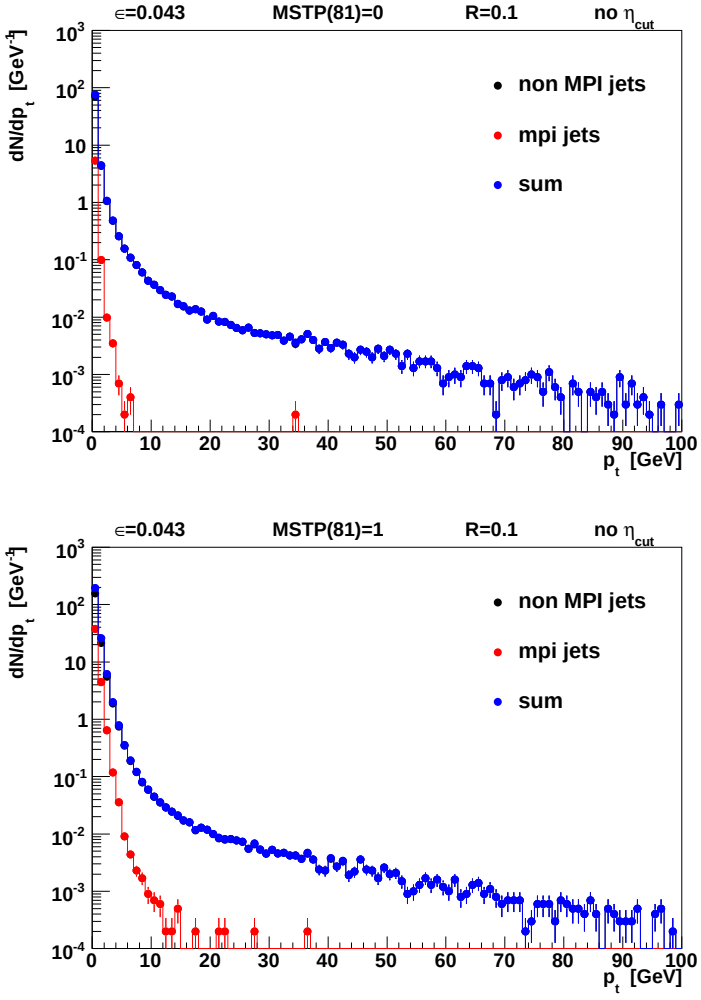

Figure 5.29: Comparison of the p_T distribution of the non MPI jets, the MPI jets and their sum. In the plot above multi parton interaction has been switched off while in the plot beneath multi parton interaction has been switched on. The distributions have been normalized with respect to the number of events.

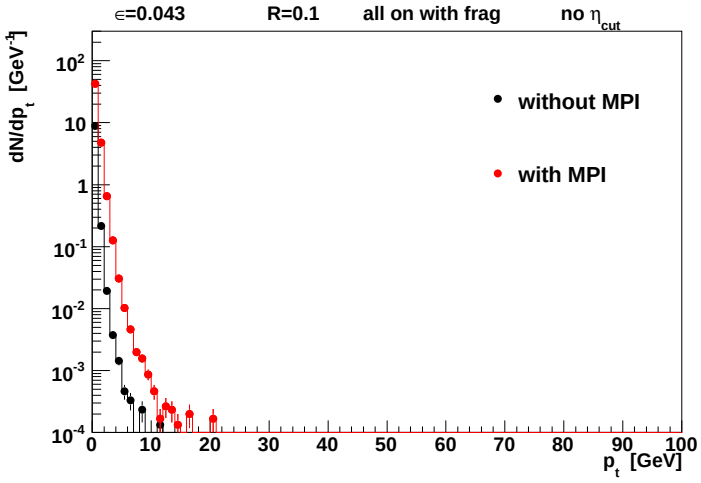

Figure 5.30: Comparison of the p_T distribution of the MPI jets. The distributions have been normalized with respect to the number of events.

value as it has been done in the previous section. The result can be seen in (5.36) where we see the comparison of the distributions for several ε values. We conclude that $\varepsilon = 0.02$ is the best choice.

In fig.(5.37) we see the comparison for the non MPI jets. We see that the agreement is rather good.

Summary and Outlook

As we see the parameter set used in the two models are quit different: while we obtained for the old model $\varepsilon = 0.043$ and $R = 0.1$ we find for the new model $\varepsilon = 0.02$ and $R = 0.1$. As discussed in the last section this difference cannot be traced back to the fact that in the new model there are also parton showers for the multi parton interactions. This has been proven by fig.(5.35) where parton showers for MPI in the new model have been switched off.

In fig.(5.38) we compare the distribution of the "true" number of MPI both in the new and in the old model. We see that there is a huge difference. That the distribution (including its shape) in the new model is so different must be traced back to the fact that in the new model a different parameter set is used. As the distribution of the "true" number of MPI is so different in the new model even when parton showers for the multi parton interaction are switched off we need for the application of the $k_\perp^{++}$ algorithm a completely

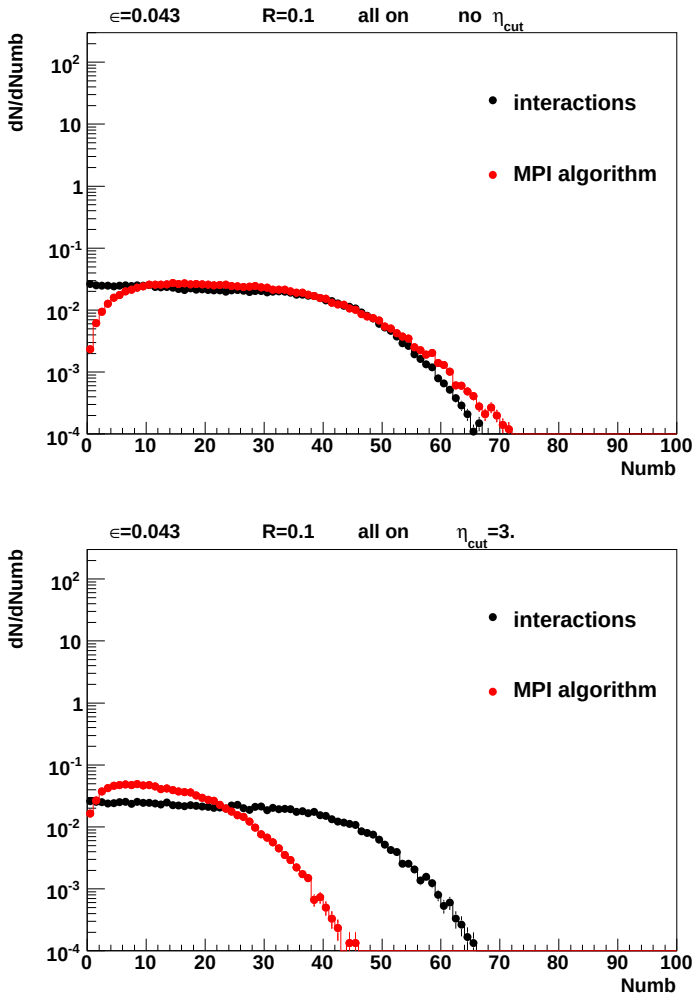

Figure 5.31: Comparison of the true number of multi parton interactions versus the number of reconstructed multi parton interactions. The distributions have been normalized with respect to the number of events. In the plot above we have no η cut while in the plot beneath we one.

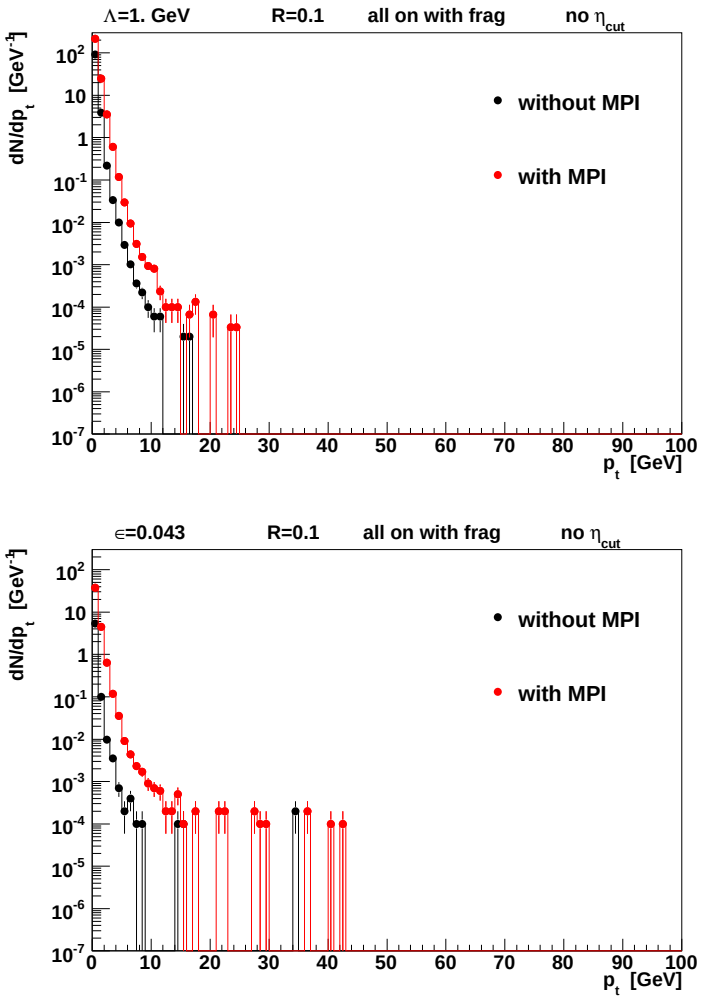

Figure 5.32: Comparison of the p_T distribution of the MPI jets. In the plot above we see the MPI jet distributions for the Λ case while in the plot beneath we see the MPI jet distributions for the ϵ case.

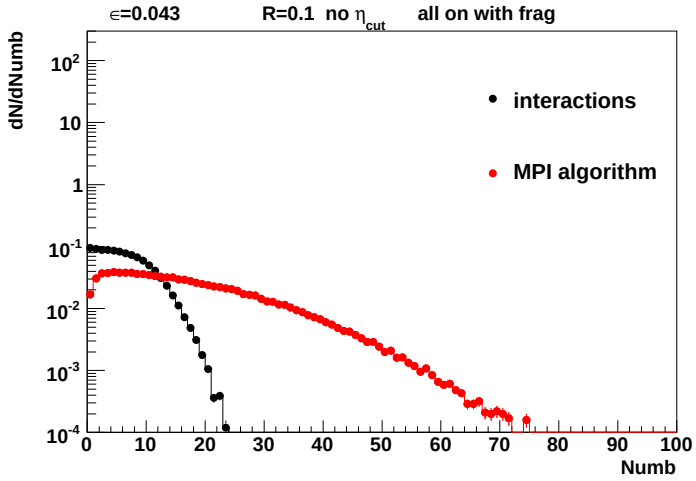

Figure 5.33: Comparison of the true number of multi parton interactions versus the number of reconstructed multi parton interactions. The simulation has been performed in the new model. The distributions have been normalized with respect to the number of events.

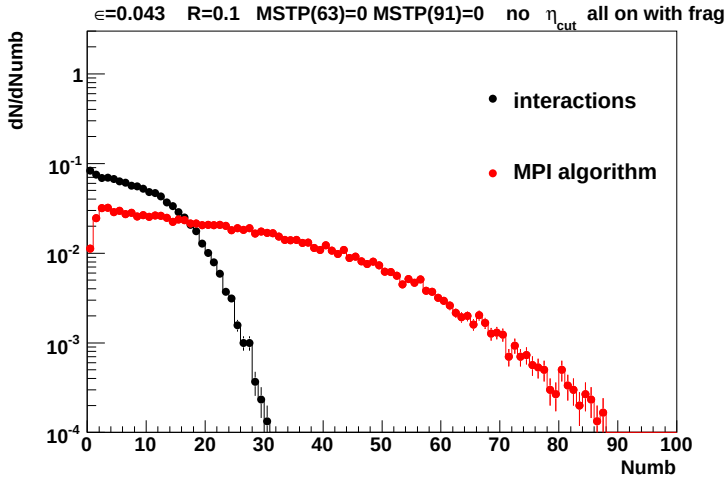

Figure 5.34: Comparison of the true number of multi parton interactions versus the number of reconstructed multi parton interactions. The simulation has been performed in the new model. The distributions have been normalized with respect to the number of events.

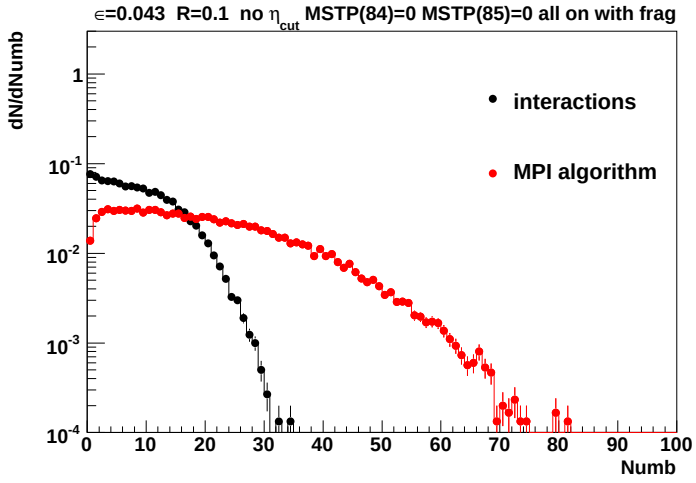

Figure 5.35: Comparison of the true number of multi parton interactions versus the number of reconstructed multi parton interactions. The simulation has been performed in the new model. The distributions have been normalized with respect to the number of events.

new ε value. This however is problematic, since we wanted to apply this algorithm for real data. The question that arises now is the following: which is the best choice for the parameter set of ε and R when we apply the algorithm for real data? As the ε values between the two models are so different this question cannot be answered in a straightforward manner. The main difference between the two models is that in the new model also parton showers for the multi parton interactions are included what is not the case in the old model. Because the new model is clearly closer to physical reality than the old model we would suggest that the parameter set $\varepsilon = 0.02$ and $R = 0.1$ is the best choice as can be seen from fig.(5.36). Such choice however would presume that the new model is close enough to physical reality (much closer than the old model) in order to justify it. To summarize we conclude that an algorithm based on a back-to-back relation for protojets is not well suited for detecting multi parton interaction.

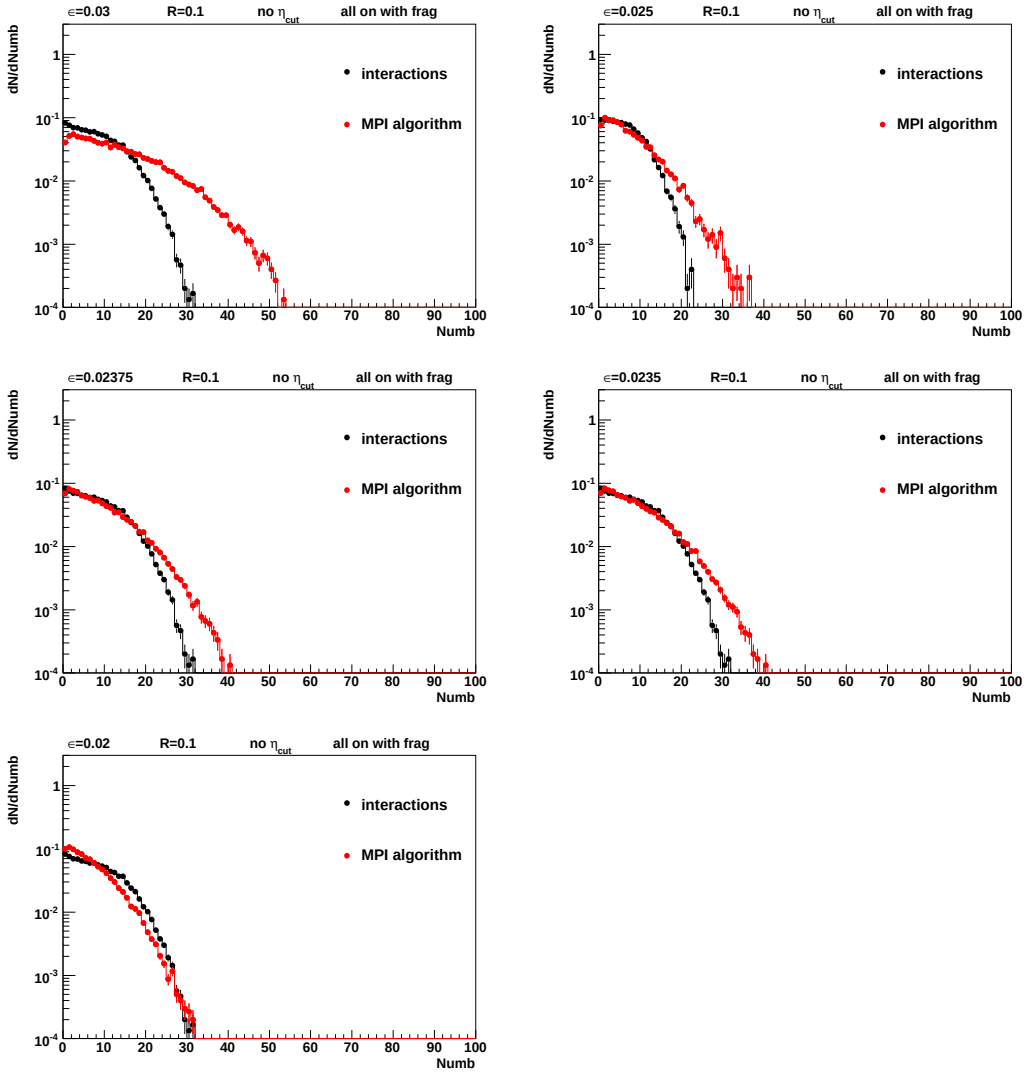

Figure 5.36: Comparison of the true number of multi parton interactions versus the number of reconstructed multi parton interactions for several ε values. The simulation has been performed in the new model. The distributions have been normalized with respect to the number of events.

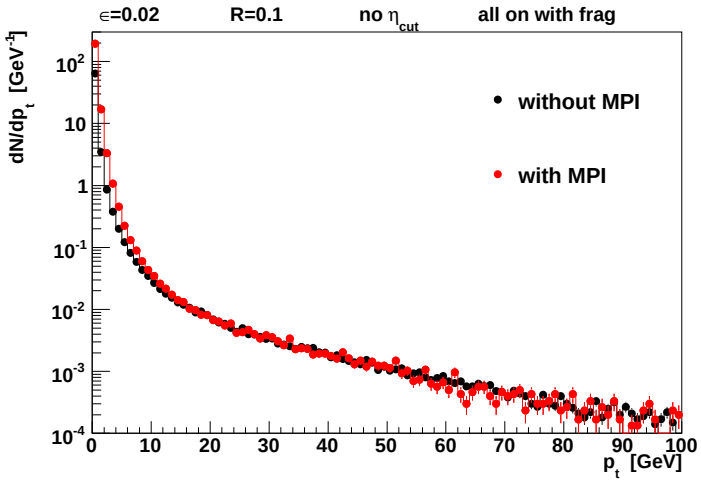

Figure 5.37: Comparison of the p_T distribution of the non MPI jets both for MPI being switched off and on. The simulation has been performed in the new model. The distributions have been normalized with respect to the number of events.

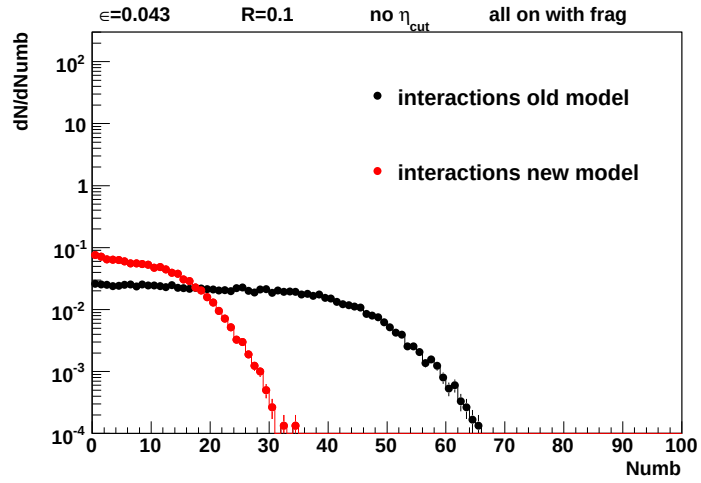

Figure 5.38: Comparison of the distribution of the number of multi parton interaction both for the old and the new model

Chapter 6

Summary

We applied an analytical formalism of parton showers to Drell Yan processes, with a dipole formalism which takes also interference effects into account. This formalism was originally developed in [1] and summarized in chapter (3). In [37] the formalism of [1] was applied to the distribution of the transverse momentum of the Z^0 boson. We used the results of [37] to show that the formalism can resum next-to-leading order logarithmic corrections. In the general case however there is a disagreement with respect to an integration boundary. This must be traced back to the usage of two different ordering variables. Else the two results agree well with each other[1]. This puts the parton shower formalism of [1] on a solid theoretical ground.
We compared the analytical result for the resummation of the energy fraction with the one obtained by the PYTHIA Monte Carlo event generator. The result was that the two approaches agree very well if the kinematical cut is properly adjusted.
What is the relation to measurements at a hadron-hadron collider like LHC? Although the energy fraction τ cannot be measured directly, the resummation of logarithmic corrections for $\tau \to 1$ is extremely important for any measurement when m_{DY} becomes large and eventually approaches $m_{\mathrm{DY}} \to \sqrt{s}$. In such a region of phase space, no hard jet in addition to the Drell Yan process can be produced. The detection of such a process was proposed as one of the interesting measurements for the high luminosity case at the LHC. A detailed measurement of this process is important for any search for new particles. $\tau \to 1$ is not only possible for $m_{\mathrm{DY}} \to \sqrt{s}$ but also when no parton emission is observed in a restricted rapidity range. The use of forward detectors with η coverage $|\eta| < 5$ in CMS/ATLAS enables such

[1] This means that the integrand is approximately equal.

measurements.
While for $\tau \to 1$ real emissions from the initial state cascade are suppressed, additional hard partons can occur from multi parton interaction, that is from secondary interaction.
We have considered a jet algorithm that was supposed to detect multi parton interactions based on a kinematical back-to-back relation for protojets. It came out that the algorithm works in an idealised case with a specially tuned parameter.

Appendix A

Integration of W_N

In this section it is our goal to perform the integration (with respect to eq.(4.83)) for the case of constant α_S. We will show that it is possible to obtain an exact result; however we will also show that this is numerically unstable. Thus even for constant α_S the numerical result obtained in section (4.3) is suitable.
For performing the integration let us take a look at eq.(4.83). Performing the $\mathbf{k}_\perp^2$ integration leads to

$$\ln W_N(Q^2;Q_0^2) = 2C_F\frac{\alpha_S}{\pi}\int_0^1 dz\frac{z^{N-1}-1}{1-z}\left\{\ln[(1-z)^2]+\ln\left[\frac{Q^2}{Q_0^2}\right]\right\} \times\theta((1-z)^2Q^2\geq Q_0^2)\ , \tag{A.1}$$

where we have relabeled ζ by z and written instead of $\ln W_{N,\,\text{resummation}}$ the expression $\ln W_N(Q^2;Q_0^2)$. Further we have explicitly introduced a θ function as a boundary condition for the z integration. The integration of the second term of this expression does not constitute a problem as we have

$$\int dz\frac{z^{N-1}-1}{1-z} = \frac{Nz^{1+N}{}_2F_1(1,1+N;2+N;z)+(1+N)(z^N+N\ln(1-z))}{N(1+N)}\ , \tag{A.2}$$

where ${}_2F_1(1,1+N;2+N;z)$ is a hypergeometric function. Now we must focus on the first term

$$2C_F\frac{\alpha_S}{\pi}\int_0^1 dz\frac{z^{N-1}-1}{1-z}\ln[(1-z)^2]\theta((1-z)^2Q^2\geq Q_0^2)\ . \tag{A.3}$$

The condition

$$(1-z)^2 Q^2 \geq Q_0^2 \tag{A.4}$$

can be written as

$$z \leq 1 - \sqrt{\frac{Q_0^2}{Q^2}} \ . \tag{A.5}$$

Thus we may write the expression given in (A.3) as

$$2C_F \frac{\alpha_S}{\pi} \int_0^{1-\sqrt{\frac{Q_0^2}{Q^2}}} dz \frac{z^{N-1}-1}{1-z} \ln[(1-z)^2] \ . \tag{A.6}$$

In principle we are able to perform an exact integration. The result however we obtain for the right side in eq.(A.1) is unstable because the expression given in eq.(A.6) contains after performing the z integration divergent terms. To overcome this problem we notice that the following relation holds[1]

$$\int z^n \ln z dz = \frac{z^{n+1}}{n+1} \ln z - \frac{z^{n+1}}{(n+1)^2} \ \ (n \neq -1; n \text{ integer}) \ . \tag{A.7}$$

Let us define the following function

$$A(x) := \int_0^x \frac{z^{N-1}-1}{1-z} \ln[(1-z)^2] dz \ \ (\text{with } 0 < x < 1) \tag{A.8}$$

with

$$x := 1 - \sqrt{\frac{Q_0^2}{Q^2}} \ . \tag{A.9}$$

By the substitution

$$\begin{aligned} b &:= 1 - z \\ \Rightarrow \frac{dz}{db} &= -1 \end{aligned} \tag{A.10}$$

A can be written as

$$A(x) = \int_{1-x}^1 db \frac{(1-b)^{N-1}-1}{b} \ln(b^2) \ . \tag{A.11}$$

[1] This relation is given in eq.(41.50) of [51] on page 69.

This can be rewritten as

$$\begin{aligned} A(x) &= 2\Bigg(\int_{1-x}^{1} \sum_{i=0}^{N-1} \left\{ \binom{N-1}{i} (-1)^i b^{i-1} \ln(b) db \right\} - \int_{1-x}^{1} \frac{\ln b}{b} db \Bigg) \\ &= 2\Bigg(\underbrace{\int_{1-x}^{1} \sum_{i=0}^{N-1} \left\{ \binom{N-1}{i} (-1)^i b^{i-1} \ln(b) db \right\}}_{C} - \int_{1-x}^{1} \frac{\ln b}{b} db \Bigg) \, . \end{aligned} \tag{A.12}$$

For the term C we can now apply eq.(A.7). This leads to

$$\begin{aligned} C &= \sum_{i=1}^{N-1} \binom{N-1}{i} (-1)^i \left[\frac{b^i}{i} \ln(b) - \frac{b^i}{i^2} \right]_{b=1-x}^{b=1} + \int_{1-x}^{1} \frac{\ln(b)}{b} \\ &= -\sum_{i=1}^{N-1} \binom{N-1}{i} (-1)^i \frac{1}{i^2} - \sum_{i=1}^{N-1} \binom{N-1}{i} (-1)^i \frac{(1-x)^i}{i} \ln(1-x) \\ &+ \sum_{i=1}^{N-1} \binom{N-1}{i} (-1)^i \frac{(1-x)^i}{i^2} + \int_{1-x}^{1} \frac{\ln(b)}{b} \, . \end{aligned} \tag{A.13}$$

To summarize, our result is now

$$\begin{aligned} A(x) = \\ 2\Bigg(&- \sum_{i=1}^{N-1} \binom{N-1}{i} (-1)^i \frac{1}{i^2} - \sum_{i=1}^{N-1} \binom{N-1}{i} (-1)^i \frac{(1-x)^i}{i} \ln(1-x) + \\ &+ \sum_{i=1}^{N-1} \binom{N-1}{i} (-1)^i \frac{(1-x)^i}{i^2} \Bigg) \, . \end{aligned} \tag{A.14}$$

Using MATHEMATICA gives

$$\begin{aligned}
&\ln W_N(Q^2,Q_0^2) = 2C_F\frac{\alpha_S}{\pi}\Bigg(\gamma_E^2+\frac{\pi^2}{6}+\\
&-2(-1+N)\sqrt{\frac{Q_0^2}{Q^2}}\,{}_4F_3\Bigg(\{1,1,1,2-N\};\{2,2,2\};\sqrt{\frac{Q_0^2}{Q^2}}\Bigg)\\
&+(-1+N)\sqrt{\frac{Q_0^2}{Q^2}}\,{}_3F_2\Bigg(\{1,1,2-N\};\{2,2\};\sqrt{\frac{Q_0^2}{Q^2}}\Bigg)\ln\left[\frac{Q_0^2}{Q^2}\right]\\
&+\frac{1}{2}\ln\left[\frac{Q_0^2}{Q^2}\right]\left(2B_\delta(N,0)+\ln\left[\frac{Q_0^2}{Q^2}\right]\right)+2\gamma_E\psi(N)+\psi(N)^2-\psi'(N)\Bigg)\,.
\end{aligned} \tag{A.15}$$

$B_\delta(N,0)$ is here a Beta function[2]. The function ψ is the Digamma function and γ_E is the Euler-Mascheroni constant. In fig.(A.1) we see the distribution of $\ln W_N(Q^2,Q_0^2)$. We took as values $Q_0^2 = 1\text{GeV}^2$, $Q^2 = M_Z^2$ with $M_Z = 91.88$ GeV and $\alpha_S = 0.2$. The range was set from $N = 1$ to $N = 1000$.
In fig.(A.1) we see that the distribution increases rather fast for decreasing N while it becomes constant for $N > 400$. This is exactly what we expect: from eq.(4.2) we see that only those $W(\tau,N)$ with $\tau \approx 1$ contribute to $W_N(Q^2)$ in the high N limit. Thus $\ln W_N(Q^2;Q_0^2)$ becomes constant for $N \gg 1$. However the expression given in eq.(A.15) shows in some regions of Q_0^2 extreme numerical instabilities ((up to $3*10^{10}$)). This is due to rounding errors (up to $3*10^{10}$). This can be seen in fig.(A.2). This instability comes from the two hypergeometric functions given in eq.(A.15). Thus even for $\alpha_S = \text{const.}$ it is meaningful to use the numerical expression which is given in eq.(4.113). In fig.(A.3) we see the same function derived by the numerical expression. We see that it is now well behaved.

A.0.4 Difference between the resummation result and the parton shower result

Here we further investigate the difference between $\ln W_{N,\text{res}}$ and $\ln W_{N,\text{PS}}$. The execution of the integral given in eq.(4.109) by MATHEMATICA yields

$$\begin{aligned}
&\ln W_{N,\text{res}} - \ln W_{N,\text{PS}} =\\
&\frac{\alpha_S}{6\pi}C_F(6\gamma_E^2+\pi^2+6\psi(N)(2\gamma_E+\psi(N))-6\psi'(N))
\end{aligned} \tag{A.16}$$

[2] with $\delta = 1-\sqrt{\frac{Q_0^2}{Q^2}}$

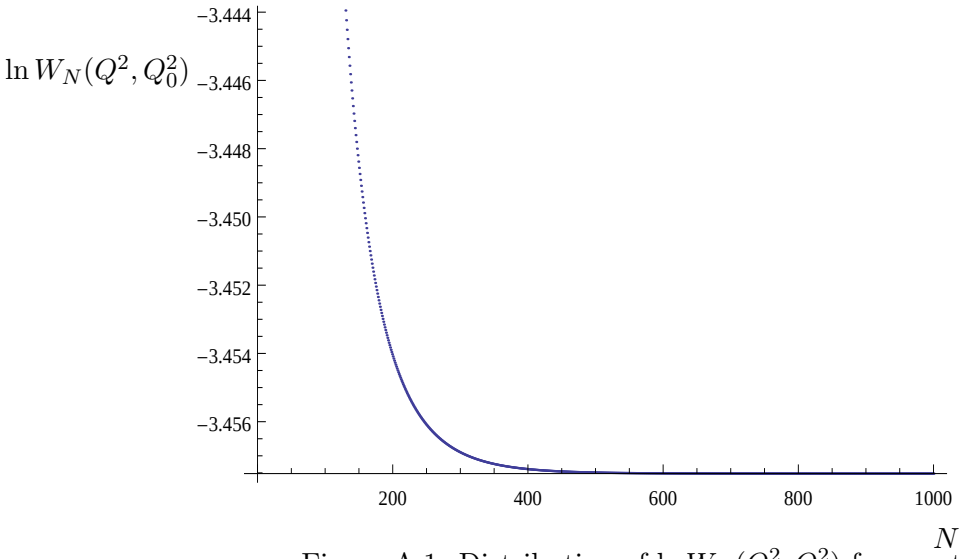

Figure A.1: Distribution of $\ln W_N(Q^2, Q_0^2)$ for constant α_S

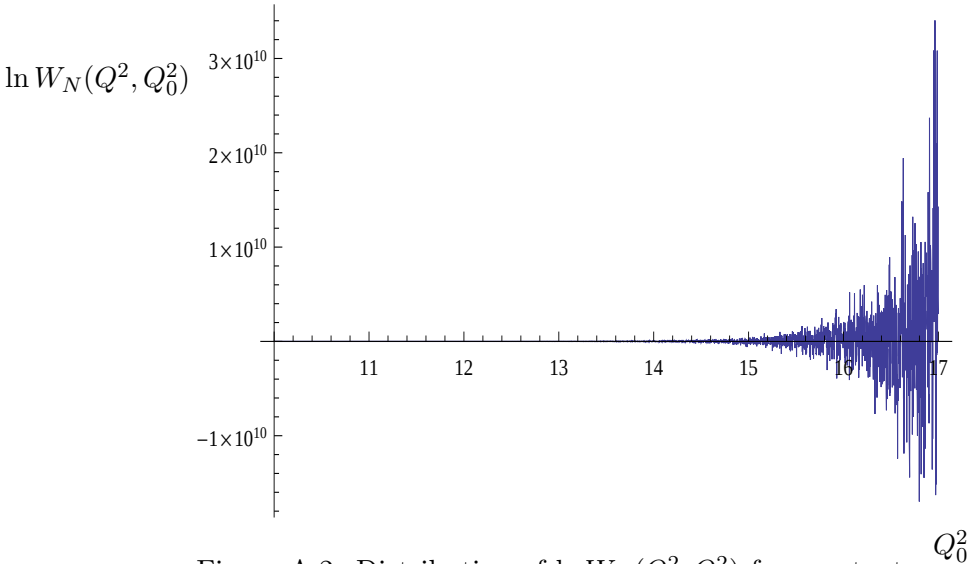

Figure A.2: Distribution of $\ln W_N(Q^2, Q_0^2)$ for constant α_S with respect to Q_0^2. N was set to 1500 while Q^2 was equal to M_Z^2 with $M_Z = 91.88$ GeV. The exact solution given in eq.(A.15) is plotted. The plot shows an extreme numerical instability due to rounding errors.

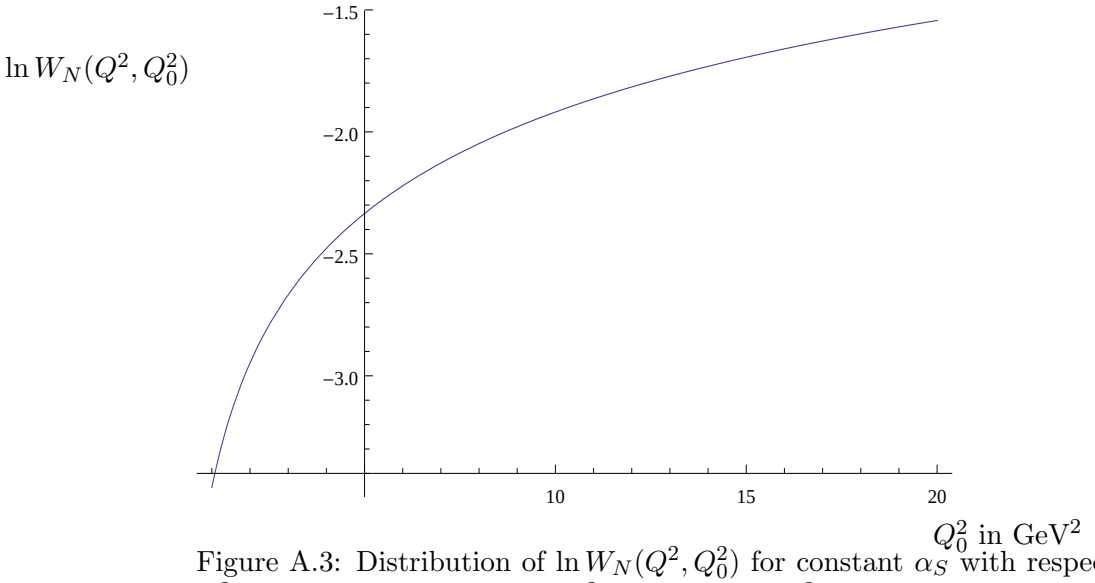

Figure A.3: Distribution of $\ln W_N(Q^2, Q_0^2)$ for constant α_S with respect to Q_0^2. N was set to 1500 while Q^2 was equal to M_Z^2 with $M_Z = 91.88$ GeV. In contrast to plot (A.2) we have now the numerical integration of eq.(4.113). Now the solution is numerically stable.

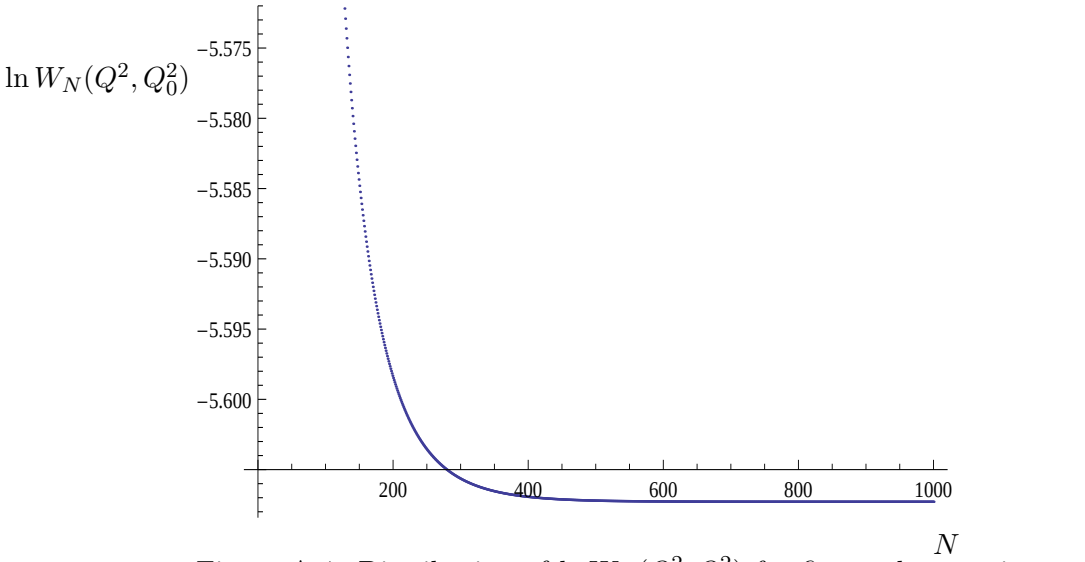

Figure A.4: Distribution of $\ln W_N(Q^2, Q_0^2)$ for first order running α_S with respect to Q_0^2.

with ψ as the digamma function.
As a next step we can look at the case of first order running α_S. In that case we have (see for that eq.(2.43) of [3])

$$\alpha_S(\mathbf{k}_\perp^2) = \frac{1}{\beta_0 \ln\left(\mathbf{k}_\perp^2/\Lambda^2\right)} \ . \tag{A.17}$$

Further we have

$$\int \frac{d\mathbf{k}_\perp^2}{\beta_0 \mathbf{k}_\perp^2 \ln\left(\mathbf{k}_\perp^2/\Lambda^2\right)} = \frac{\ln\left(\ln(\mathbf{k}_\perp^2/\Lambda^2)\right)}{\beta_0} \ . \tag{A.18}$$

With that we can rewrite $\ln W_{N,\,\mathrm{res}}$ and $\ln W_{N,\,\mathrm{PS}}$ as

$$\ln W_{N,\,\mathrm{res}} = 2\frac{C_F}{\pi\beta_0}\int_0^1 dz \left\{\ln\left(\ln\left(\frac{(1-z)^2Q^2}{\Lambda^2}\right)\right) - \ln\left(\ln\left(\frac{Q_0^2}{\Lambda^2}\right)\right)\right\} \tag{A.19}$$

and

$$\ln W_{N,\,\mathrm{PS}} = 2\frac{C_F}{\pi\beta_0}\int_0^1 dz \left\{\ln\left(\ln\left(\frac{(1-z)Q^2}{\Lambda^2}\right)\right) - \ln\left(\ln\left(\frac{Q_0^2}{\Lambda^2}\right)\right)\right\} \ . \tag{A.20}$$

This yields

$$\begin{aligned} &\ln W_{N,\,\mathrm{res}} - \ln W_{N,\,\mathrm{PS}} = \\ &2\frac{C_F}{\pi\beta_0}\int_0^1 dz \left\{\ln\left[\ln\left(\frac{(1-z)^2Q^2}{\Lambda^2}\right)\right] - \ln\left(\frac{(1-z)Q^2}{\Lambda^2}\right)\right\} = \\ &2\frac{C_F}{\pi\beta_0}\int_0^1 dz \ln\left[\frac{\ln\left[\frac{(1-z)^2Q^2}{\Lambda^2}\right]}{\ln\left[\frac{(1-z)Q^2}{\Lambda^2}\right]}\right] \end{aligned} \tag{A.21}$$

Such an integral can be only numerically solved.

Bibliography

[1] Zoltan Nagy and Davison E. Soper, "Parton showers with quantum interference," *JHEP*, **09**(2007), 114, 0706.0017.

[2] S. Catani and L. Trentadue, "Resummation of the QCD Perturbative Series for Hard Processes," *Nucl. Phys.*, **B327**(1989), 323.

[3] R. Ellis, W.Stirling, and B.Webber, QCD and Collider Physics, Camebridge University Press, 2003.

[4] Victor S. Fadin, E. A. Kuraev, and L. N. Lipatov, "On the Pomeranchuk Singularity in Asymptotically Free Theories," *Phys. Lett.*, **B60**(1975), 50.

[5] E. A. Kuraev, L. N. Lipatov, and Victor S. Fadin, "Multi - Reggeon Processes in the Yang-Mills Theory," *Sov. Phys. JETP*, **44**(1976), 443, [Zh. Eksp. Teor. Fiz.71,840(1976)].

[6] I. I. Balitsky and L. N. Lipatov, "The Pomeranchuk Singularity in Quantum Chromodynamics," *Sov. J. Nucl. Phys.*, **28**(1978), 822, [Yad. Fiz.28,1597(1978)].

[7] Marcello Ciafaloni, "Coherence Effects in Initial Jets at Small q**2 / s," *Nucl. Phys.*, **B296**(1988), 49.

[8] S. Catani, F. Fiorani, and G. Marchesini, "QCD Coherence in Initial State Radiation," *Phys. Lett.*, **B234**(1990), 339.

[9] S. Catani, M. Ciafaloni, and F. Hautmann, "High-energy factorization and small x heavy flavor production," *Nucl. Phys.*, **B366**(1991), 135.

[10] Giuseppe Marchesini, "QCD coherence in the structure function and associated distributions at small x," *Nucl. Phys.*, **B445**(1995), 49, hep-ph/9412327.

[11] Bo Andersson *et al.* (Small x), "Small x phenomenology: Summary and status," *Eur. Phys. J.*, **C25**(2002), 77, hep-ph/0204115.

[12] Hannes Jung, "k(t) factorization and CCFM: The Solution for describing the hadronic final states: Everywhere?" *Mod. Phys. Lett.*, **A19**(2004), 1, hep-ph/0311249.

[13] Torbjorn Sjostrand, Stephen Mrenna, and Peter Z. Skands, "PYTHIA 6.4 Physics and Manual," *JHEP*, **05**(2006), 026, hep-ph/0603175.

[14] Torbjorn Sjostrand, "The Lund Monte Carlo for Jet Fragmentation and e+ e- Physics: Jetset Version 6.2," *Comput. Phys. Commun.*, **39**(1986), 347.

[15] Torbjorn Sjostrand and Mats Bengtsson, "The Lund Monte Carlo for Jet Fragmentation and e+ e- Physics. Jetset Version 6.3: An Update," *Comput. Phys. Commun.*, **43**(1987), 367.

[16] Leif Lonnblad, "ARIADNE version 4: A Program for simulation of QCD cascades implementing the color dipole model," *Comput. Phys. Commun.*, **71**(1992), 15.

[17] G. Marchesini and B. R. Webber, "Monte Carlo Simulation of General Hard Processes with Coherent QCD Radiation," *Nucl. Phys.*, **B310**(1988), 461.

[18] G. Marchesini, *et al.*, "HERWIG: A Monte Carlo event generator for simulating hadron emission reactions with interfering gluons. Version 5.1 - April 1991," *Comput. Phys. Commun.*, **67**(1992), 465.

[19] Stephen D. Ellis and Davison E. Soper, "Successive combination jet algorithm for hadron collisions," *Phys. Rev.*, **D48**(1993), 3160, hep-ph/9305266.

[20] Gavin P. Salam and Gregory Soyez, "A Practical Seedless Infrared-Safe Cone jet algorithm," *JHEP*, **05**(2007), 086, 0704.0292.

[21] Matteo Cacciari, Gavin P. Salam, and Gregory Soyez, "The Anti-k(t) jet clustering algorithm," *JHEP*, **04**(2008), 063, 0802.1189.

[22] Vardan Khachatryan *et al.* (CMS), "Distributions of Topological Observables in Inclusive Three- and Four-Jet Events in pp Collisions at sqrt(s) = 7 TeV," *Eur. Phys. J.*, **C75**(2015) (7), 302, 1502.04785.

[23] Georges Aad *et al.* (ATLAS), "Measurement of three-jet production cross-sections in *pp* collisions at 7 TeV centre-of-mass energy using the ATLAS detector," *Eur. Phys. J.*, **C75**(2015) (5), 228, 1411.1855.

[24] S. Catani, B. R. Webber, and G. Marchesini, "QCD coherent branching and semiinclusive processes at large x," *Nucl. Phys.*, **B349**(1991), 635.

[25] J. Alwall, *et al.*, "The automated computation of tree-level and next-to-leading order differential cross sections, and their matching to parton shower simulations," *JHEP*, **07**(2014), 079, 1405.0301.

[26] S. Agostinelli *et al.* (GEANT4), "GEANT4: A Simulation toolkit," *Nucl. Instrum. Meth.*, **A506**(2003), 250.

[27] John Allison *et al.*, "Geant4 developments and applications," *IEEE Trans. Nucl. Sci.*, **53**(2006), 270.

[28] Andy Buckley *et al.*, "General-purpose event generators for LHC physics," *Phys. Rept.*, **504**(2011), 145, 1101.2599.

[29] M. Bahr *et al.*, "Herwig++ Physics and Manual," *Eur. Phys. J.*, **C58**(2008), 639, 0803.0883.

[30] H. Jung *et al.*, "The CCFM Monte Carlo generator CASCADE version 2.2.03," *Eur. Phys. J.*, **C70**(2010), 1237, 1008.0152.

[31] Torbjorn Sjostrand, Stephen Mrenna, and Peter Z. Skands, "A Brief Introduction to PYTHIA 8.1," *Comput. Phys. Commun.*, **178**(2008), 852, 0710.3820.

[32] T. Sjostrand and Peter Z. Skands, "Multiple interactions and the structure of beam remnants," *JHEP*, **03**(2004), 053, hep-ph/0402078.

[33] C. Adloff *et al.* (H1), "A Measurement of the proton structure function f2 (x, q**2) at low x and low q**2 at HERA," *Nucl. Phys.*, **B497**(1997), 3, hep-ex/9703012.

[34] C. Adloff *et al.* (H1), "Deep inelastic inclusive e p scattering at low x and a determination of alpha(s)," *Eur. Phys. J.*, **C21**(2001), 33, hep-ex/0012053.

[35] F. D. Aaron *et al.* (ZEUS, H1), "Combined Measurement and QCD Analysis of the Inclusive e+- p Scattering Cross Sections at HERA," *JHEP*, **01**(2010), 109, 0911.0884.

[36] A. Donnachie and P. V. Landshoff, "Total cross-sections," *Phys. Lett.*, **B296**(1992), 227, hep-ph/9209205.

[37] Zoltan Nagy and Davison E. Soper, "On the transverse momentum in Z-boson production in a virtuality ordered parton shower," *JHEP*, **03**(2010), 097, 0912.4534.

[38] S. Catani and M. H. Seymour, "A General algorithm for calculating jet cross-sections in NLO QCD," *Nucl. Phys.*, **B485**(1997), 291, [Erratum: Nucl. Phys.B510,503(1998)], hep-ph/9605323.

[39] F.Mandl and G.Shaw, Quantenfeldtheorie
(German version), Aula Verlag, 1993.

[40] M.Peskin and D.Schroeder, An introduction to Quantum Field Theory, Westview Press, 1995.

[41] Jack E. Paton and Hong-Mo Chan, "Generalized veneziano model with isospin," *Nucl. Phys.*, **B10**(1969), 516.

[42] Frits A. Berends and W. Giele, "The Six Gluon Process as an Example of Weyl-Van Der Waerden Spinor Calculus," *Nucl. Phys.*, **B294**(1987), 700.

[43] Michelangelo L. Mangano, Stephen J. Parke, and Zhan Xu, "Duality and Multi - Gluon Scattering," *Nucl. Phys.*, **B298**(1988), 653.

[44] Michelangelo L. Mangano, "The Color Structure of Gluon Emission," *Nucl. Phys.*, **B309**(1988), 461.

[45] Zoltan Nagy and Davison E. Soper, "Parton showers with quantum interference: Leading color, spin averaged," *JHEP*, **03**(2008), 030, 0801.1917.

[46] John C. Collins, Davison E. Soper, and George F. Sterman, "Transverse Momentum Distribution in Drell-Yan Pair and W and Z Boson Production," *Nucl. Phys.*, **B250**(1985), 199.

[47] S. Catani, M. Ciafaloni, and G. Marchesini, "NONCANCELLING INFRARED DIVERGENCES IN QCD COHERENT STATE," *Nucl. Phys.*, **B264**(1986), 588.

[48] John C. Collins and Davison E. Soper, "The Theorems of Perturbative QCD," *Ann. Rev. Nucl. Part. Sci.*, **37**(1987), 383.

[49] John C. Collins, Davison E. Soper, and George F. Sterman, "Soft Gluons and Factorization," *Nucl. Phys.*, **B308**(1988), 833.

[50] URL `http://www.wolfram.com/mathematica/`.

[51] M. Abramowitz and I. Stegun, Handbook of mathematical functions with formulas, graphs and mathematical tables, Dover Publications, Boston, 1972.